Monolayer Helium Adsorbed on Rare Gas Plated Graphite - A Heat Capacity Study

by

Selden B. Crary

A dissertation submitted in partial fulfillment
of the requirements for the degree of

Doctor of Philosophy

University of Washington

1978

Approved by Oscar Vilches

Program Authorized
to Offer Degree Physics

Date July 5, 1978

UNIVERSITY OF WASHINGTON

Date: June 21, 1978

We have carefully read the dissertation entitled "Monolayer Helium Adsorbed on Rare Gas Plated Graphite - A Heat Capacity Study"

submitted by Selden B. Crary in partial fulfillment of the requirements of the degree of Ph.D. and recommend its acceptance. In support of this recommendation we present the following joint statement of evaluation to be filed with the dissertation.

Mr. Crary has chosen for his experimental work a topic of current interest in physical adsorption. In particular, he has addressed the question of how the thermodynamic properties of an adsorbed layer of helium are modified by well controlled changes in the surface where the helium layer is formed. He has found that while ^{4}He on graphite has, at low densities, a condensation temperature around 1.2K, on an Ar coated graphite surface the condensation temperature moves to 2.1K. On the other hand, Ne coating decreases the condensation temperature to about 0.8K. Similar effects are observed with ^{3}He. While there is no unique interpretation for the shift, Mr. Crary has explored two possibilities: condensation into a liquid phase, and condensation into an array partially registered with the substrate. The interpretations are in the context of the literature currently available as well as unpublished work of theorists at the U. of Washington. The dissertation is very well written.

DISSERTATION READING COMMITTEE: Oscar Vilches

O. E. Vilches (Chairman)

R. Puff

J. G. Dash

In presenting this dissertation in partial fulfillment of the requirements for the Doctoral degree at the University of Washington, I agree that the Library shall make its copies freely available for inspection. I further agree that extensive copying of this dissertation may be referred to University Microfilms, 300 North Zeeb Road, Ann Arbor, Michigan 48106, to whom the author has granted "the right to reproduce and sell (a) copies of the manuscript in microform and/or (b) printed copies of the manuscript made from microform."

Signature Selden B. Gray

Date July 5, 1978

TABLE OF CONTENTS

Table of Contents, cont'd

LIST OF FIGURES

List of Figures, cont'd

LIST OF TABLES

ACKNOWLEDGEMENTS

The author is indebted to Professor Oscar E. Vilches for his assistance and encouragement throughout all phases of the experiment, its interpretation, and the preparation of the manuscript. In addition, he would like to thank Professor J. G. Dash for several stimulating conversations, especially in regard to the various interpretations of the data.

The author also wishes to express his sincere appreciation to Mr. Steven Van Sciver for providing instruction in the operation of the dilution refrigerator and heat capacity apparatus; to Messrs. Carlos Kohan and Olegario Ferreira for their expert assistance with data acquisition and reduction; to Mrs. Beverly Dexter and Mr. John Stoltenberg for their special efforts in providing an uninterrupted supply of cryogenic liquids; and to Ms. Lorie Lucky and Mrs. Daris Healy for cheerfully allowing the author to make changes in the manuscript and figures even as they were being typed and drafted.

Finally, a special acknowledgement is due the author's wife, Susan F. Engert, for her support and encouragement during the years in which this study was prepared.

Chapter 1

INTRODUCTION

1.1 Motivation

In recent years it has been demonstrated that submonolayer coverage films of rare gas atoms can be prepared which have properties describable by two-dimensional models. Analogues of the three-dimensional gas, liquid, and solid phases have been identified, and in addition, film phases which have no three-dimensional counterpart have been discovered and studied.[1,2-6]

Adsorbed films of ^{3}He and ^{4}He have been of particular interest because they closely approximate two-dimensional Fermi-Dirac and Bose-Einstein systems, respectively. They thus provide a test of theories of interacting quantum systems in reduced dimensionality and offer the possibility of studying phase transitions in two-dimensions.

The properties of submonolayer helium films have been studied on a variety of surfaces, including unplated and plated copper sponge,[7-12] vycor glass,[13,14] the surface of liquid ^{4}He,[15] graphitized carbon black,[16] and exfoliated graphite.[17] A primary goal of these studies has been to find an adsorbing surface which, although confining the helium to a planar geometry, minimizes the influence of the substrate on the ideal two-dimensional properties of the film. The only successful surface in this regard has been exfoliated graphite,[18] in part because of its high degree of chemical purity and structural perfection, but also because of the relatively small variation in helium-substrate potential energy along its surface.[19].

Heat capacity and vapor pressure measurements[2,20,21] of ^{4}He adsorbed on graphite have revealed a number of thermodynamic phases. The phase diagram which has been constructed from the heat capacity data is shown in Fig. 1.1, where the circles indicate the positions of peaks in constant coverage heat capacity data. Over the majority of the areal density-temperature plane of the figure, the ^{4}He film heat capacity has the temperature and density dependence of a two-dimensional gas of interacting Bose particles.[2,22,23]

As the gas is cooled, peaks are observed in the heat capacity and these have been interpreted as signals of phase transitions to various low temperature phases depending upon the density of the atoms of the film. At densities near monolayer completion, which has been determined to occur at an areal density $n \approx 0.114$ Å^{-2}, the low temperature phase is a "two-dimensional Debye solid" with heat capacity proportional to the square of the temperature.[2,20,24] Over a relatively narrow density range near $n \approx 0.0636$ Å^{-2}, the gas on cooling becomes registered with the surface atomic structure of the graphite substrate in a structure with one helium atoms for every six surface carbon atoms.[2,20,25-27] A few percent of vacancies or interstitials are allowed in the structure, however, and this accounts for the range of areal densities for which this phase occurs. The structure is shown in Fig. 1.2 with the helium atoms shown as disks with diameter $\rho = 2.87$ Å. At densities intermediate to the solid and registered phases, the nature of the low temperature film has not been identified with certainty, although it is possibly a two-phase mixture of solid and registered phases.[28]

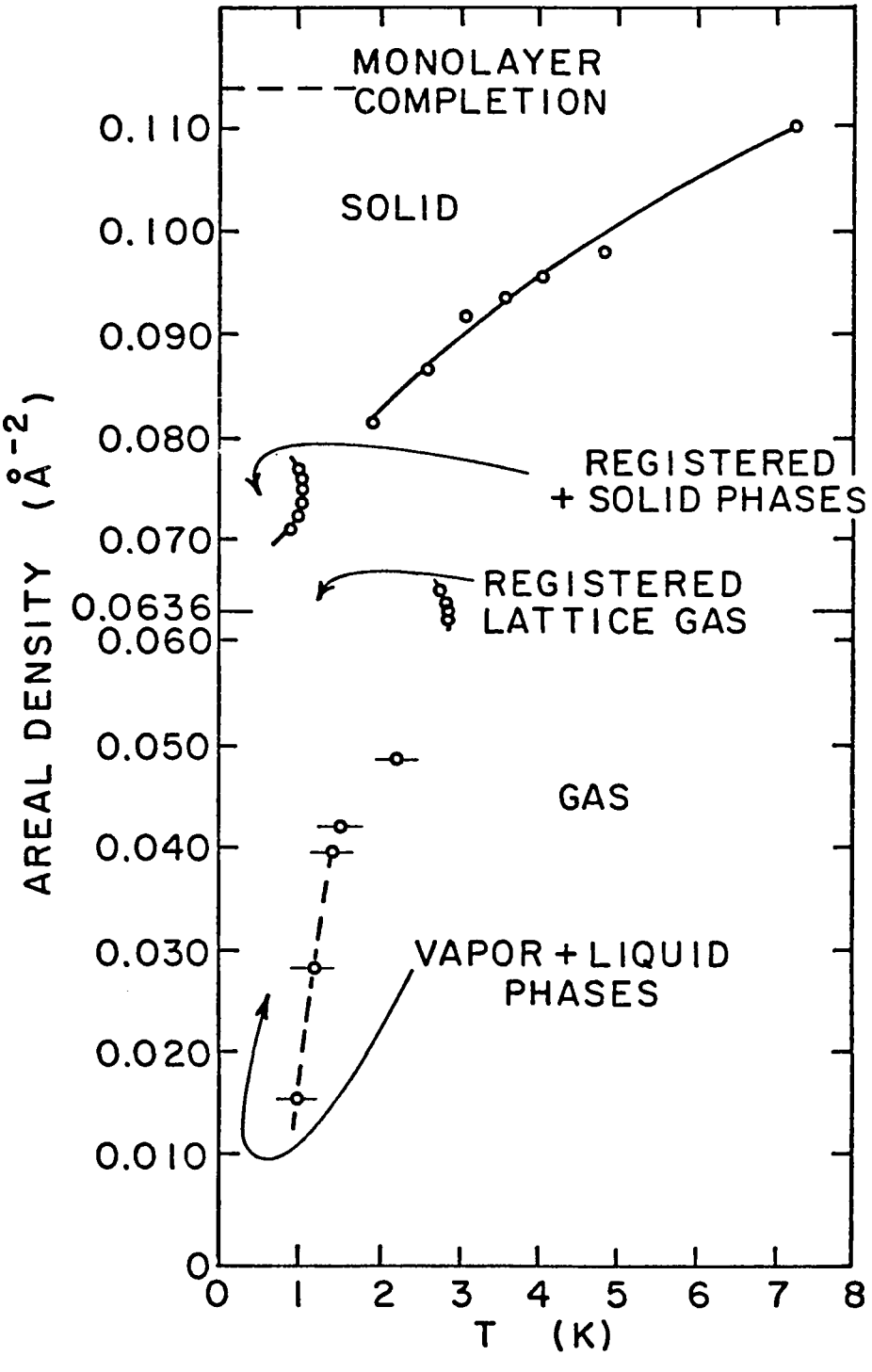

Figure 1.1 Phase diagram for ^{4}He/Gr.

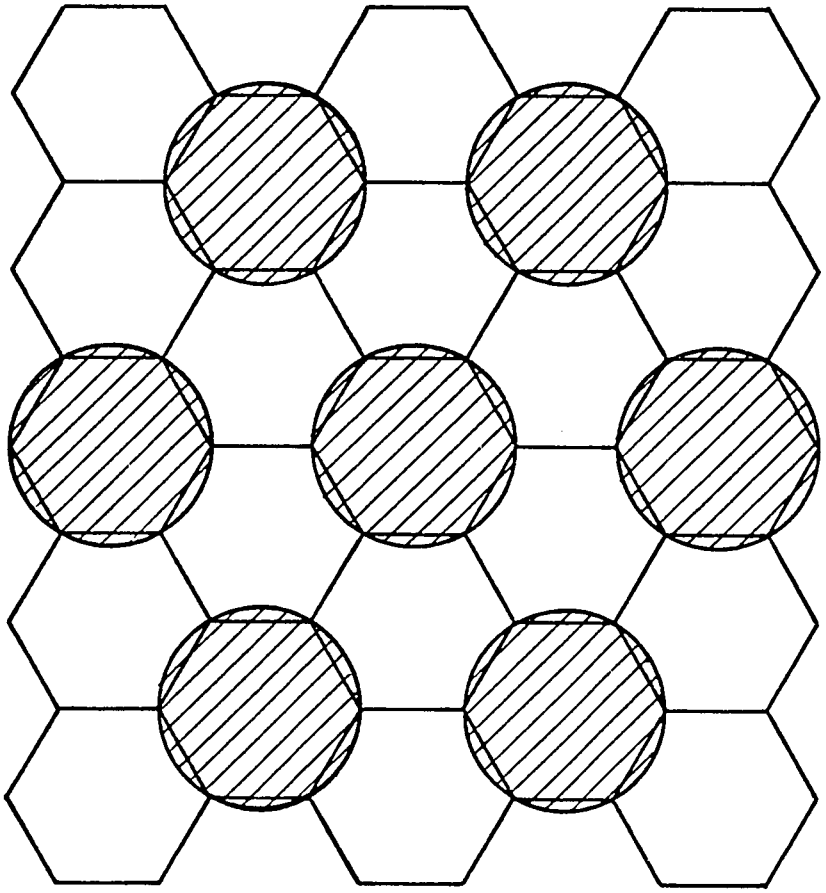

Figure 1.2 The geometry of the registered phase of ^{4}He/Gr.

At densities $n<0.060\ \text{Å}^{-2}$ peaks are seen in specific heat measurements below 4 degrees Kelvin[2,29] (Fig. 1.3), and one interpretation has been that these peaks are the signal of a low temperature region of coexisting gas and liquid phases.[22,30] Theoretical calculations of helium on an ideally two-dimensional surface[31-34] or on the periodic graphite substrate[34] predict a liquid phase at T=0, although in the realistic substrate case the stability of the phase with respect to a registered phase is not conclusive. Thus it is also possible that the low temperature region for $n<0.060\ \text{Å}^{-2}$ is a region of coexisting gas and registered phases.

Although the properties of adsorbed submonolayer helium have been studied using a variety of substrates, graphite is the only one which has a well-characterized crystalline surface. The other substrates are either liquid or amorphous in structure or have surfaces which are inhomogeneous to helium adsorption.

In order to distinguish between those properties of helium films which are a result of the two-dimensional character of the film and those which are induced by the periodic nature of the substrate, it is necessary to find well-characterized substrates.other than graphite. Magnesium oxide powder (MgO) has been suggested as a possibility, and its adsorption properties are currently being investigated.[35] An alternative approach is to plate graphite with one or more layers of a noble gas and to use the plated graphite system as the new substrate.

This study was undertaken with this alternative approach in mind. Argon and neon were chosen as preplating atoms because theoretical

Figure 1.3 The specific heat of three ^{4}He/Gr runs from Refs. 2 and 29.

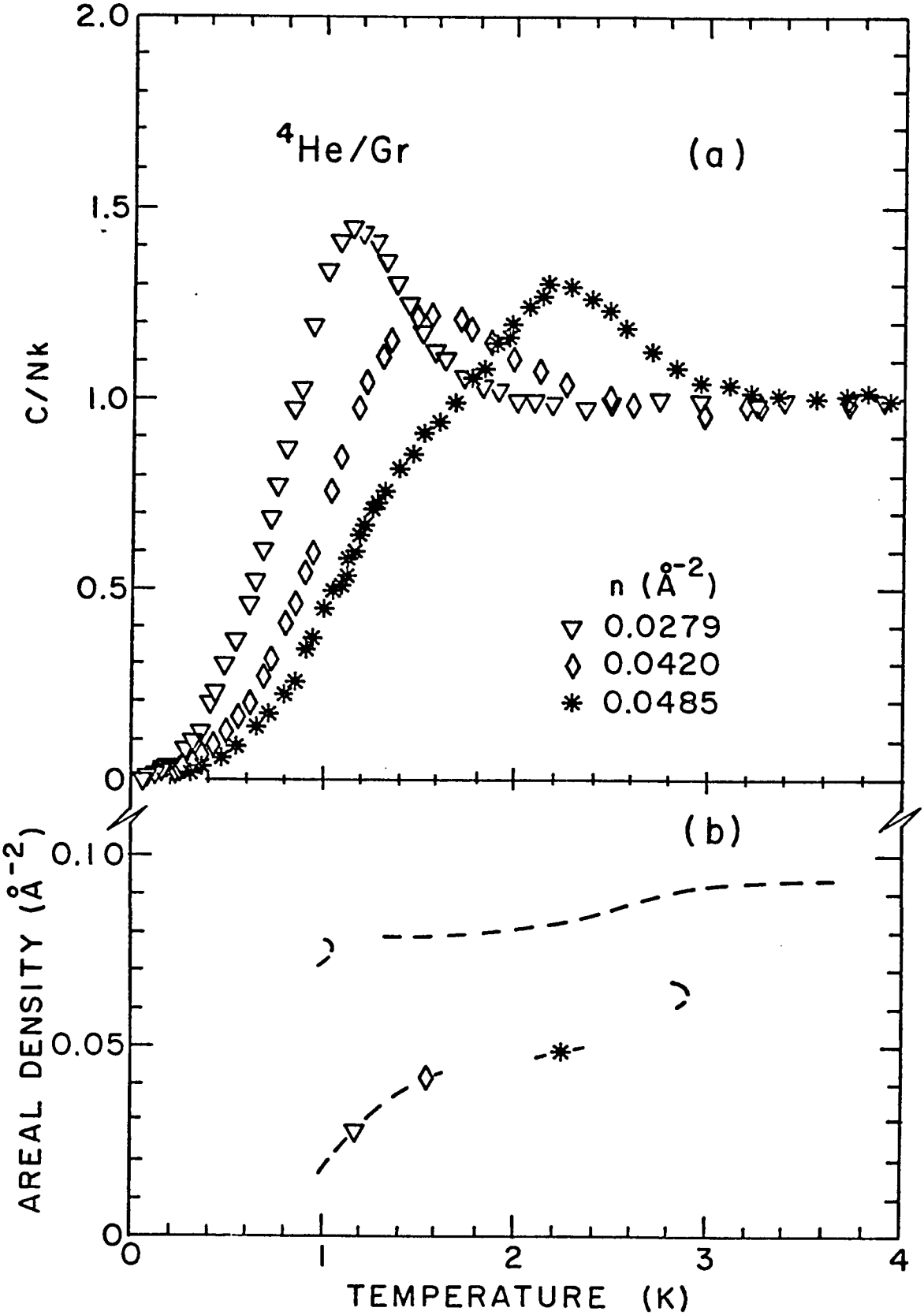
2.0
1.5
1.0
0.5
0
C/Nk
^{4}He/Gr
(a)
n (Å^{-2})
0.0279
0.0420
0.0485
(b)
0.10
0.05
0
AREAL DENSITY (Å^{-2})
0
1
2
3
4
TEMPERATURE (K)

results indicated that the properties of a helium film would be significantly altered if the adsorbent were graphite plated with a monolayer of either of these two rare gas atoms.[34] The experimental plan was to plate a pre-existing graphite substrate with a monolayer of argon and to measure the heat capacity of a series of submonolayer coverages of He in the temperature range $0.1<T<4.0$ K. Evidence would be sought for the existence of the various phases observed for the system ^{4}He on unplated graphite, with special attention given to coverages less than one-half monolayer. The cell could then be warmed to room temperature, the adsorbed gas removed, and the experiment repeated using neon as the plating atom.

The remainder of this chapter details some of what is known about the interaction of helium with the surfaces of interest: graphite, argon-plated graphite, and neon-plated graphite. It also includes a discussion of some of the superlattice structures possible on the plated surfaces. Chapters 2 and 3 describe the experimental apparatus and procedures, respectively, and Chapter 4 describes the methods of data reduction. The data is presented in Chapter 5 which is followed by a discussion in Chapter 6. Chapter 7 provides a conclusion.

1.2 Helium-Substrate Potential Energy

The interaction energy between two similar noble gas atoms is commonly approximated by the Lennard-Jones potential:

$$V(r) = -4\epsilon\left[\left(\frac{\sigma}{r}\right)^6 - \left(\frac{\sigma}{r}\right)^{12}\right],$$

where r is the distance between the centers of the atoms, ϵ is the

maximum depth of the potential, and σ is the distance at which the potential energy changes sign.[36] This potential has also been used to describe the interaction between carbon atoms in different planes of graphite. From knowledge of the Lennard-Jones parameters σ and ε for the helium-helium and carbon-carbon interactions, estimates of the two body helium-carbon interaction have been made[37] using the interpolation formulas $\sigma_{He-C} = (\sigma_{He} + \sigma_C)/2$ and $\varepsilon_{He-C} = (\varepsilon_{He-He}\varepsilon_{C-C})^{\frac{1}{2}}$. The interaction of a helium atom with a graphite substrate can then be approximated by a lattice summation of interactions of Lennard-Jones form using the values σ_{He-C} and ε_{He-C}..

This method has been used by Hagen, Milford, and Novaco[37] to calculate the potential energy as a function of the distance normal to three fixed points in the plane of the graphite surface, and their results are shown in Fig. 1.4. The distance normal to the surface is expressed in units of the distance between adjacent graphite hexagons, a=2.45 $\mathring{A}$. It can be determined from the figure that the energetically most favorable position is approximately 2.9 $\mathring{A}$ above the plane of the carbon atoms and equidistant from the six nearest carbon atoms. The figure also shows the binding energy (long horizontal lines) for the two helium isotopes as well as the energies of vertically excited states. The difference in energy between the minimum of the curves and the binding energies is a measure of the zero-point kinetic energy of a single atom on the surface. Thus, an isolated helium atom is expected to have high mobility on a perfect graphite surface.

The calculated helium-substrate potential energy is qualitatively

Figure 1.4 Potential energy of an isolated helium atom as a function of displacement normal to three fixed points in the graphite surface plane, as given in Ref. 37. The long horizontal lines show the binding energy of isolated helium atoms in the ground state. The shorter horizontal lines show the energy of vertically excited states. The length scale a is the distance between adjacent graphite hexagons: $a = 2.45$ Å.

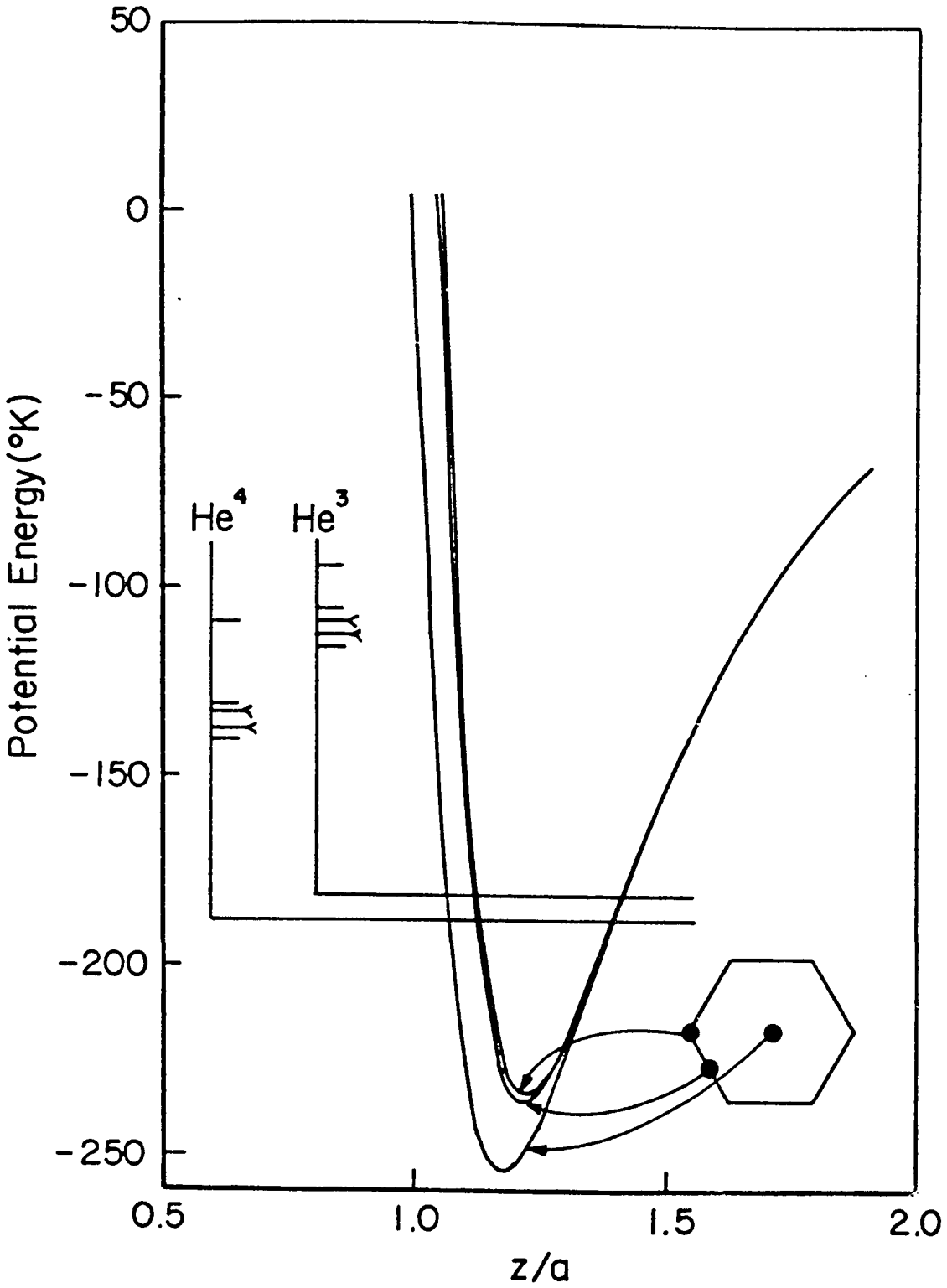
50
0
-50
-100
-150
-200
-250
Potential Energy (°K)
He⁴
He³
0.5
1.0
1.5
2.0
z/a

changed if the substrate consists of graphite pre-plated with a monolayer of argon. Neutron scattering studies[38] have shown that an argon monolayer on graphite forms a triangular lattice with a nearest neighbor distance of 3.9 Å at 4 K. Fig. 1.5(a) is a representation of the relative sizes of argon atoms adsorbed on the basal plane of graphite. It can be seen that the argon overlayer has a greater areal density than the registered configuration of Fig. 1.2. The unit cell of this argon-plated substrate and the calculated helium-substrate potential energy above three fixed points in the unit cell are shown in Fig. 1.6 as reported by Novaco and Milford.[39].

A comparison between this figure and Figs. 1.4 and 1.5(a) shows the following differences between the systems of helium adsorbed on graphite (He/Gr) and helium adsorbed on argon-plated graphite (He/Ar/Gr):

(1) The calculated minimum potential energy directly over an adsorption site is reduced from -254 K for He/Gr to -112 K for He/Ar/Gr.

(2) The maximum variation in the potential energy across the substrate is increased from 21 K to 47 K. However, the variation in energy from the equilibrium position directly above a site to a position directly above a point halfway between substrate atoms is reduced from 18 K for He/Gr to 14 K for He/Ar/Gr.

(3) The lattice of the top layer of substrate atoms is changed from honeycomb to close-packed.

(4) The lattice of sites is changed from triangular to honeycomb.

(5) The distance between sites is decreased from 2.46 Å for He/Gr to 2.3 Å for He/Ar/Gr.

Figure 1.5 (a) Representation of the relative size of argon atoms on a graphite surface plane. The nearest neighbor distance is 3.9 Å.

(b) Neon monolayer adsorbed on graphite. The nearest neighbor distance is 3.1 Å.

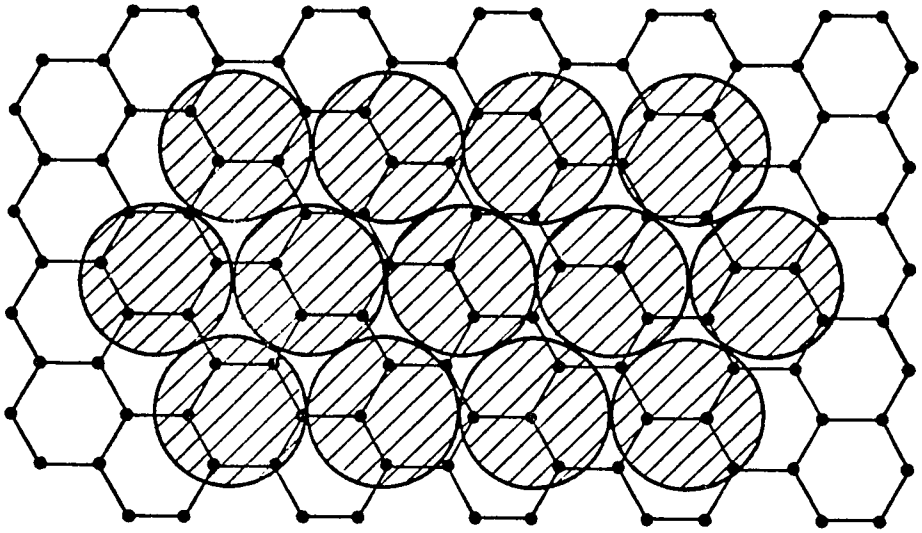

(a) Ar/Gr

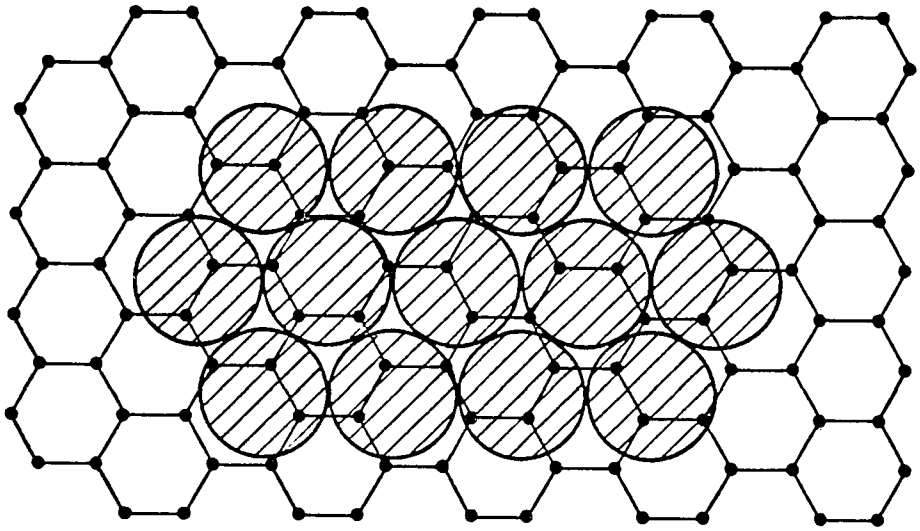

(b) Ne/Gr

Figure 1.6 Helium-substrate potential energy for the argon-plated graphite system, as given in Ref. 39.

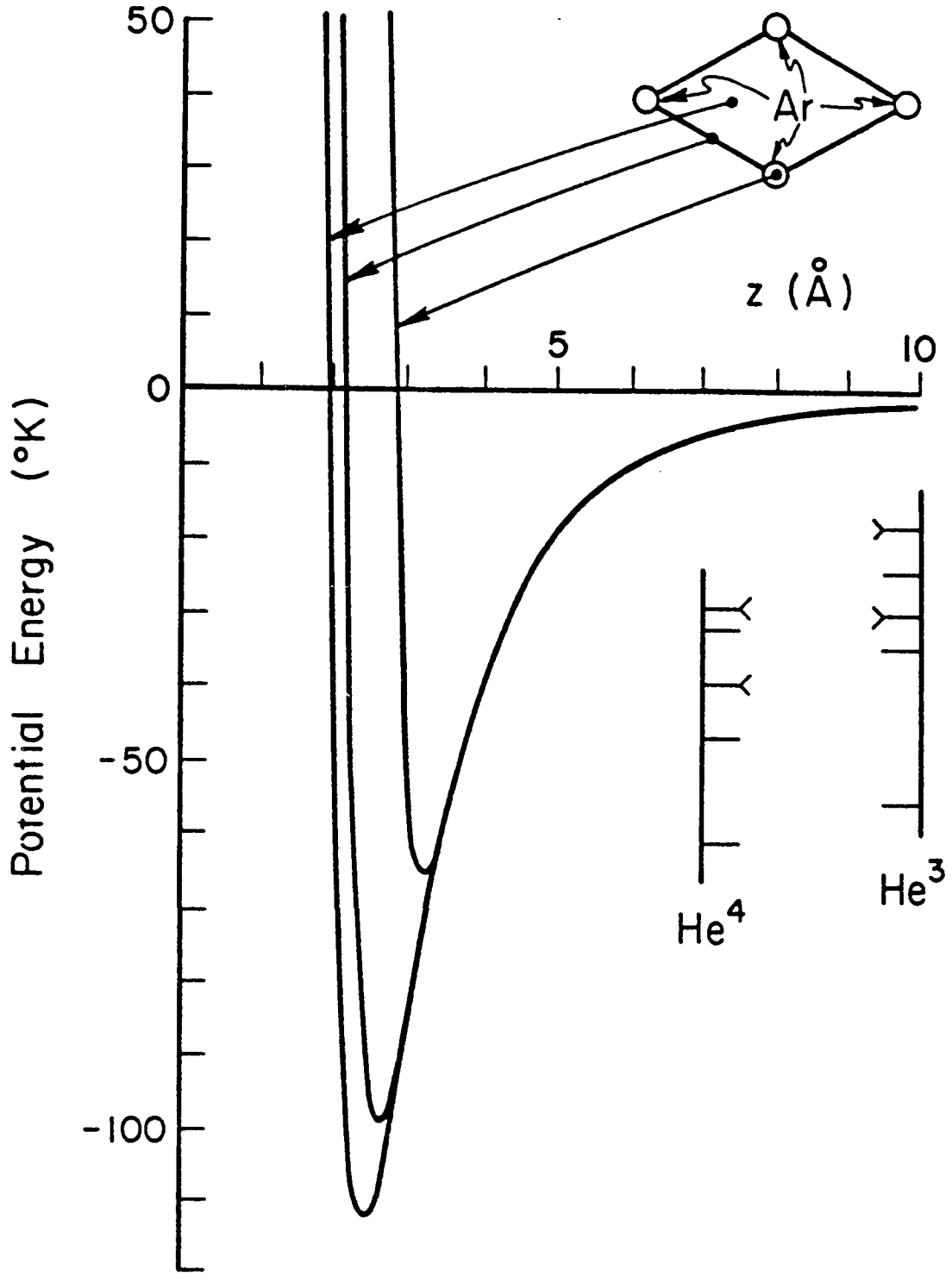
50
0
-50
-100
Potential Energy (°K)
z (Å)
5
10
Ar
He4
He3

These differences are reported in tabular form in Table 1.1 which includes the results of calculations for He/Ne/Gr as well.[40] The potential energy curve for He/Ne/Gr calculated by Novaco[40] is shown in Fig. 1.7 and the geometry of the assumed close-packed structure of the neon monolayer is shown in Fig. 1.5(b).

1.3 Superlattice Geometries

A common feature of systems of adsorbed atoms and molecules on crystal surfaces is the occurrence of superlattice structures which are in registry with adsorption sites of the adsorbate-surface interaction.[41] In the case of helium adsorbed on graphite, a structure with one helium atom localized in every three adsorption sites has been observed[2,25,26,42] and is represented in Fig. 1.2. A possible superlattice structure of the He/Gr which is thought not to occur[43] corresponds to the adsorption of one helium atom for every four adsorption sites. These two structures are denoted $(\sqrt{3} \times \sqrt{3})R\text{-}30^{\circ}$ and (2x2), respectively, using the terminology for classifying superlattice structures[41] and are represented in Fig. 1.8 where a circle denotes an occupied site. There are, of course, many other possible structures.

The notation (m x n) denotes a structure with unit cell vectors whose magnitudes are in the ratio m and n to the magnitudes of the substrate unit cell vectors. The additional notation R-Θ indicates that the superlattice unit cell is rotated an angle Θ from the substrate unit cell.[41] It has been suggested [44] that the notation be further appended to distinguish phases with the same (m x n)R-Θ denotation but which have different average site occupation numbers Xg(Xg = Number of

Table 1.1

V_S, V_A, and V_{SP} are the minimum potential energies directly above an adsorption site, a substrate atom, and the saddle point half-way between substrate atoms, respectively.

d_{A-A} and d_{S-S} are the distances between nearest neighbor substrate atoms and between nearest neighbor sites, respectively.

H and T denote honeycomb and triangular lattices, respectively.

System	V_S (K)	V_A-V_S (K)	$V_{SP}-V_S$ (K)	Lattices: Substrate	Lattices: Sites	d_{A-A} (Å)	d_{S-S} (Å)
He/Gr	-254	21	18	H	T	1.42 (Ref. 2)	2.46
He/Ar/Gr	-112	47	14	T	H	3.9 (Ref. 38)	2.3
He/Ne/Gr	-100	32	9	T	H	3.1 (Ref. 34)	1.8

Figure 1.7 Potential energy of an isolated helium atom as a function of displacement normal to the surface carbon plane of the neon-plated graphite system, as given in Ref. 40. The energy has been calculated for positions normal to neon atoms (A), normal to the "sites" equidistant from three neon atoms (S), and normal to the "saddle points" midway between two neon atoms. The dashed lines are the result of calculations assuming that the neon atoms are fixed. When neon oscillations normal to the surface are included, the potential is shifted somewhat (solid lines).

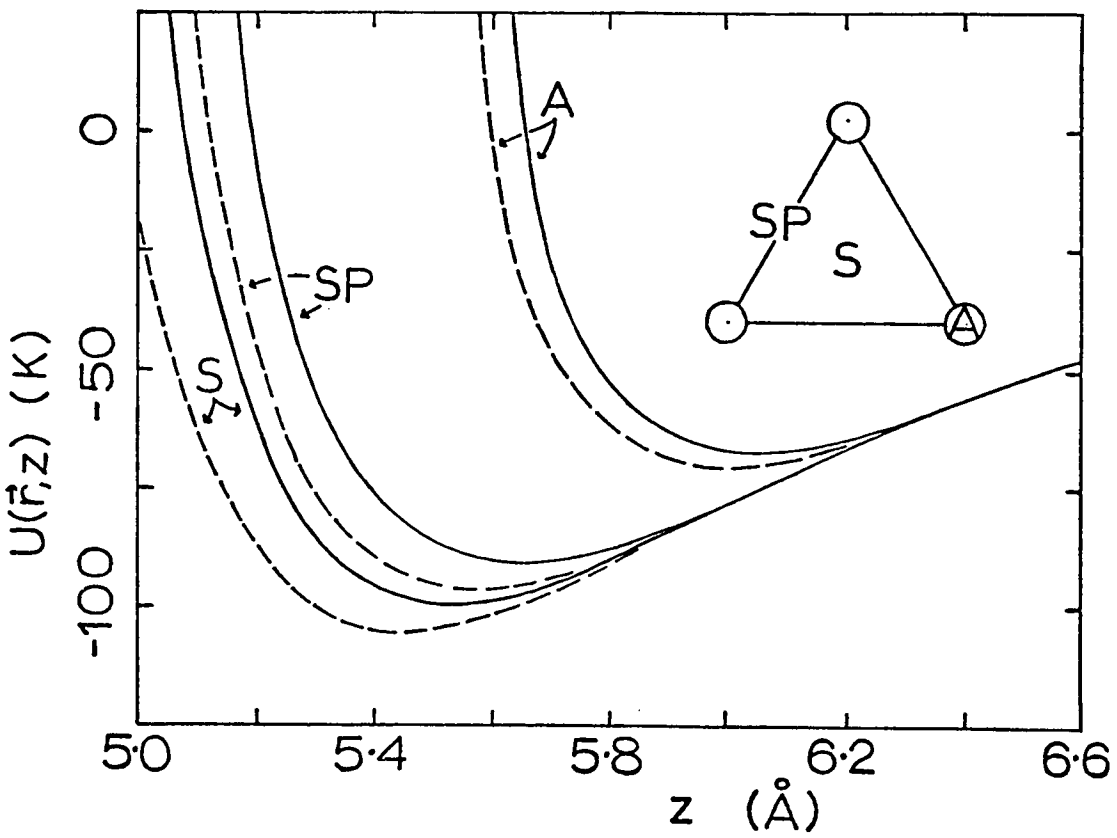
A
SP
S
SP
S
A
0
-50
-100
U(r̂,z) (K)
5·0
5·4
5·8
6·2
6·6
z (Å)

Figure 1.8 Some possible superlattice structures on a triangular lattice of sites [(a) and (b)] and on a honeycomb lattice of sites [(c) - (f)].

(a) $(\sqrt{3} \times \sqrt{3})R\text{-}30^{\circ}$

(b) (2×2)

(c) $(1 \times 1)[\frac{1}{2}]$

(d) $(\sqrt{3} \times \sqrt{3})R\text{-}30^{\circ}[\frac{1}{3}]$

(e) $(2 \times 2)[\frac{1}{4}]$

(f) $(\sqrt{3} \times \sqrt{3})R\text{-}30^{\circ}[\frac{1}{6}]$

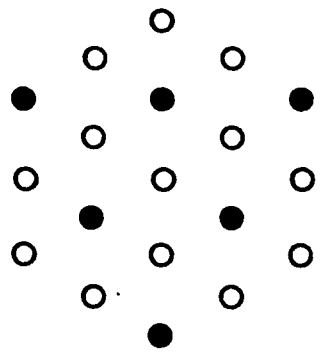

(a)

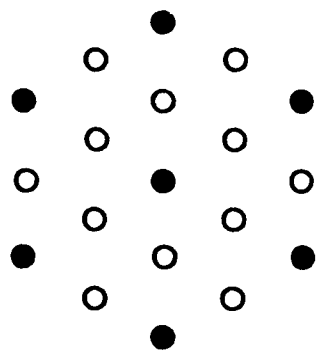

(b)

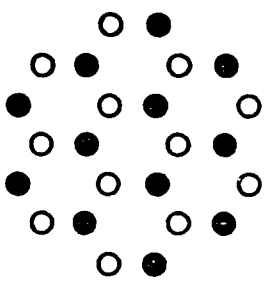

(c)

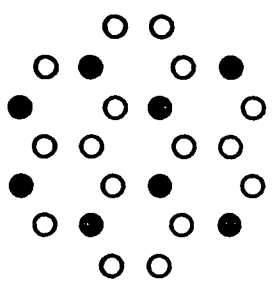

(d)

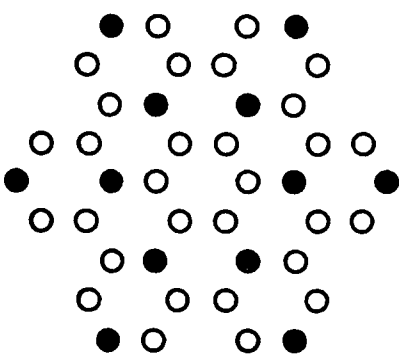

(e)

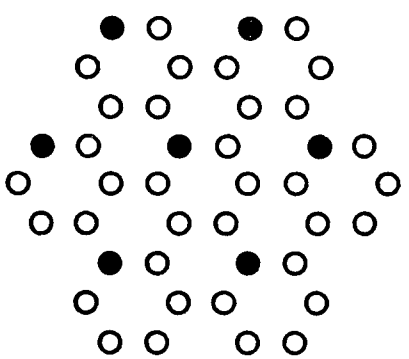

(f)

sites occupied/Number of sites). The structures represented in Figs. 1.8(d) and 1.8(f) are distinguished in this way.

Because the symmetry of sites is changed when graphite is plated with a monolayer of argon or neon, the possible superlattice structures are also changed. Four possible structures are represented in Fig. 1.8(c)-(f) corresponding to values $1/6 \leq Xg \leq 1/2$. The densities these structures would have on various rare gas plated graphite substrates are given in Table 1.2 using the nearest neighbor values of the plating atoms from Table 1.1.

Table 1.2

Structure (see Fig. 1.8)	X_g	Areal Density ($\mathring{A}^{-2}$)		
		He/Gr	He/Ar/Gr	He/Ne/Gr
(a) $(\sqrt{3} \times \sqrt{3})R\text{-}30^\circ$	1/3	0.0636	-	-
(b) (2 x 2)	1/4	.0477	-	-
(c) $(1 \times 1)[\frac{1}{2}]$	1/2	-	0.076	0.12
(d) $(\sqrt{3} \times \sqrt{3})R\text{-}30^\circ[\frac{1}{3}]$	1/3	-	.051	.080
(e) $(2 \times 2)[\frac{1}{4}]$	1/4	-	.038	.060
(f) $(\sqrt{3} \times \sqrt{3})R\text{-}30^\circ[\frac{1}{6}]$	1/6	-	.025	.040

Chapter 2

EXPERIMENTAL APPARATUS

2.1 The Calorimeter

A schematic diagram of the calorimeter used for the heat capacity measurements is shown in Fig. 2.1. The configuration is identical to that used in previous experiments,[29,45] except for minor modification of the thermal link to the mixing chamber, the placement of resistance thermometers, and an increase in the mass of CMN used for thermometry.

The primary adsorbent is a form of exfoliated graphite available commercially with the tradename "Grafoil". Grafoil combines the favorable properties of high specific surface area, exceptional uniformity to adsorption, good thermal conductivity, and purity from surface contamination.[18] In different forms it has been used successfully in experimental situations including heat capacity, NMR, magnetic susceptibility, neutron diffraction, and x-ray diffraction.

The Grafoil sample used in this study is referred to as "cell B" in the literature.[2] Its surface area for helium adsorption is approximately 268 m^2.[46] It is enclosed by a copper container to which has been attached a 104.1 Ω Evanohm wire heater, a 56 Ω Allen-Bradley ¼-watt carbon resistor, and a 110 Ω Speer ¼-watt carbon resistor. In addition, two crystals of CMN with a total mass of 13.6 mg are attached with Apiezon N grease to a short copper tail of the cell. A magnetic field of approximately 5 gauss is trapped inside a small niobium shield around the tail of the cell. Inside the shield an Epibond

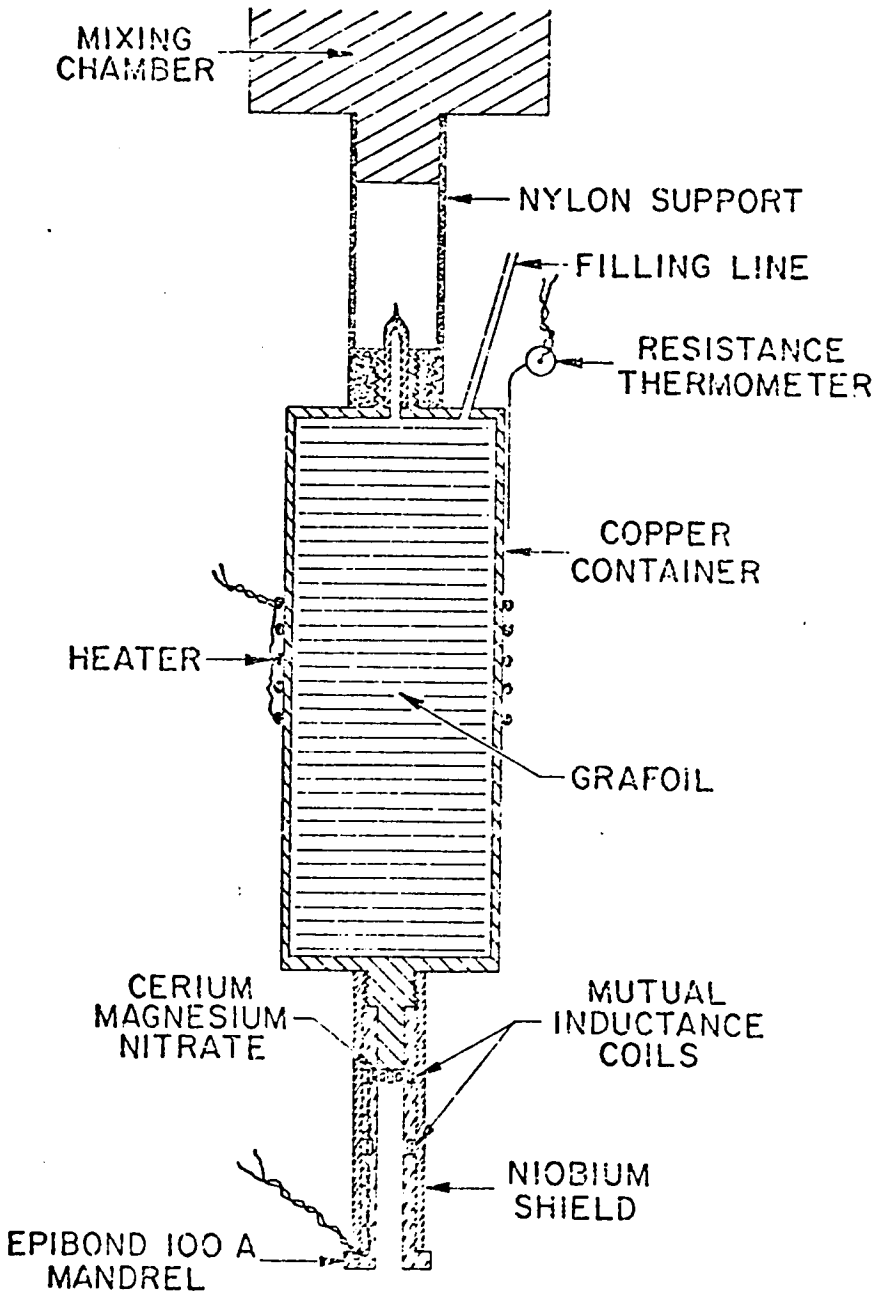

Figure 2.1 The calorimeter used for heat capacity measurements.

100A epoxy mandrel holds two astatically wound niobium wire coils for SQUID thermometry.[47] Electrical leads to the cell heater and resistance thermometers are made of Pb-coated manganin wire and are thermally grounded to the mixing chamber.

The cell is connected to the mixing chamber of a dilution refrigerator by a nylon support of small cross-sectional area. In addition, the entire cell is surrounded by a copper radiation shield which is greased to the sides of the mixing chamber.

A filling line of 0.016" O.D. x 0.004" wall stainless steel tubing is connected to the cell and is thermally anchored at the mixing chamber and the still of the dilution refrigerator. Above the still the filling line is connected to a vacuum jacketed piece of 0.031" O.D. x 0.005" wall Cu-Ni tubing with a 1000 Ω bifilar heater wound along its length.

A dilution refrigerator with a two stage continuous heat exchanger was used to cool the calorimeter. No heat switch was employed. Starting from 1.2 K the cell could be cooled to 0.1 K in about 4 hours of continuous operation of the refrigerator. Cooling of the calorimeter to 0.5 K was possible in less than one hour by operating the refrigerator as a $^3He/^4He$ evaporator.

2.2 Thermometry

Temperatures in the range $0.10<T<1.5$ K were measured using a SQUID system which measured the changing magnetic susceptibility of the two CMN crystals attached to the tail of the cell. Output readings on a

Hewlett-Packard Model 7100B strip chart recorder allowed an experimental resolution $\Delta T^{-1} \simeq 10^{-4} K^{-1}$. This resolution decreases somewhat above 1.5 K because of noise in the SQUID/chart recorder electronics, whereas $10^{-4} K^{-1}$ resolution was possible in the range $1.0 < T < 4.0$ K from resistance thermometry using a 56 Ω carbon resistor and a standard 3-wire AC Wheatstone Bridge[48] with a PAR Model 120 lock-in amplifier. The 100 Ω carbon resistor was used as a back-up thermometer for temperatures below 1 K.

2.3 Thermometer Calibrations

The two carbon resistors had been calibrated previously[29] using a CryoCal germanium resistor as the primary thermometer. The 56 Ω Allen-Bradley carbon resistor had a history of stability. Its calibration had been checked and found not to have changed four years after the initial calibration,[45] and as part of this study no temperature shift was observed in a repetition of a heat capacity run made five years earlier. The same calibration was therefore used for the present study.

The output voltage of the CMN/SQUID thermometer system is inversely proportional to the temperature. It can therefore be conveniently calibrated against the 56 Ω carbon resistor in the range $1.5 < T < 4.2$ K and a linear extrapolation made to greater values of T^{-1}. This was done after each series of heat capacity measurements using this thermometer. The extrapolation introduces an uncertainty of less than 1% in the value of T.

The temperature dependence of the resistance of the 100 Ω Speer

carbon resistor has been observed to change upon thermal cycling to room termperature[45] and was therefore used only as a back-up thermometer.

2.4 Power and Time Interval Measurement

The voltage across a precision 1000 Ω resistor in series with the calorimeter heater allowed a measurement of the heater current. Measurement of the voltage across the heater using the standard 4-wire method then allowed an accurate determination of the power applied. In practice the resistance of the heater was found to be constant so that only the voltage across the precision resistor was measured for each heating interval. A Dana Model 5500 voltmeter was used for the measurement.

The heating time interval was measured with an accuracy of 0.005 sec[49] using a Monsanto Model 100c Counter-Timer.

2.5 Gases and Gas Dosing

The gases used for the plating were purchased from Air Reduction Corporation and were guaranteed to have less than 0.004% impurities. The ^{3}He was obtained from Monsanto Research Corporation which specified 99.98% purity, and the ^{4}He was repurified from the boiloff of the cryostat by passage over a molecular sieve at 77 K to a nominal purity of 99.9%.

The volume of gas admitted to the calorimeter was accurately measured using a 114.1 cm^3 calibrated volume, a Baratron type 77-1000 capacitance pressure gauge, and a thermometer. A Thermo-Vac TM201 pressure gauge,

manufactured by Leybold-Heraeus[50] and capable of operating in the pressure range $0.001<P<10$ torr was used to monitor the pressure in the room temperature portion of the fill line.

Chapter 3

EXPERIMENTAL PROCEDURES

3.1 Preliminaries

As a preliminary, the heat capacity of a film previously measured by Hickernell[29] was re-measured and found to be identical to the earlier result within experimental uncertainty. The film had an areal density $n=0.0281\ \text{Å}^{-2}$. This provided a general check on the experimental procedures and the method of data reduction.

After the preliminary run, the cell was warmed to room temperature, pumped out for several days with a trapped diffusion pump, and then cooled to liquid nitrogen temperature (77 K).

3.2 Argon Pre-plating

The Grafoil had an argon monolayer capacity at 77 K of 81-83 cm^3 STP as determined by a vapor pressure isotherm,[2] and in order to allow for contraction of the argon film as it cooled, a shot of somewhat greater quantity (84.84 cm^3 STP) was used. The gas was admitted to the cell in a series of doses, with the pressure of each dose kept well below the vapor pressure (≈200 torr) of bulk liquid argon at 77 K[51].

The cell was then cooled slowly to 4.2 K with care taken that the argon did not block the fill line. Added assurance of a clear fill line was provided later when helium was successfully admitted to the cell. It is assumed that the Grafoil was completely plated at 77 K, and that the number of argon atoms in the first layer above the Grafoil increased as the cell was cooled. The exact extent of such rearrangement is, however,

unknown. Assuming that all the argon atoms were adsorbed on the first layer, and using the area of the cell as determined from earlier studies,* the average areal density of the argon film was 0.0863 Å^{-2}. In the assumed two-dimensional close-packed arrangement this corresponds to a nearest neighbor distance of 3.7 Å. A recent neutron scattering study of argon films adsorbed on Grafoil confirms the assumption of close-packing and gives a nearest neighbor distance of 3.9 Å.(38)

The calorimeter with argon pre-plating was then cooled to 0.1 K and a heat capacity run taken to 4.0 K. The heat capacity was a monotonic function of T (Fig. 3.1) and was easily fitted above 0.1 K with a ninth order polynomial of the form

$$C(T) = \sum_{n=0}^{9} A_n T^n. \tag{3.1}$$

The heat capacity of the argon was determined by subtracting the heat capacity of the empty cell as determined by Van Sciver(45) and was found to have the T^2 dependence characteristic of a two-dimensional solid at low temperatures. In analogy to the procedure in three dimensions,(52) an effective two-dimensional Debye temperature can be defined from the slope of the specific heat versus T^2:

$$\Theta_D^2 = 28.85\left[\frac{d(C/Nk)}{d(T^2)}\right]^{-1} \tag{3.2}$$

This procedure gave a value $\Theta_D = 70\pm2$ K at T = 4 K, close to the value

*The area of the cell used is that determined by assuming that the tallest specific heat signal of the ^{4}He/Gr registry-deregistry transition occurs when there is exactly one ^{4}He atom for every three graphite hexagons available for adsorption.(2)

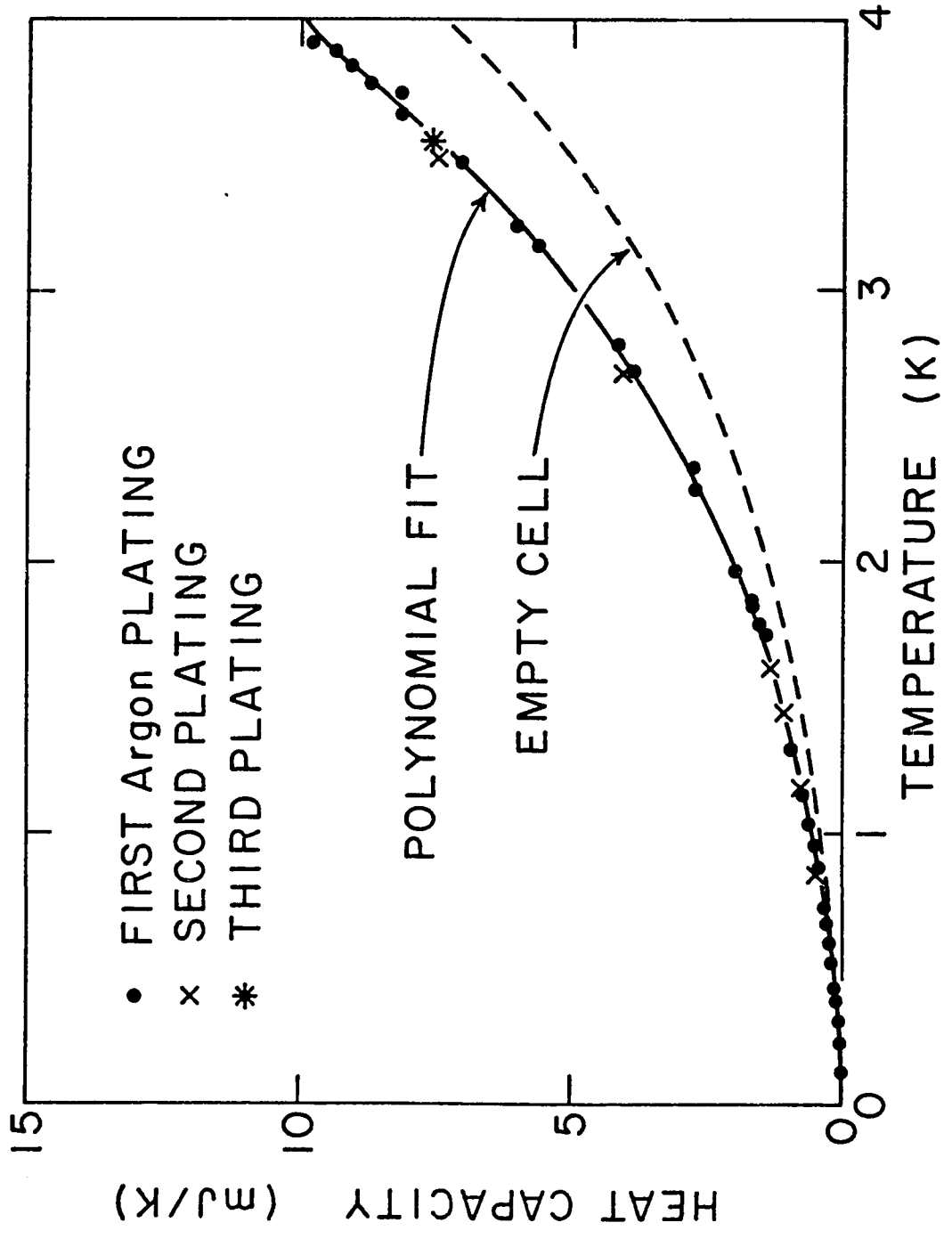

Figure 3.1 Heat capacity of the calorimeter with and without argon plating.

74±2 K extrapolated to 4 K from measurements of Chung( ) at higher temperatures of an argon film with a coverage of 0.77 monolayers.

Despite the good agreement between the effective Debye temperature of the earlier experiment and the value presented here, it is not known with certainty that the entire Grafoil adsorption surface was coated with argon at the lowest temperatures. At some point in the contraction of the film as it is cooled from 77 K the argon in the second layer may lose its interlayer mobility, resulting in a partially filled first layer. Adsorption of helium will then preferentially occur in the gaps left by the shrinking argon film. The actual areal density of the subsequently adsorbed helium film in the next layer will then be somewhat different from the stated value calculated from the relation $n = N/A$, where N is the total number of helium atoms and A is the area available for ^{4}He adsorption on the first layer. It should be kept in mind that although the helium areal densities are reported with three "significant figures", this is only a reflection of the accuracy to which N and A can be determined. The actual areal density of the helium film may be somewhat different because of possible adsorption in the first layer, or because the area available for adsorption in the second layer is not the same as A.

A helium film which was calculated to have an areal density $n = N/A = 0.0280$ Å^{-2} was prepared and admitted to the cell slowly so as to keep the cell temperature below 7 K. The cell was then allowed to cool back to 4-5 K over a period of several hours. In order to assure uniform film density throughout the sample, the annealing procedure

developed by Hering[46] was then followed. This involved raising the temperature of the cell until the vapor pressure above the sample was about 0.2 torr and holding the temperature constant for at least one hour. The heaters were then turned off and the sample allowed to drift slowly to 4.2 K.

The calorimeter was next cooled to 1.2 K and heat capacity data taken to 4.0 K. The data was reduced and a helium film with higher density prepared by admitting additional helium to the cell.

The annealing and cooling procedure outlined above was then repeated for the new coverage. The heat capacity of helium films with five different coverages were measured on the first argon pre-plating. The coverages were n=0.0280, 0.0327, 0.0374, 0.0846, and 0.0887 Å^{-2}. The results are discussed in Chapters 5 and 6.

Following a period of cryostat maintenance, the cell was again pumped out and then a second argon plating prepared as before. The heat capacity was measured for a few temperatures and was found to reproduce the earlier results (Fig. 3.1). Helium films with densities n=0.0093, 0.0140, 0.0187, 0.0233, and 0.0515 Å^{-2} were measured on this second argon pre-plating.

The ^{4}He was then removed by warming the cell to 36 K and successively expanding the desorbed helium into the calibrated volume and pumping it away. On the assumption that all the gas which was removed was ^{4}He, 99.1% of the gas which was put into the cell was accounted for. The cell was again cooled to the experimental range and a single heat capacity point taken to confirm that the background heat capacity had not changed.

The measured value was consistent with the earlier background measurements and is included on Fig. 3.1.

Two ^{3}He coverages were then prepared and their heat capacities measured. The coverages were n=0.0233 Å^{-2} and 0.0374 Å^{-2}. Following these two runs the cryostat was warmed to room temperature and the protected fill line installed in preparation for the neon-plated study.

3.3 Neon Pre-plating

The areal density of a monolayer of neon adsorbed on Grafoil at T=20 K has been determined by Huff[54] to be 0.122 Å^{-2}. This agrees with the value 0.121 Å^{-2} obtained by assuming that the neighboring neon atoms are separated by the distance corresponding to the minimum of the neon-neon interatomic potential, 3.09 Å (Ref. 55). In order to plate the Grafoil it was decided to admit to the cell the quantity of neon which corresponds to an areal density 0.124 Å^{-2}, that is, about 2% more than the estimate of the required amount. A shot of 122.3 STPcc was prepared and admitted to the cell at 77 K.

Because of its weaker attraction to graphite, the majority of the neon was in the bulk vapor phase at 77 K and it was therefore necessary to cool the sample cell very slowly in the temperature range 20<T<30 K in order to avoid condensation of bulk neon in the filling line. Figure 3.2 shows the temperature dependence of the vapor pressure of bulk liquid and solid normal neon,[56] the triple point,[54] and the equilibrium pressure above a Grafoil surface plated with 1.00 and 1.04 monolayers of neon as determined from the adsorption isotherms of Huff.[54]

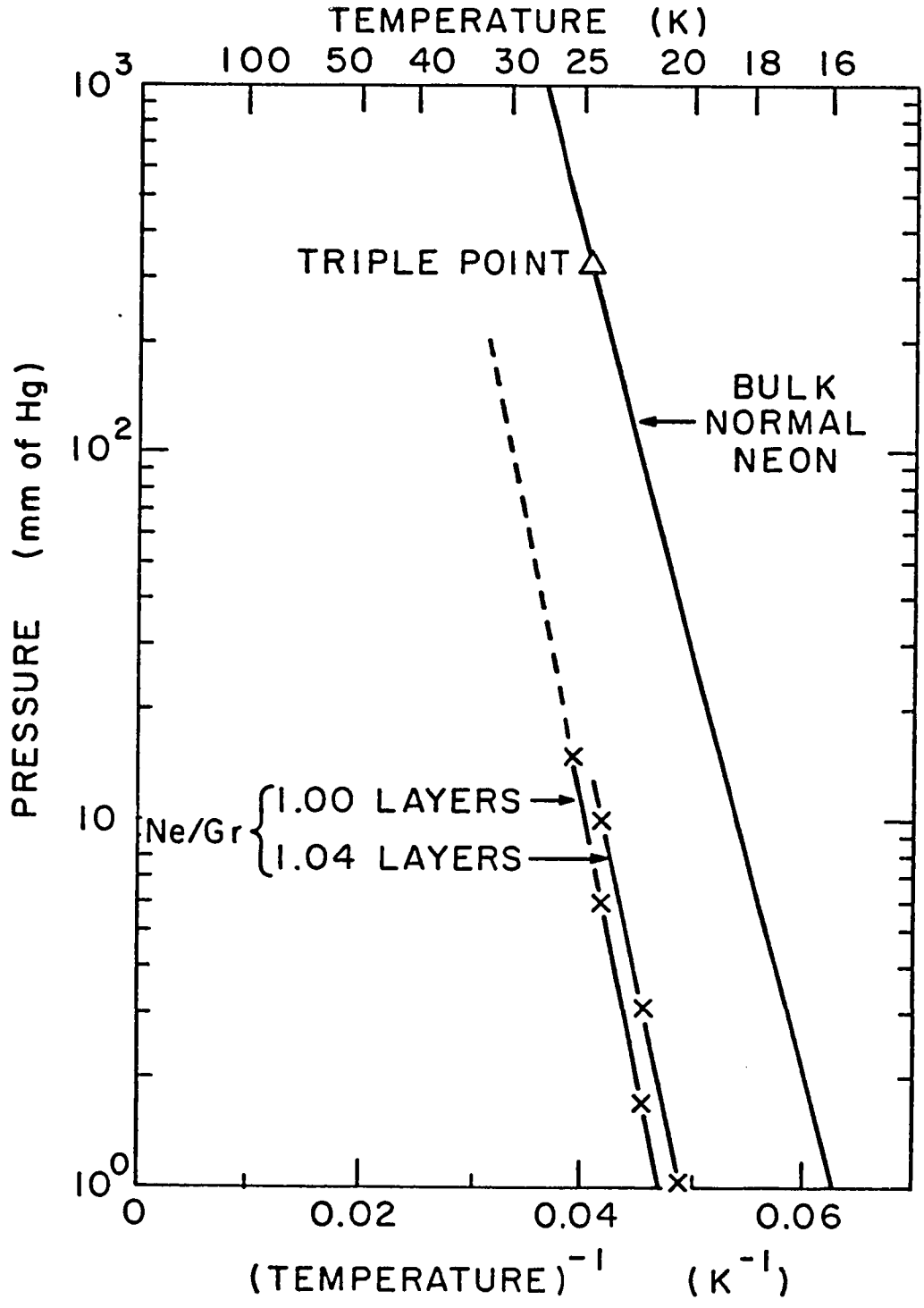

Figure 3.2 Vapor pressure of bulk neon and of Ne/Gr neon monolayer completion as determined from Ref. 54.

At 30 K the pressure above the cell is approximately 84 torr which is the vapor pressure of bulk neon at approximately 22 K. Thus if any section of the fill line is at a temperature less than 22 K, solid bulk neon will block the tube. More generally, in the temperature range of concern, bulk solid will condense in the fill line if any part of the line has an inverse temperature which differs from the cell's by more than 0.13 K^{-1}.

The cell and dilution refrigerator were cooled to approximately 10 K by exchange gas in the vacuum can during the initial transfer of liquid helium into the cryostat. During this procedure the protected fill line heater was dissipating about 0.8 watts of power. This was sufficient to keep the protected section of the fill line from plugging. However, the unprotected bottom section of the fill line was thermally grounded to the dilution refrigerator at both the still and mixing chamber, and a plug formed in this section. The plug was removed by warming the cell and dilution refrigerator to 30 K and then allowing the cell to cool very slowly without exchange gas. The cooling was primarily by thermal conduction between the helium evaporator ("4-pot") and the vacuum can. The helium evaporator was thus the coldest part and the cell the warmest part of the refrigerator/cell system.

The temperature profile of the dilution refrigerator and cell was measured frequently and the evaporator's inverse temperature kept within 0.13 K^{-1} of the cell's inverse temperature. The cell reached 11 K in about one day using this procedure. The pressure of neon gas above the cell was then sufficiently low (approximately 300 μm) that exchange gas

could be admitted to the vacuum can and the cell cooled quickly to 4 K without plugging the fill line. On the basis of the fill line volume and cell dead volume, less than 0.1% of the neon was in the bulk gas phase when the exchange gas was admitted.

A background heat capacity was then taken of the neon-plated Grafoil cell and a seventh order polynomial fitted to the data (Fig. 3.3). At 4K the two-dimensional Debye temperature of the neon film was Θ_D = 65±3 K, somewhat higher than the value 54 K obtained by linearly extrapolating the submonolayer results of Huff[54] to monolayer completion. It may be that the effective Debye temperature in the case of neon is strongly dependent on areal density as monolayer completion is neared, and that the disagreement is a result of the linear extrapolation from 0.84 to 1.00 monolayers. Because the heat capacity had the T^2 temperature dependence of a two-dimensional solid and was considerably greater than the heat capacity of an equal quantity of bulk solid neon, it was reasonable to assume that the neon had plated most of the Grafoil. However, as in the argon-plating case, the neon heat capacity did not provide an independent determination of the exact extent of plating, and the uncertainty in this regard must be kept in mind.

A series of ^{4}He coverages were then prepared and their heat capacities measured in the temperature range 0.10<T<4.0 K. During admission of the ^{4}He the temperature of the cell never rose above 7.0 K. Each coverage was annealed by the procedure discussed earlier. Coverages with areal densities n=0.0140, 0.0236, 0.0329, 0.0422, 0.0562, and 0.0702 Å^{-2} were measured before the cryostat was accidentally allowed

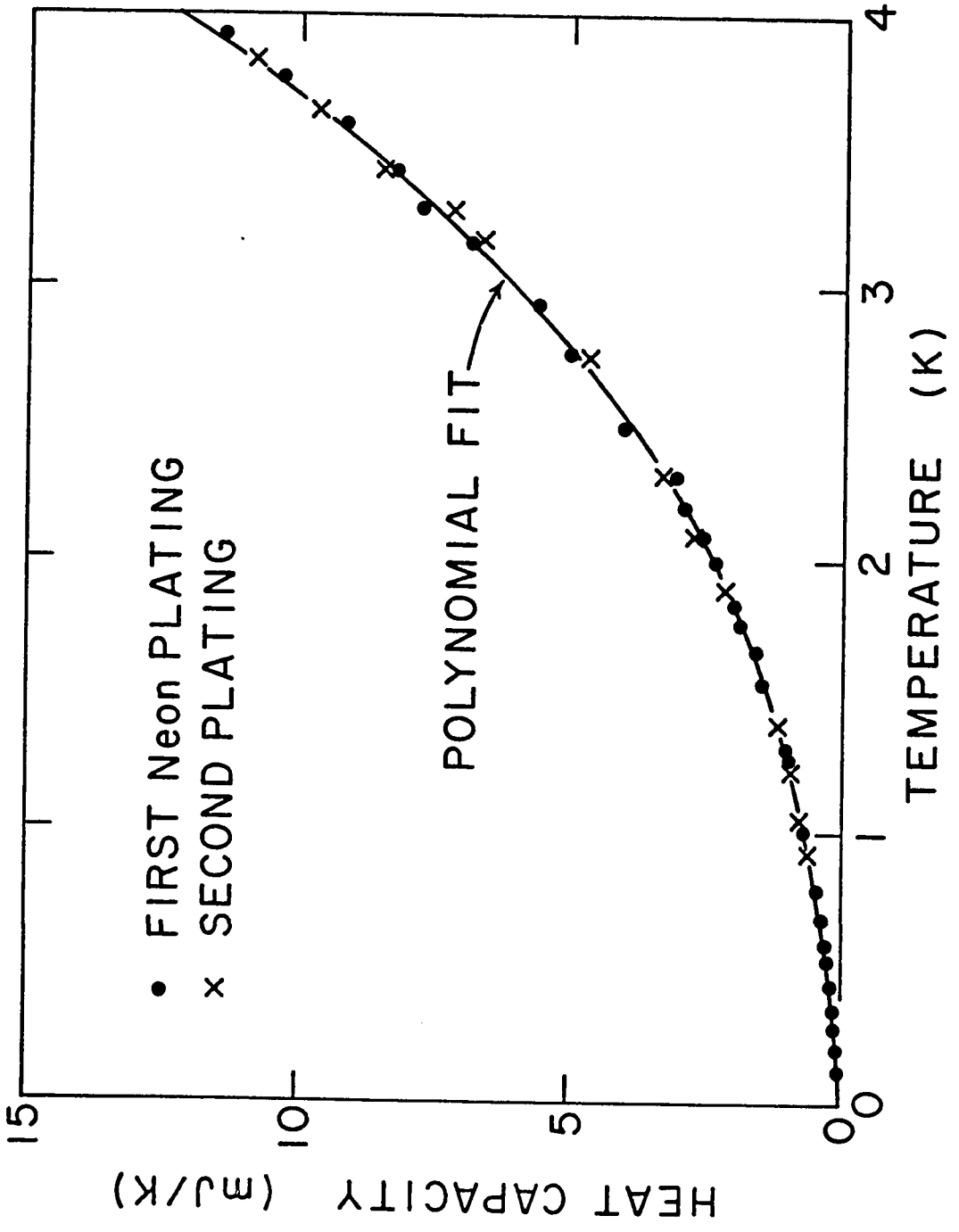

Figure 3.3 Background heat capacity with neon plating.

to warm to approximately 30 K. At this temperature a neon monolayer has a vapor pressure of approximately 70 torr, and it was estimated that about 15% of the neon was desorbed at this point. The cell was cooled back to the experimental range following the procedure for neon plating given above, except that in this case there was a substantial fill line partial pressure due to the desorbed helium. A heat capacity run did not reproduce the earlier result for the areal density 0.0702 Å^{-2}, and the entire cryostat was warmed to room temperature and the cell pumped for two days with a trapped diffusion pump.

The cell was pre-plated with another neon monolayer using a shot of 122.1 STPcc and following the same procedure as before. The background heat capacity was taken and was identical to the earlier background (Fig. 3.3). Two ^{4}He coverages with areal densities n=0.0329 Å^{-2} and 0.0702 Å^{-2} were then prepared and their heat capacities measured as a check on experimental reproducibility. The background and the ^{4}He film heat capacities agreed with the earlier measurements. Films with densities n=0.0841 Å^{-2} and 0.0888 Å^{-2} were then measured. Following the run with n=0.0888 Å^{-2} it was decided to try to remove some ^{4}He from the cell in order to take more detailed data of the run with areal density 0.0841 Å^{-2}. In order to do this the cell was warmed to approximately 7.2 K, the ^{4}He allowed to desorb, and the appropriate quantity removed. The second run with n=0.0841 Å^{-2} agreed well with the first, and provided another check on the reproducibility of the system. Following this run the cell was again warmed to room temperature and pumped for a few days.

An effort was made to reproduce the n=0.0841 Å^{-2} results and to study films with areal densities close to this value. A third pre-plating

using 122.6 STPcc of neon was introduced to the cell, cooled, and a heat capacity run taken. Although the amount of neon admitted to the cell for this plating differed from the two earlier platings by less than 0.5%, the heat capacity proved to be somewhat greater and a new seventh order polynomial was fitted to the data and used as the background. After subtracting off the empty cell contribution, the neon film was found to have a heat capacity about 20% greater than previously, and had an effective Debye temperature Θ_D = 59±3 K.

Nine ^{4}He films were measured over a limited temperature range on this pre-plating, but the results of the previous two n=0.0841 Å^{-2} runs were never reproduced. Several interesting features did emerge, however, and will be discussed in Chapter 6. The coverages in chronological order were n=0.0794, 0.0841, 0.0889, 0.0905, 0.0899, 0.0867, 0.0856, 0.0874, and 0.0813 Å^{-2}.

In addition to the ^{4}He films, the heat capacity of two ^{3}He films, with coverages n=0.0232 Å^{-2} and 0.0840 Å^{-2} were measured.after the cell had been plated with neon a fourth time. A shot of 122.3 STPcc was used, and the neon heat capacity and its effective Debye temperature were the same as those of the third plating.

Chapter 4

DATA REDUCTION

4.1 Helium Heat Capacity

A typical heat capacity point is shown in Fig. 4.1. Following a period of pre-heating drift, a current i was applied to the cell heater for a time interval Δt. This was followed by a period of post-heating drift. The temperature of the resistance thermometer showed considerable overshoot due to the fact that the resistor was in better thermal contact with the heater than with the film. A record was kept of the instrument settings, specifically, the lock-in amplifier sensitivity and time constant, the bridge sensitivity, and the chart recorder sensitivity and speed.

The data was reduced by extrapolating the pre-heating and post-heating drifts to the midpoint of the heating time interval and noting the displacement of the chart recorder pen at these two points. The displacement of the pen was then converted to a resistance by mimicking the cell resistor with a decade resistance box and dialing the value of resistance which produced the identical chart recorder displacement.

This substitution method had the advantage of allowing the bridge to be operated off balance and avoided the need to calibrate the sensitivity of the chart recorder displacement for each heat capacity point. In addition, it bypassed the problem of non-constant sensitivity across a chart page which arises when the resistance being measured exceeds the value of the fixed arms of the bridge (10 KΩ).

Figure 4.1 Typical heat capacity point. Note that the baseline resistance was changed during the heating interval.

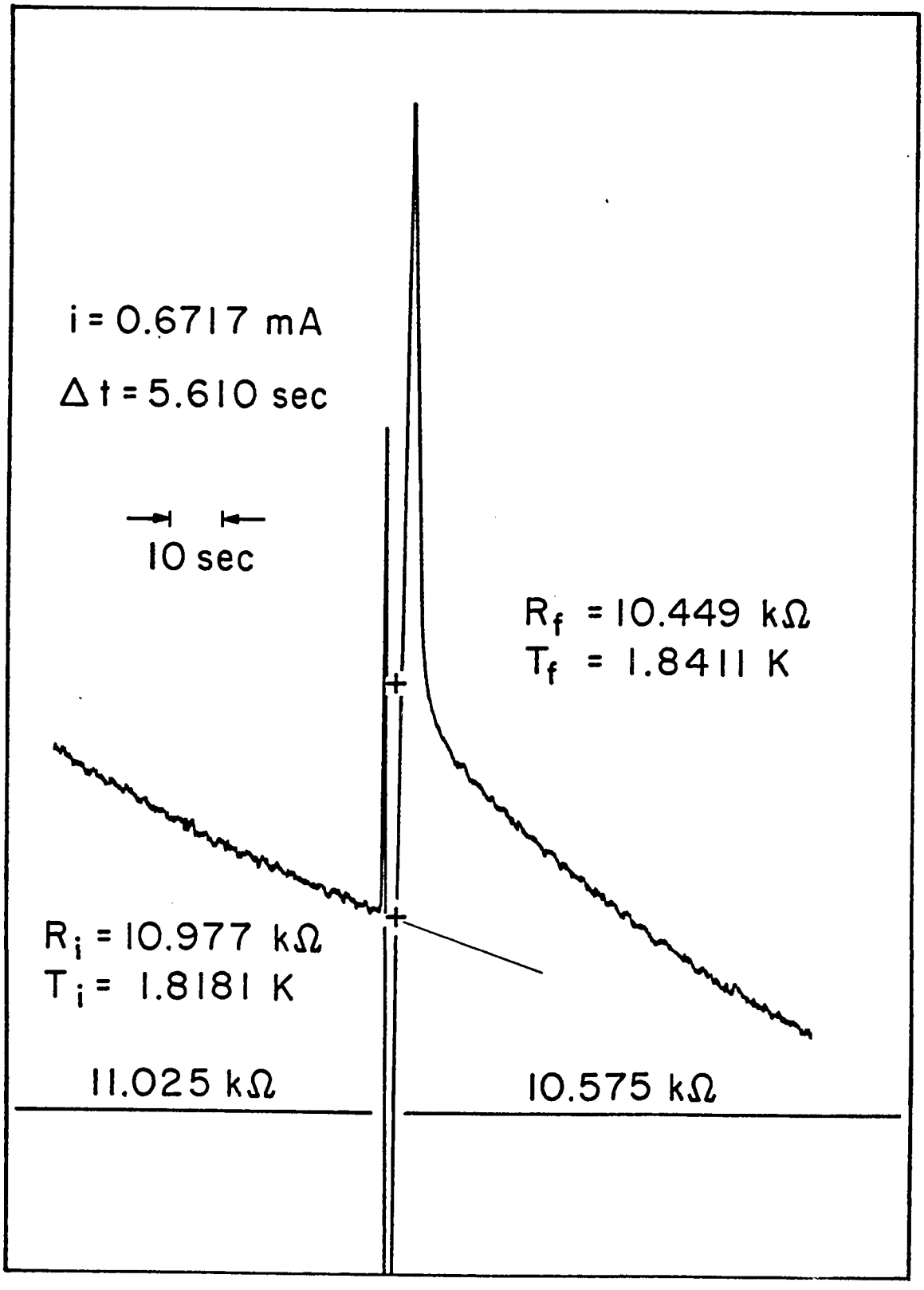
i = 0.6717 mA
Δt = 5.610 sec
10 sec
R_f = 10.449 kΩ
T_f = 1.8411 K
R_i = 10.977 kΩ
T_i = 1.8181 K
11.025 kΩ
10.575 kΩ

Using the calibration of the resistance thermometers, the two values of resistance were converted to an initial and final temperature for the heat capacity point. These temperatures were used to determine the average temperature, $\overline{T}$, and the temperature interval, ΔT. The heat capacity was then calculated as

$$C(\overline{T}) = \frac{i^2 R \Delta t}{\Delta T} \qquad (4.1)$$

where R is the heater resistance which had been determined to be 104.1 Ω.

4.2 Heat Capacity Errors

The largest potential source of systematic error in the determination of the heat capacity came from the temperature calibration. The germanium sensor was provided by the manufacturer with a calibration accuracy of ±0.2%, but the necessary calibration of the secondary carbon resistors including polynomial fitting increased the error to ±0.4%. The SQUID calibration used for lower temperatures was based on an extrapolation from the region of carbon resistance thermometry and had a potential systematic error which increased from ±0.4% at 1.5 K to approximately ±1.5% at 0.1 K. A detailed breakdown of the errors in the measurement using the apparatus has been reported by McLean.[49]

The substitution method mentioned earlier allowed an efficient method of data acquisition and reduction, without increasing the random error in the measurement of the heat capacity above that associated with measurements made with the bridge operated in the balance condition.[49] Generally the random error in the helium heat capacity was approximately ±1% for the data taken using the SQUID system, and ±2% for the data

taken with the resistance thermometer, although the scatter near T=4 K was somewhat higher because of the increased difficulty of graphical extrapolation of the post-heating drift as the thermal isolation of the cell decreased.

Because the preheating drift was monitored in real time on a chart recorder, it was sometimes possible to adjust the drifts for successive points to be nearly identical. This then allowed a tradeoff between random and systematic errors, with the result that the scatter in the heat capacity using carbon thermometry could be decreased to approximately 0.5%.

4.3 Areal Density Errors

The stated areal densities for the various heat capacity runs are calculated by dividing the number of helium atoms admitted to the cell, N, by the area of the cell determined from earlier measurements, (cf. footnote, Sec.3.2). The major sources of error in the value of N are a ±0.5% uncertainty in the value of the calibrated volume used for the measurements and a ±0.2% uncertainty in the pressure measurement of a typical helium "shot" using the Baratron system.[49] In addition, a random error of approximately ±0.2% is introduced by the pressure and temperature measurement of each shot, and because new coverages were frequently prepared by admitting additional helium to the cell, the error is somewhat greater for coverages at the end of a series of runs.

As noted earlier, the actual areal density of a helium film adsorbed on a Grafoil surface may be somewhat different from the stated value, even when the magnitude of the possible systematic and random errors in the

measurement of N is taken into account. Both incomplete and more than complete plating of the Grafoil are possibilities because of thermal contraction of the plating layer, and these will affect the actual film density. Although it is not possible to be very quantitative, the error involved is probably of the order of a few percent, judging from the fact that some of the ^{4}He/Ne/Gr results seem to fit together if the areal density of one of the series of runs is shifted by 3% (cf. Sec. 5.3 and Fig. 5.9).

4.4 Desorption Heat Capacity, ^{4}He/Ar/Gr

Above 3 K the measured heat capacity of the two highest coverage ^{4}He/Ar/Gr films must be corrected for desorption of helium from the surface. To estimate this desorption contribution, the vapor pressure measurements and isosteric heat of adsorption calculations of Lerner and Daunt[57] for ^{4}He/Ar/Gr were used. Their vapor pressure isotherms were made using a capacitance pressure gauge operated at 4.2 K, thus avoiding the difficult problem of correcting for thermomolecular pressure differences in small tubes.

Lerner and Daunt's plot of the isosteric heat of adsorption at ∿10 K was extrapolated to the two densities for which corrections were estimated to be important for this study, namely n=0.0846 Å^{-2} and 0.0887 Å^{-2}. The extrapolated values are q_{st}/k = 53 K and 42 K respectively. However, values of the isosteric heat at 4 K were desired, and this required an assumption concerning the nature of the film. In the model of an ideal mobile two-dimensional film, the temperature dependence of the isosteric heat is given by

$$\frac{q_{st}}{k} = -\epsilon_b + \frac{3}{2}T \quad , \tag{4.2}$$

where ϵ_b is the binding energy of the film at T=0. For other models the coefficient of the temperature dependent term is somewhat different. For example, it is 5/2 for a highly localized film.[58]

The coefficient 3/2 was assumed and gave the values q_{st}/k = 44 K and 33 K for the two films. These values were then used along with approximate values of the 4.2 K vapor pressure, P, taken from Lerner and Daunt's isotherm. Using the fact that $q_{st}/k = (d\ln P/dT^{-1})_N$, equation 4.2, and P(4.2 K), it was possible to estimate P(T) in the range $3.0 \leq T \leq 4.0$ K. The approximate desorption heat capacity was calculated from the equation given by Dash, Peierls, and Stewart,[59]

$$C_d = \frac{PV}{T}\left[\frac{3}{2} + \left(\frac{q_{st}}{kT} - 1\right)^2\right] \quad , \tag{4.3}$$

and the desorption contribution then subtracted from the total measured heat capacity. For the highest density run, the correction was ∿17% at 4 K and ∿6% at 3 K. For the run with density n=0.0846 Å^{-2} the correction was ∿12% at 4 K and ∿2% at 3 K.

4.5 Desorption Heat Capacity, ^{4}He/Ne/Gr

No vapor pressure isotherms were available in the literature for the ^{4}He/Ne/Gr system and therefore pressure measurements were necessary in order to estimate the desorption heat capacity.

The vapor pressure measurements made on the Thermo-Vac gauge were corrected for gas species according to calibration curves supplied by the manufacturer. Thermomolecular pressure corrections were required to

determine the actual pressure in the cell and the low temperature parts of the fill line. As pointed out by McConville,[60] cleaned stainless steel tubes and tubes "as received" can require quite different pressure corrections because of differences in the character of their inner surfaces. The values for tubes "as received" were used.

The thermomolecular corrections were in some cases sizable. For example, with the cell at 4.0 K and a ^{4}He pressure of 0.62 torr at room temperature, the pressure in the cell is estimated to be 0.43 torr.

It was then possible, using values for the room temperature and cell temperature dead volumes (26.4 cm^3 and 8.33 cm^3, respectively), to determine the quantity of unadsorbed helium. At T=4.0 K this amounted to $\sim$1.0 % for the n=0.0888 Å^{-2} film and to less than 0.5% for all other coverages. Knowledge of the unadsorbed fraction of the helium shot allowed an estimate of what the vapor pressure in the cell would have been under isosteric conditions. The isosteric pressure at various temperatures was then used to calculate the isosteric heat of adsorption q_{st} at 4.0 K. Calculations for the films with areal densities n=0.0841 Å^{-2} and 0.0888 Å^{-2} fell in the range q_{st}/k = 43±4 K. The desorption heat capacity was then calculated using equation 4.3 with q_{st}/k = 43 K + 3(T - 4.0 K)/2 and using P(T) calculated as before from the cell pressure and the isosteric heat of adsorption.

Chapter 5

DATA PRESENTATION

5.1 ^{4}He/Ar/Gr

The heat capacity results for ^{4}He adsorbed on argon plated Grafoil (^{4}He/Ar/Gr) are shown in Fig. 5.1(a). The runs with areal densities n=0.0093, 0.0233, 0.0846, and 0.0887 Å^{-2} contain most of the data taken at these coverages. A similar number of specific heat points were taken for all other coverages, but for clarity only smooth lines with a few experimental points are shown. The dominant feature is a rounded specific heat peak that moves to higher temperature as the coverage is increased, the strongest peak ($C/Nk \simeq 3.5$) occurring for n=0.0233 Å^{-2} and T=2.28 K (Fig. 5.2). The positions of the peaks in the density versus temperature plane are shown in Fig. 5.1(b), where peak positions for ^{4}He on unplated Grafoil (^{4}He/Gr) are shown by a dashed line.

The phase for ^{4}He/Gr on the high temperature side of the boundary defined by the dashed line in Fig. 5.1(b) is a two-dimensional (2D) interacting Bose gas.[2] On the low temperature side of the dashed line the film is believed to be a 2D solid above n=0.08 Å^{-2}, a substrate registered lattice gas for $n \simeq 0.06$ Å^{-2}, and a coexisting gas and liquid or a coexisting gas and registered phase for n<0.05 Å^{-2}. The small region between n=0.07 and 0.08 Å^{-2} could be a substrate ordered phase or a region of coexisting substrate ordered and solid phases.[21] The peaks measured using the Ar-plated Grafoil fall on a curve very different from those obtained using the unplated substrate,

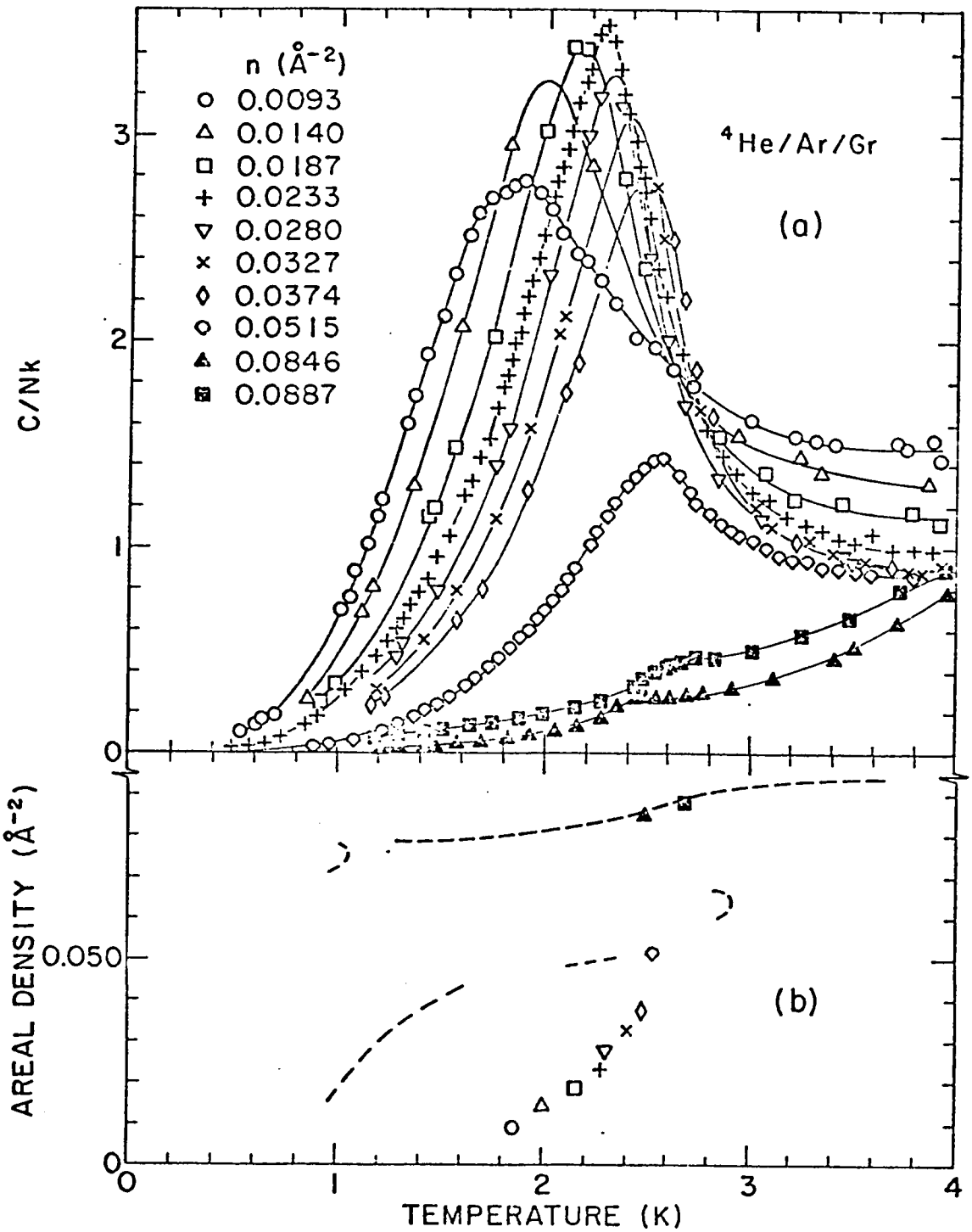

Figure 5.1 (a) Specific heat of ^{4}He/Ar/Gr. (b) Corresponding phase diagram. Dashed lines outline phase diagram for ^{4}He/Gr.

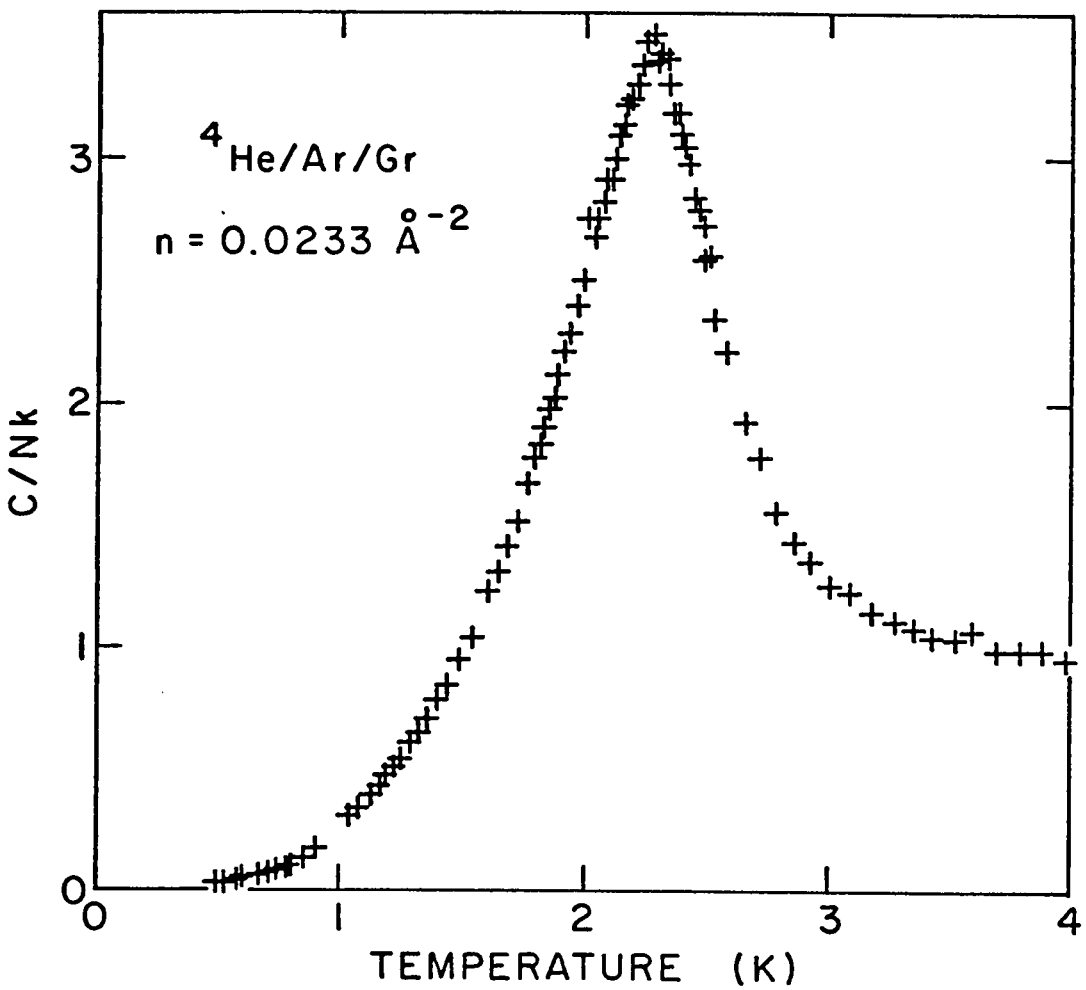

Figure 5.2 Specific heat of the ^{4}He/Ar/Gr film with areal density n=0.0233 Å^{-2}.

except for the highest two densities where the same melting line appears to be followed. This agreement may be coincidental and will be discussed in more detail in Chapter 6.

5.2 ^{3}He/Ar/Gr

Specific heat runs were also made for two ^{3}He coverages on Ar-plated Grafoil and the results are shown in Fig. 5.3. The lower density run ($n = 0.0233$ Å^{-2}) had the coverage value that had given the highest peak for ^{4}He. The other ($n = 0.0374$ Å^{-2}) had a substantially larger coverage, but one still in the range measured by Hickernell, McLean, and Vilches[61] on unplated Grafoil. Their results show that the heat capacity of ^{3}He on bare Grafoil for $T>0.5$ K and lower densities is like that of an interacting 2D Fermi gas. At lower temperature, a rounded anomaly at $T \simeq 0.2$ K shows the effect of strong ^{3}He-^{3}He interactions.

In the Ar-plated case, there is no evidence of the type of peaks seen for ^{4}He at temperatures in the range $1 \leq T \leq 4$ K. For $n = 0.0233$ Å^{-2} a peak was found at $T = 0.74$ K. This peak decreases in height and almost disappears for the higher coverage. This last coverage, the only Ar-plated run taken to 0.13 K also shows some evidence of the behavior observed by Hickernell, McLean, and Vilches[61] below 0.3 K.

5.3 ^{4}He/Ne/Gr and ^{3}He/Ne/Gr

The results of the specific heat measurements of ^{4}He adsorbed on Ne-plated Grafoil are remarkably different from either the bare Grafoil or the Ar-plated results. The low density ($n \leq 0.0702$ Å^{-2}) specific

Figure 5.3 Specific heat, ^{3}He/Ar/Gr

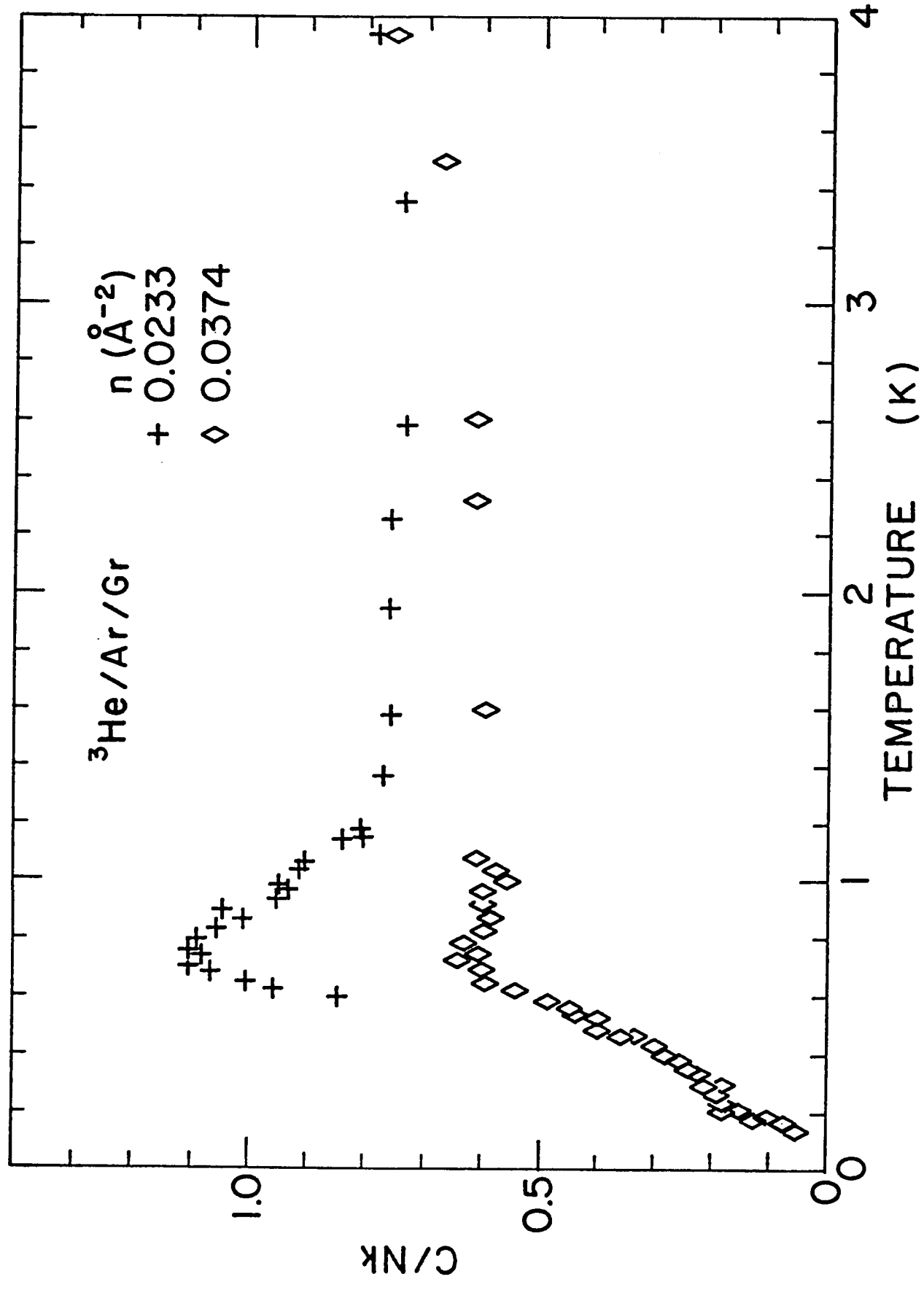
^{3}He/Ar/Gr
n (Å^{-2})
+ 0.0233
◇ 0.0374
C/Nk
1.0
0.5
0
0
1
2
3
4
TEMPERATURE (K)

heat curves corrected for desorption are shown in Fig. 5.4(a). A peak is observed at approximately T=0.75 K for the lowest coverage studied, n = 0.0140 Å^{-2}. As the film coverage increases, the peak decreases in height and broadens but remains at approximately the same temperature. The positions of the peaks in the density versus temperature plane are shown in Fig. 5.4(b) along with the unplated results which are shown with a dashed line. For the five lowest coverages each successive specific heat curve lies almost entirely below the preceding one. The run with density 0.0702 Å^{-2} departs from this trend at low temperatures as can be seen in Fig. 5.5, which is a plot of the specific heat at low temperatures. It was at the completion of this run that the cryostat warmed to 30 K because of an accident (see Sec. 3.3) and an estimated 10% of the neon preplating desorbed. The cell was cooled again, and the specific heat was found to have changed, and showed signs of a peak at approximately 0.90 K (Fig. 5.6). However, after the cryostat was warmed to room temperature, pumped out, and a new neon preplating prepared, new runs with areal densities n=0.0329 and 0.0702 Å^{-2} were found to reproduce the original results.

An interesting question is raised as a result of the accident: Despite the reproducibility of the results using the standard annealing procedure, is it possible that the procedure was inadequate for the film with areal density 0.0702 Å^{-2} and that warming the cell to 30 K would have been a better technique? This question is not answered by this study.

Figure 5.4 (a) Specific heat, ^{4}He/Ne/Gr. (b) Corresponding phase diagram.

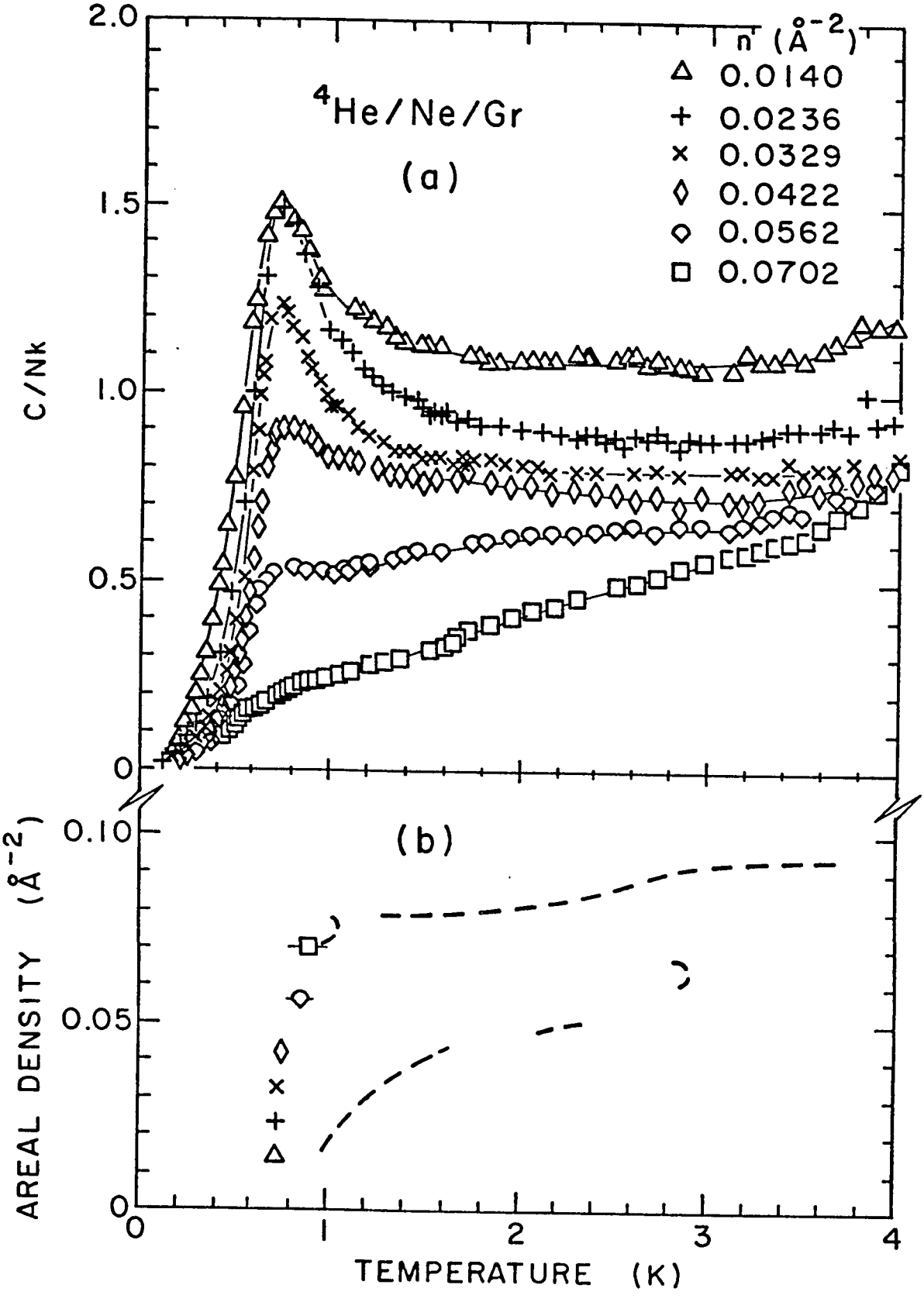
2.0
1.5
1.0
0.5
0
C/Nk
^{4}He/Ne/Gr
(a)
n (Å^{-2})
0.0140
0.0236
0.0329
0.0422
0.0562
0.0702
0.10
0.05
0
AREAL DENSITY (Å^{-2})
(b)
0
1
2
3
4
TEMPERATURE (K)

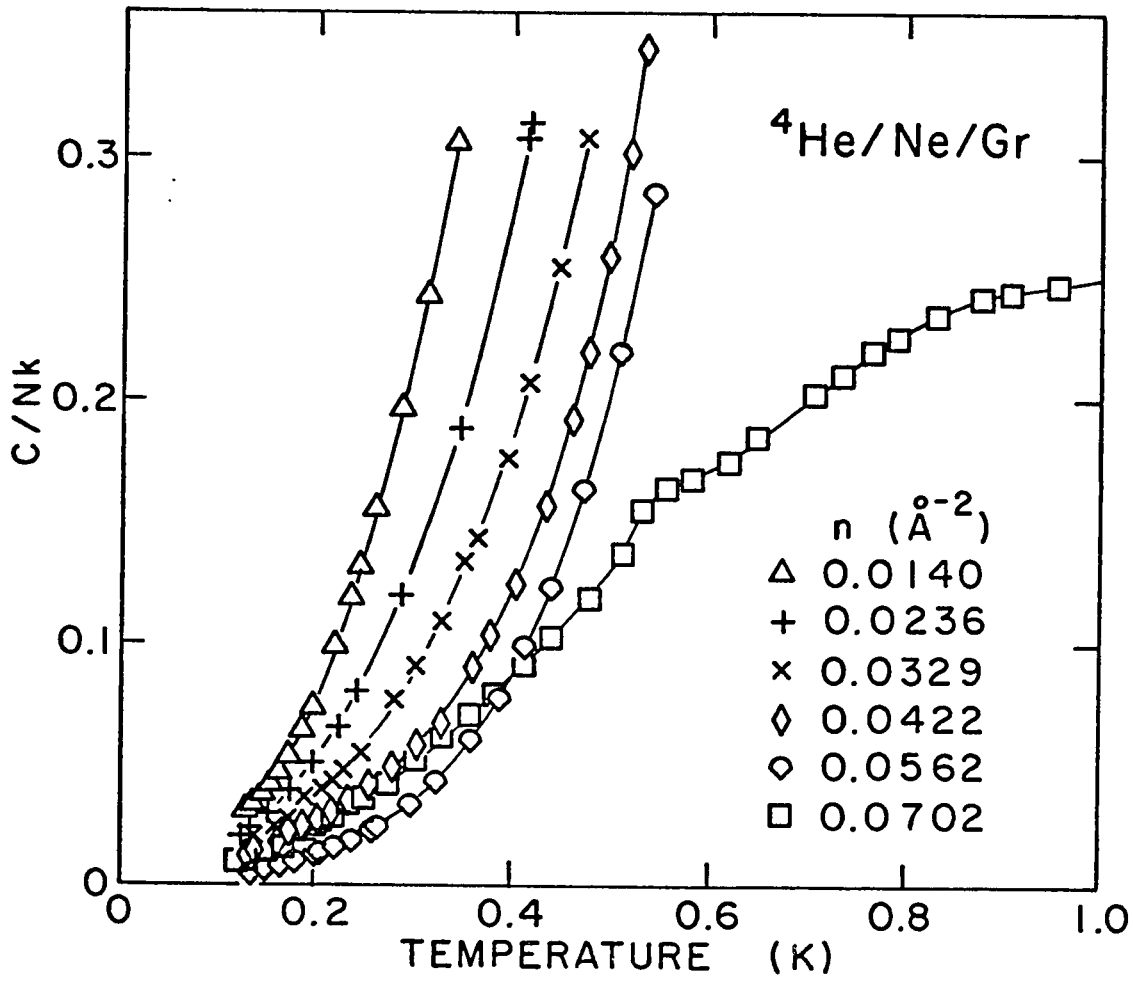

Figure 5.5 Low temperature specific heat, ^{4}He/Ne/Gr.

Figure 5.6 Low temperature specific heat of the ^{4}He/Ne/Gr run with areal density n=0.0702 $\mathring{A}^{-2}$.

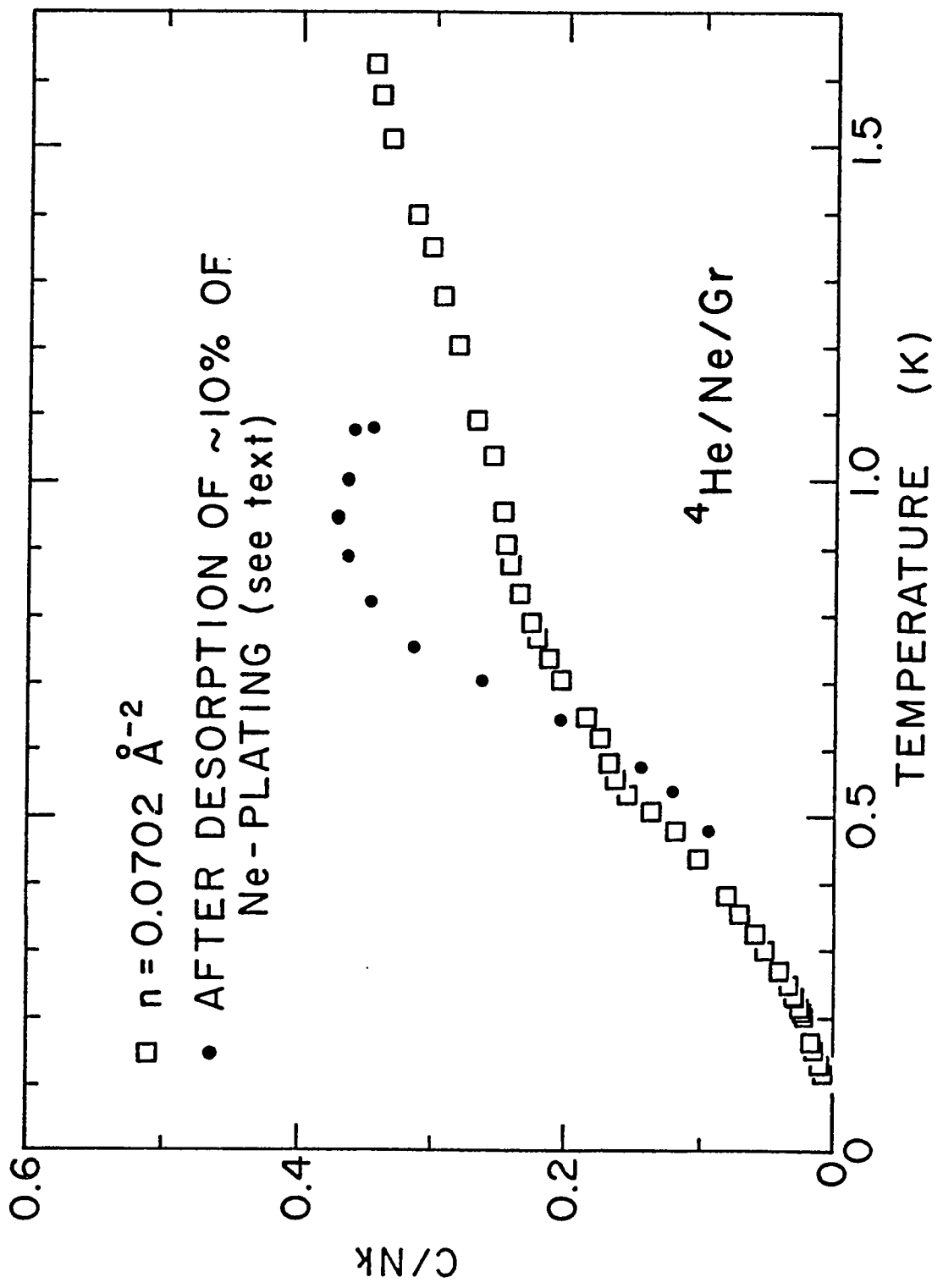
C/Nk
0.6
0.4
0.2
0
0
0.5
1.0
1.5
TEMPERATURE (K)
^{4}He/Ne/Gr
□ n=0.0702 Å^{-2}
• AFTER DESORPTION OF ~10% OF
Ne-PLATING (see text)

At still higher densities a series of specific heat runs was taken [Figs. 5.7(a), 5.8, and 5.9(a)]. The runs appear to show a melting line and a series of peaks similar to those reported by Hering, Van Sciver, and Vilches[21] for ^{3}He/Gr and ^{4}He/Gr. The estimated magnitude of the desorption contribution to the specific heat is indicated in Fig. 5.7(a). The data in this areal density and temperature range were taken using two separate neon platings, and it is possible that the area available for helium adsorption was somewhat different in the two cases. If this possibility is allowed and the "third neon preplating" data are shifted down in areal density by 3% as in Fig. 5.9(b) then the four runs now with highest areal density all fall on what appears to be a common melting line. Further, the relatively sharp peak seen at areal density n=0.0841 Å^{-2} then appears in the same density range as the other peaks seen at densities below the melting line. It is not clear why the "third neon preplating" runs did not reproduce this sharp peak, but two additional pieces of information should be pointed out. First, the specific heat of the sharp peak was remeasured at the end of the "second neon preplating" runs after the removal of the appropriate quantity of helium, and was found to be reproducible. This repeat run provided the opportunity to explore the peak region in detail. Secondly, a peak of similar shape and with a maximum at approximately the same temperature was found when a ^{3}He/Ne/Gr run was made at the same coverage. Figure 5.7(b) shows the specific heat for this run and Fig. 5.10 shows the only other ^{3}He/Ne/Gr run which was measured (n=0.0232 Å^{-2}).

Figure 5.7 High areal density specific heat

(a) ^{4}He/Ne/Gr, second neon plating

(b) ^{3}He/Ne/Gr, fourth neon plating

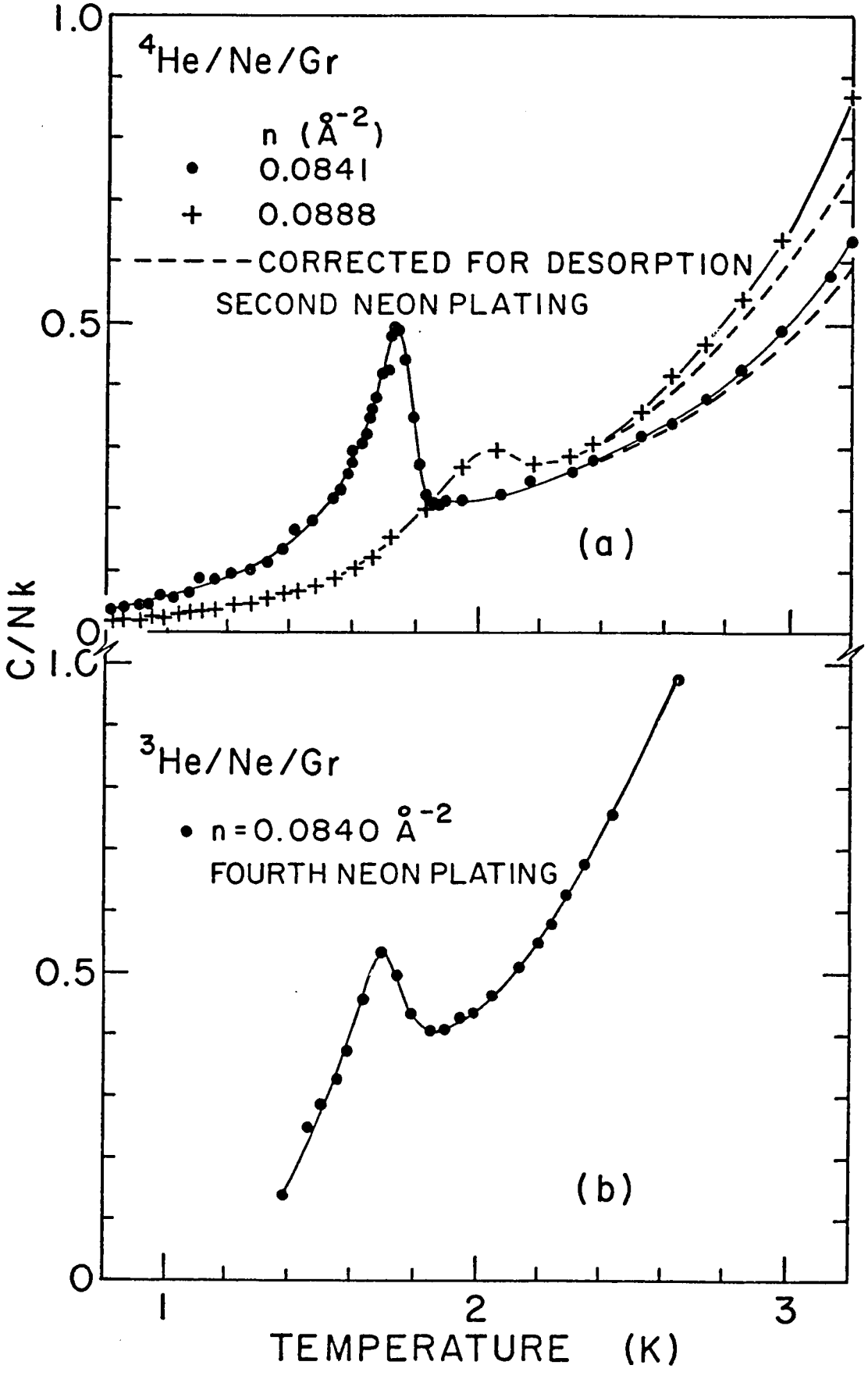
1.0
^{4}He/Ne/Gr
n (Å^{-2})
• 0.0841
+ 0.0888
CORRECTED FOR DESORPTION
SECOND NEON PLATING
0.5
0
(a)
C/Nk
1.0
^{3}He/Ne/Gr
• n=0.0840 Å^{-2}
FOURTH NEON PLATING
0.5
0
(b)
1
2
3
TEMPERATURE (K)

Figure 5.8 High areal density specific heat, ^{4}He/Ne/Gr

(a) and (b) Third neon plating.

(c) Third neon plating. The second neon plating run with areal density n=0.0888 $\mathring{A}^{-2}$ is shown for comparison.

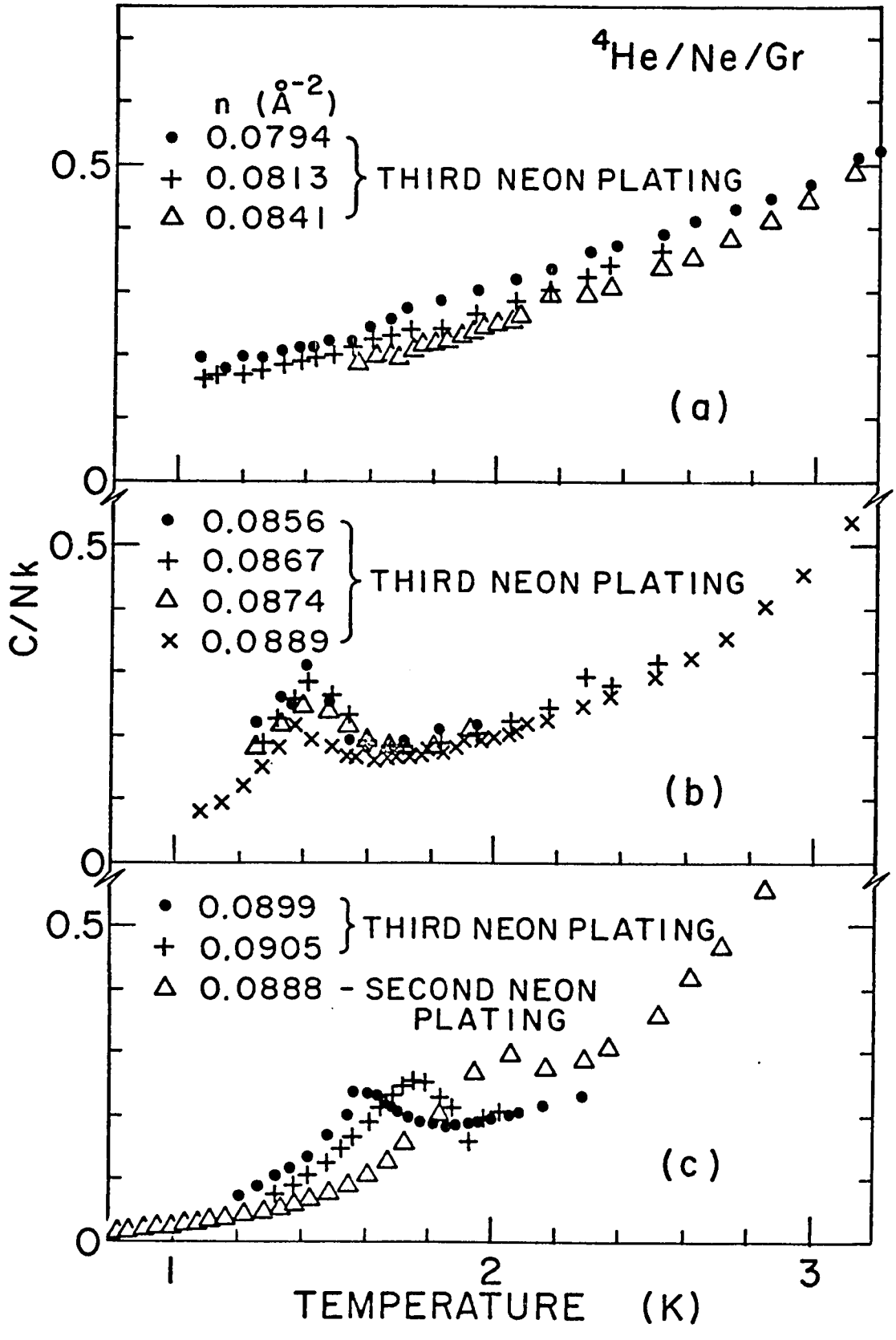
^{4}He/Ne/Gr
n (Å^{-2})
• 0.0794
+ 0.0813
△ 0.0841
THIRD NEON PLATING
(a)
• 0.0856
+ 0.0867
△ 0.0874
× 0.0889
THIRD NEON PLATING
(b)
• 0.0899
+ 0.0905
THIRD NEON PLATING
△ 0.0888 - SECOND NEON PLATING
(c)
C/Nk
0.5
0
1
2
3
TEMPERATURE (K)

Figure 5.9 High areal density phase diagram for ^{4}He/Ne/Gr

(a) Unshifted.

(b) After a 3% shift in areal density of the third neon plating results.

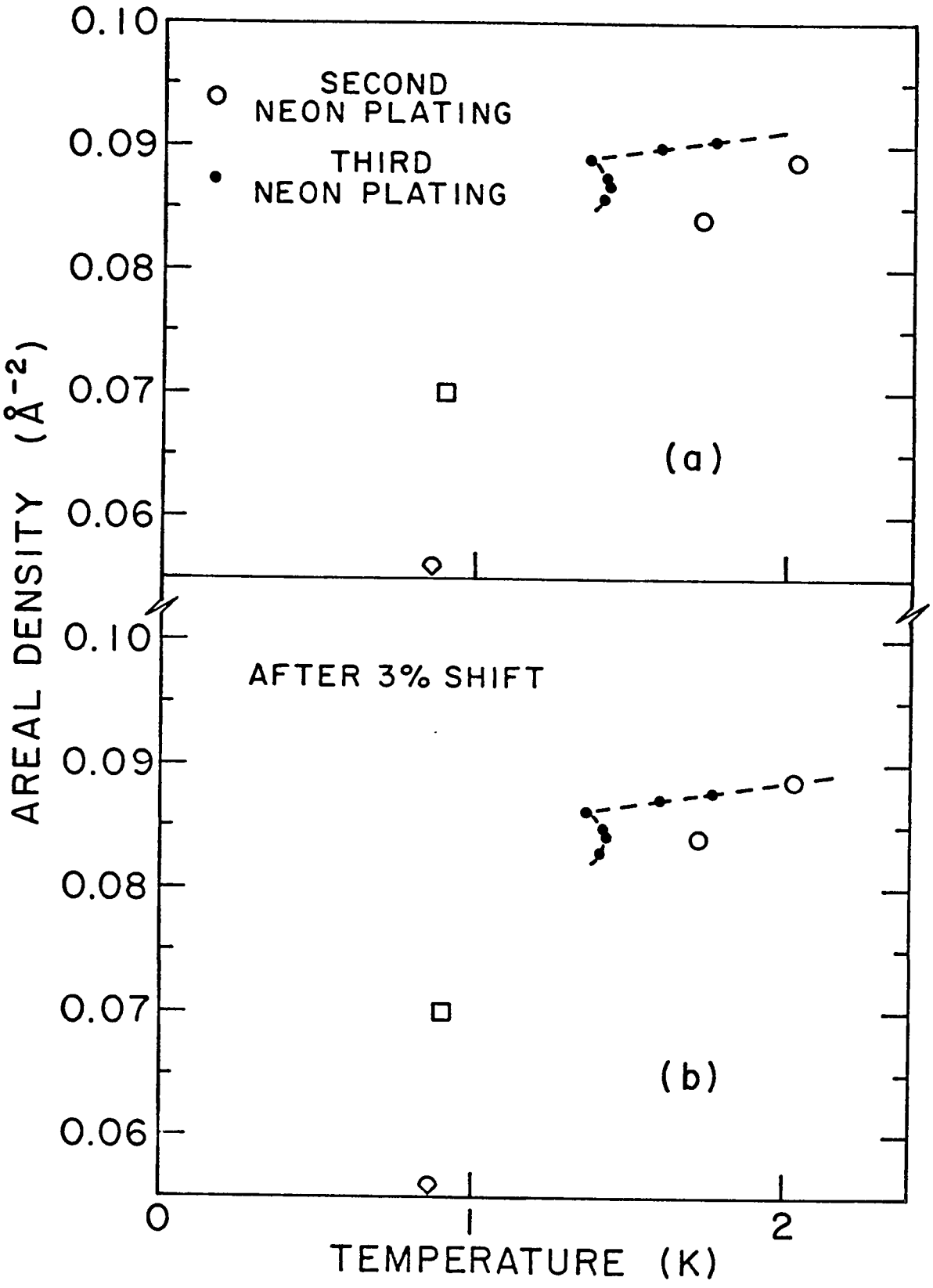
0.10
0.09
0.08
0.07
0.06
SECOND
NEON PLATING
THIRD
NEON PLATING
(a)
AFTER 3% SHIFT
(b)
AREAL DENSITY (Å⁻²)
0
1
2
TEMPERATURE (K)

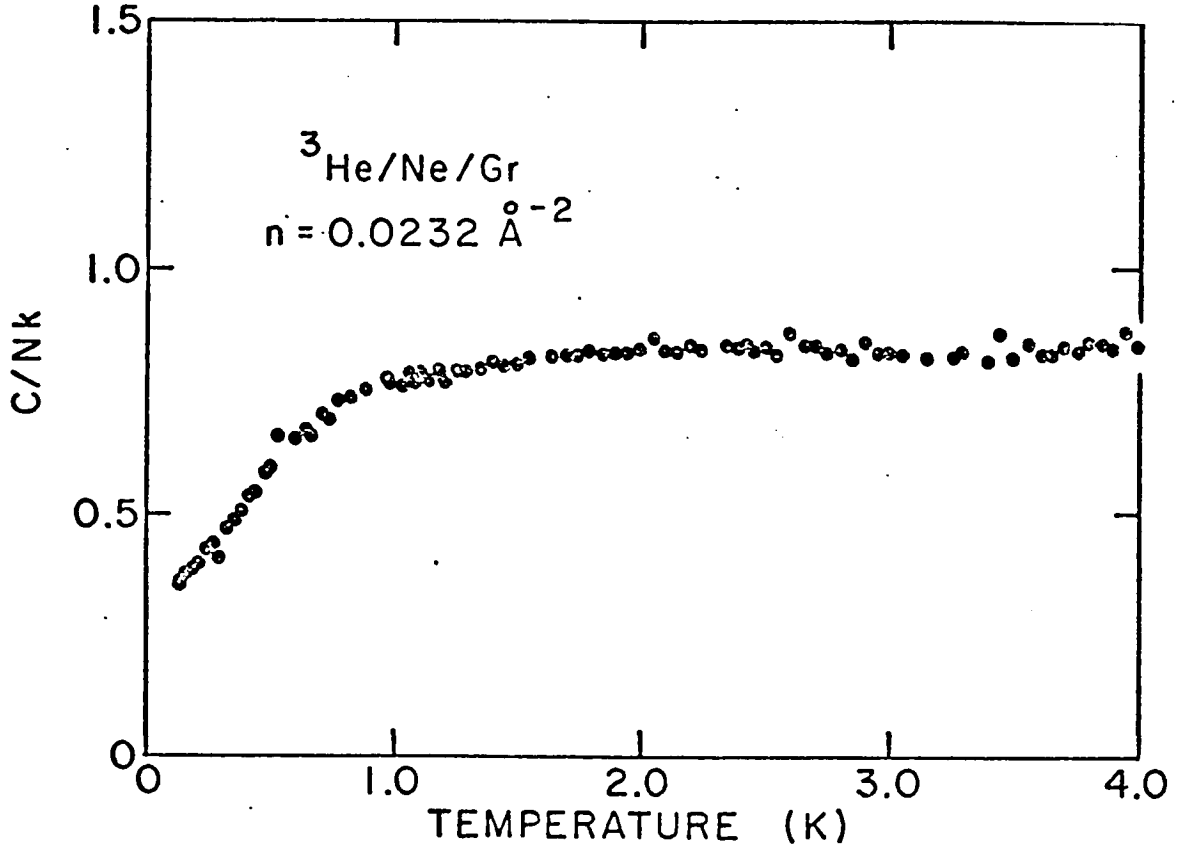

Figure 5.10 Specific heat, ^{3}He/Ne/Gr run with areal density $n=0.0232$ Å^{-2}.

5.4 Heat Capacity Isotherms and 4 K Entropies.

The low temperature ^{4}He/Ar/Gr and ^{4}He/Ne/Gr results are shown plotted as isotherms of the heat capacity versus areal density in Figs. 5.11 and 5.12. No points are shown on the 1.0 K ^{4}He/Ar/Gr isotherm for the three runs with areal densities between 0.02 and 0.04 Å^{-2} because for these runs data was taken only in the range $1.1<T<4.0$ K. The lines connecting the points are intended as a guide for the eye.

The entropies at 4.0 K calculated from smoothed heat capacity curves extrapolated to T=0 are shown in Fig. 5.13 along with the 4.0 K entropy of a 2D ideal gas of mass-4 particles.[62] The extrapolation assumes a power law temperature dependence of the specific heat for temperatures below the experimental range and accounts for less than 7% of the 4.0 K value of the ^{4}He/Ar/Gr entropies and less than 0.8% of the 4.0 K value of the ^{4}He/Ne/Gr entropies. The smooth curve drawn through the calculated entropy points for ^{4}He/Ar/Gr shows an inflection point at low density similar to that reported by Elgin and Goodstein in the case of ^{4}He/Gr.[20]

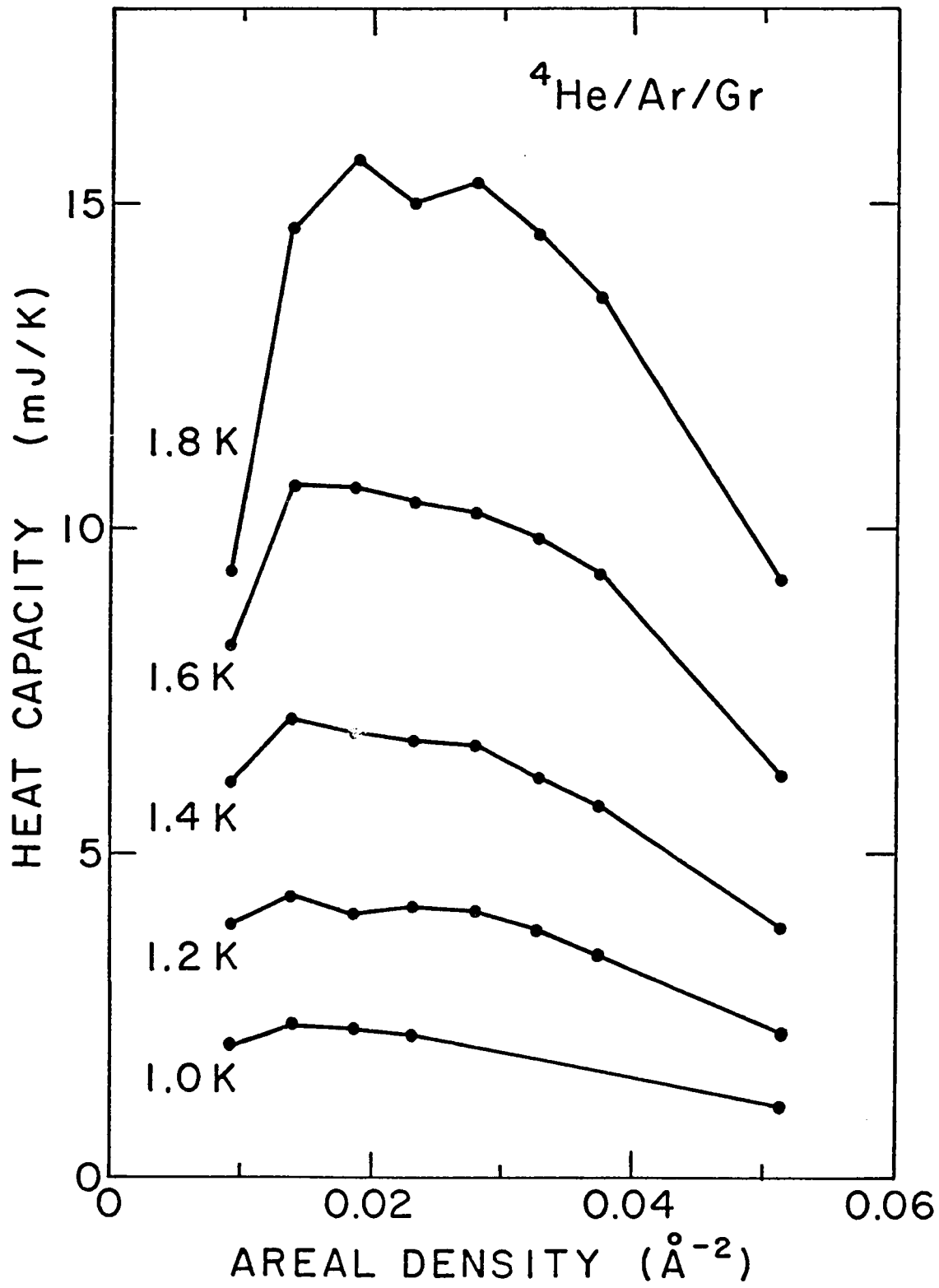

Figure 5.11 Heat capacity vs. areal density isotherms, ^{4}He/Ar/Gr.

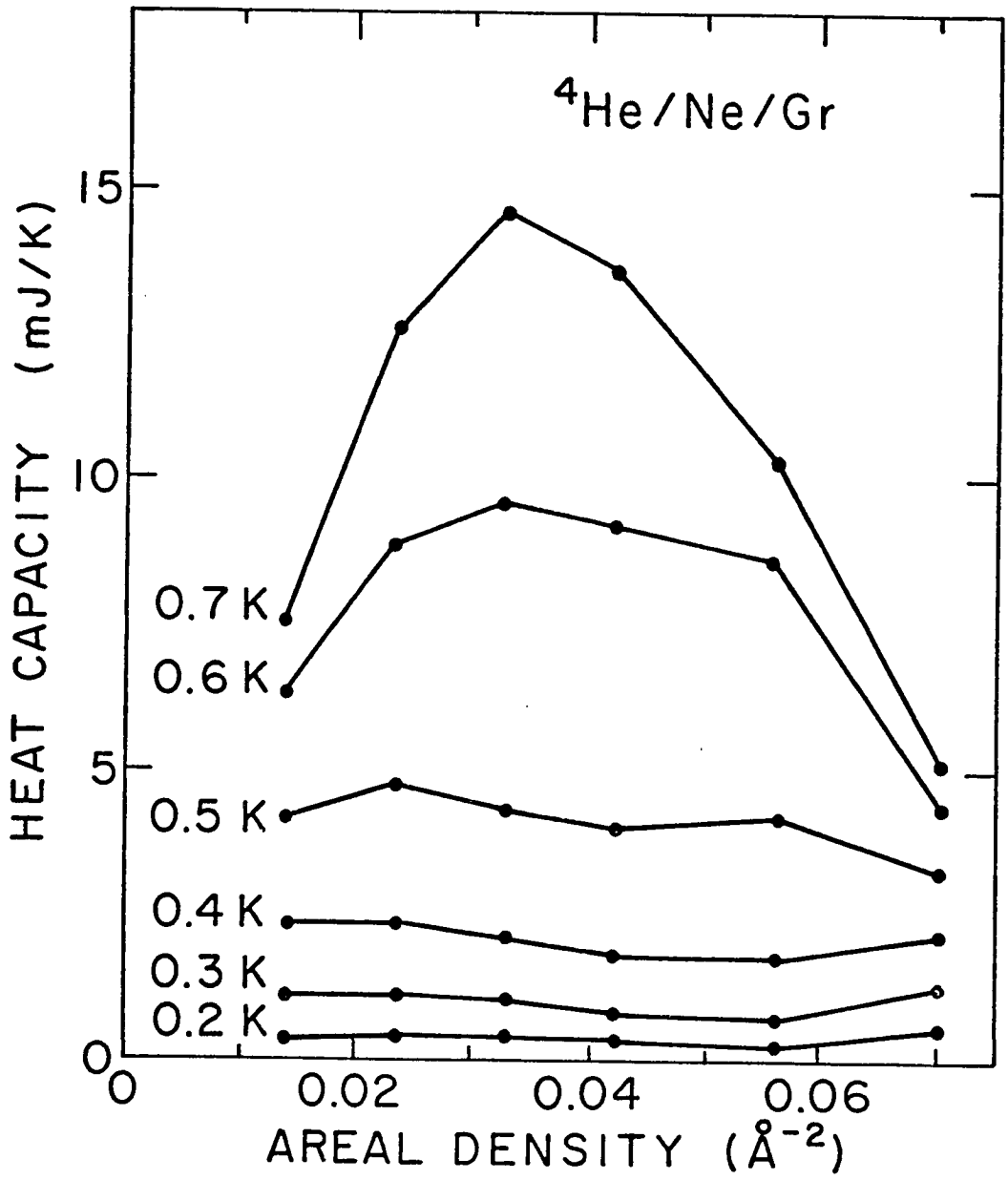

Figure 5.12 Heat capacity vs. areal density isotherms, ^{4}He/Ne/Gr.

Figure 5.13 Specific entropy vs. areal density isotherm at T=4.00 K, ^{4}He/Ar/Gr and ^{4}He/Ne/Gr.

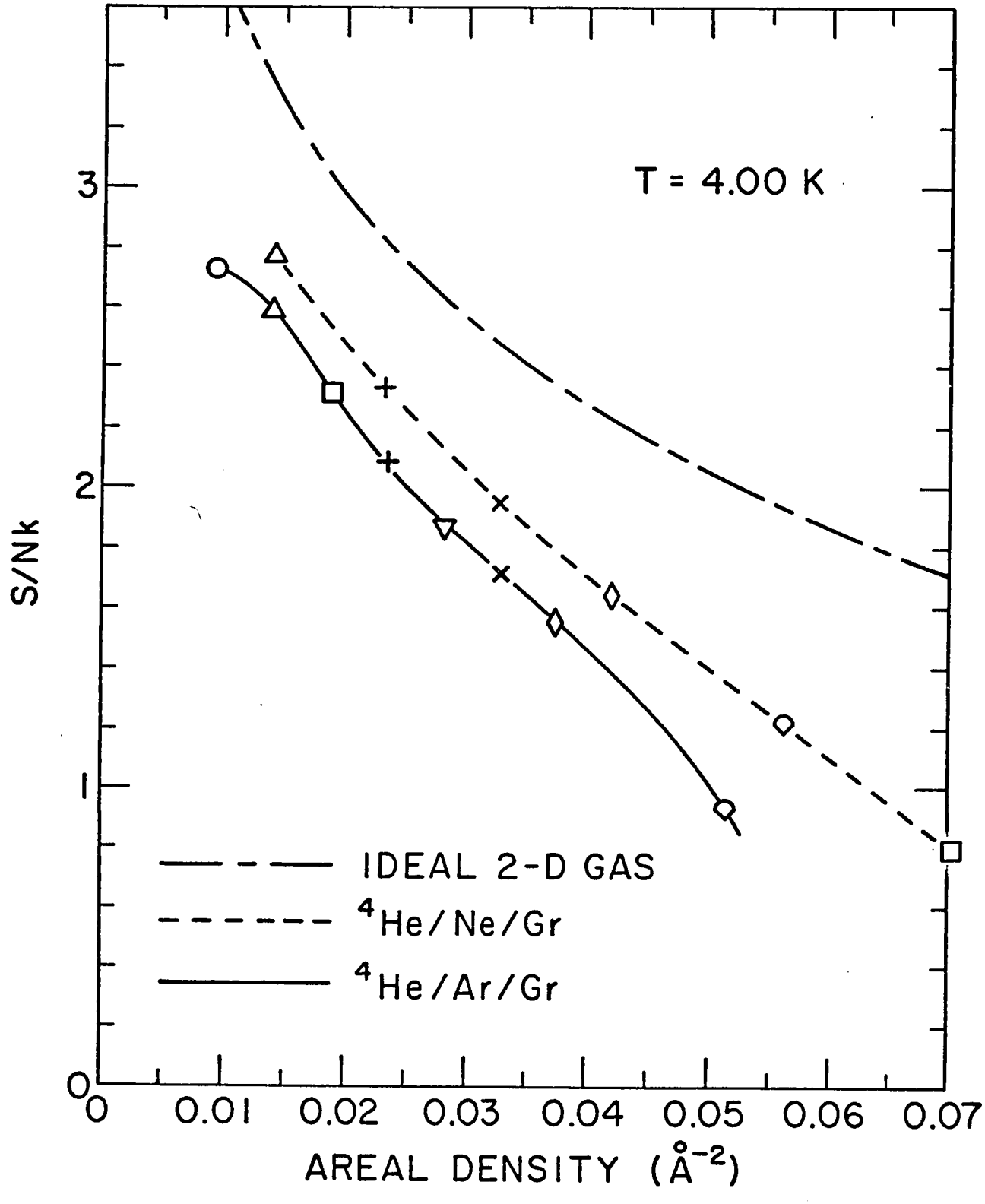
T = 4.00 K
S/Nk
AREAL DENSITY (Å^{-2})
IDEAL 2-D GAS
^{4}He/Ne/Gr
^{4}He/Ar/Gr
0
1
2
3
0.01
0.02
0.03
0.04
0.05
0.06
0.07

Chapter 6

INTERPRETATION AND DISCUSSION

6.1 Introduction

The data presented in the last chapter reveal both remarkable similarities and differences in the thermal properties of submonolayer helium films adsorbed on unplated, Ar-plated, and Ne-plated Grafoil. A series of heat capacity peaks which move to higher temperatures as the density is increased over a certain range is observed in each case. However, the temperatures at which the peaks occur and the details of the phase diagrams are all different.

This chapter will discuss the results and offer possible interpretations for the observed similarities and differences. Sections 6.2-6.5 deal mainly with the lower areal density runs with particular emphasis on the interpretation of the peaks as signaling two dimensional liquefaction. Later sections deal with the two platings separately and discuss other possible interpretations.

6.2 High Temperature, Low Density Region

The heat capacity signal of ^{4}He/Ar/Gr for $T>T_{peak}$ and $n\leq 0.0515$ A^{o-2} is markedly different from the signal of ^{4}He/Gr in the same range of areal density. Siddon and Schick[22] have shown that the trend of the ^{4}He/Gr and ^{3}He/Gr specific heats can be described by a virial expansion to the equation of state of a two dimensional gas on a structureless substrate. They calculated the quantum mechanical second virial coefficient B(T) and its first two derivatives and

determined the specific heat to first order in n:

$$C/Nk = 1 - n\beta^2 d^2B/d\beta^2 \qquad (6.1)$$

where $\beta=(kT)^{-1}$. When results are correctly described by Eq. 6.1 , the expression $[(C/Nk)-1]n^{-1}$ is a function of T alone. Fig. 6.1 is a plot of the three lowest density ^{4}He/Gr runs shown in Fig. 1.3 using the same cell as was employed in this study. The theoretically predicted increase in specific heat with decreasing temperature at about 2 K is seen for the two densities n=0.0279 and 0.0420 Å^{-2}. The agreement is not as good for the film with density n=0.0485 Å^{-2}, perhaps because of the importance of higher terms in the virial expansion, or perhaps because this density is close enough to the registered density (n=0.0637 Å^{-2}, see Table 1.2) that the periodic substrate structure is beginning to play a significant role. On the other hand, the specific heat at this density was not reproducible[2] and the discrepancy may be due to some as yet undetermined experimental problem.

There is better agreement between experiment and the virial calculation for ^{3}He/Gr[22], in which case the deviation of the specific heat is in the opposite sense, i.e., to lower values as T is decreased. This improved agreement may be coincidental or may be a reflection of the change in statistics. The important feature of the virial expansion theory is that it predicts the increase (decrease) in specific heat for ^{4}He/Gr (^{3}He/Gr) at approximately the correct

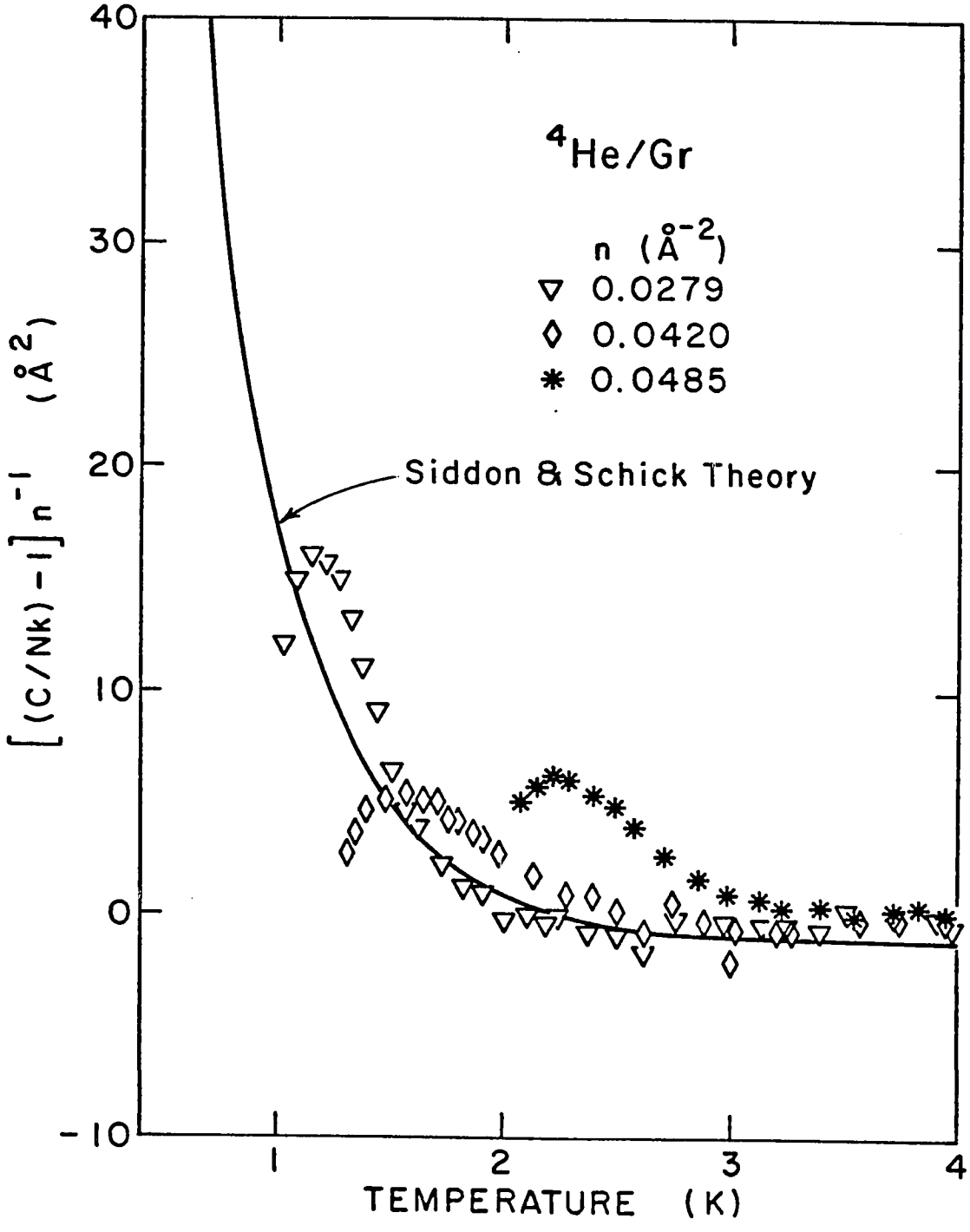

Figure 6.1 ^{4}He/Gr specific heat data from Refs. 2 and 29 compared to the theory of Siddon and Schick[22].

temperature.

The ^{4}He/Ar/Gr results for $n \leq 0.0515$ Å^{-2} are shown in Fig. 6.2 along with the calculation of Siddon and Schick for ^{4}He/Gr. The points for the four coverages in the density range $0.0233 \leq n \leq 0.0374$ Å^{-2} define a single curve from which the points for each run deviate after reaching their respective peaks as temperature is decreased. The value of the ordinate at which the 0.0233 Å^{-2} run turns over is approximately 108 Å^2. The three lowest density runs do not fall on the same curve, but rather have specific heats in excess of that expected if the single curve defined by the other runs were followed. The very low density specific heats for ^{4}He/Gr in the range $n \leq 0.010$ Å^{-2} show this same behavior.

It is likely that the low density specific heats for both the ^{4}He/Ar/Gr and the ^{4}He/Gr systems are influenced by the presence of inhomogeneities in the form of adsorption sites of stronger than average binding energy. The 4.0 K entropy of the lowest density ^{4}He/Ar/Gr film (Fig. 5.13) is lower than would be expected from a smooth extrapolation from the higher density 4.0 K entropy values. This trend is similar to that observed for ^{4}He/Gr films at low density (Fig. 7 of Ref. 20) and is attributed to substrate inhomogeneities. Simple models of adsorption in which it is assumed that a fixed number of the total number of atoms in the film are adsorbed on these preferential sites, each contributing a certain heat capacity independent of the film density, give dependences on n of the form

Figure 6.2 symbols: ^{4}He/Ar/Gr specific heat data

_____ : Siddon and Schick theory for two-dimensional helium.

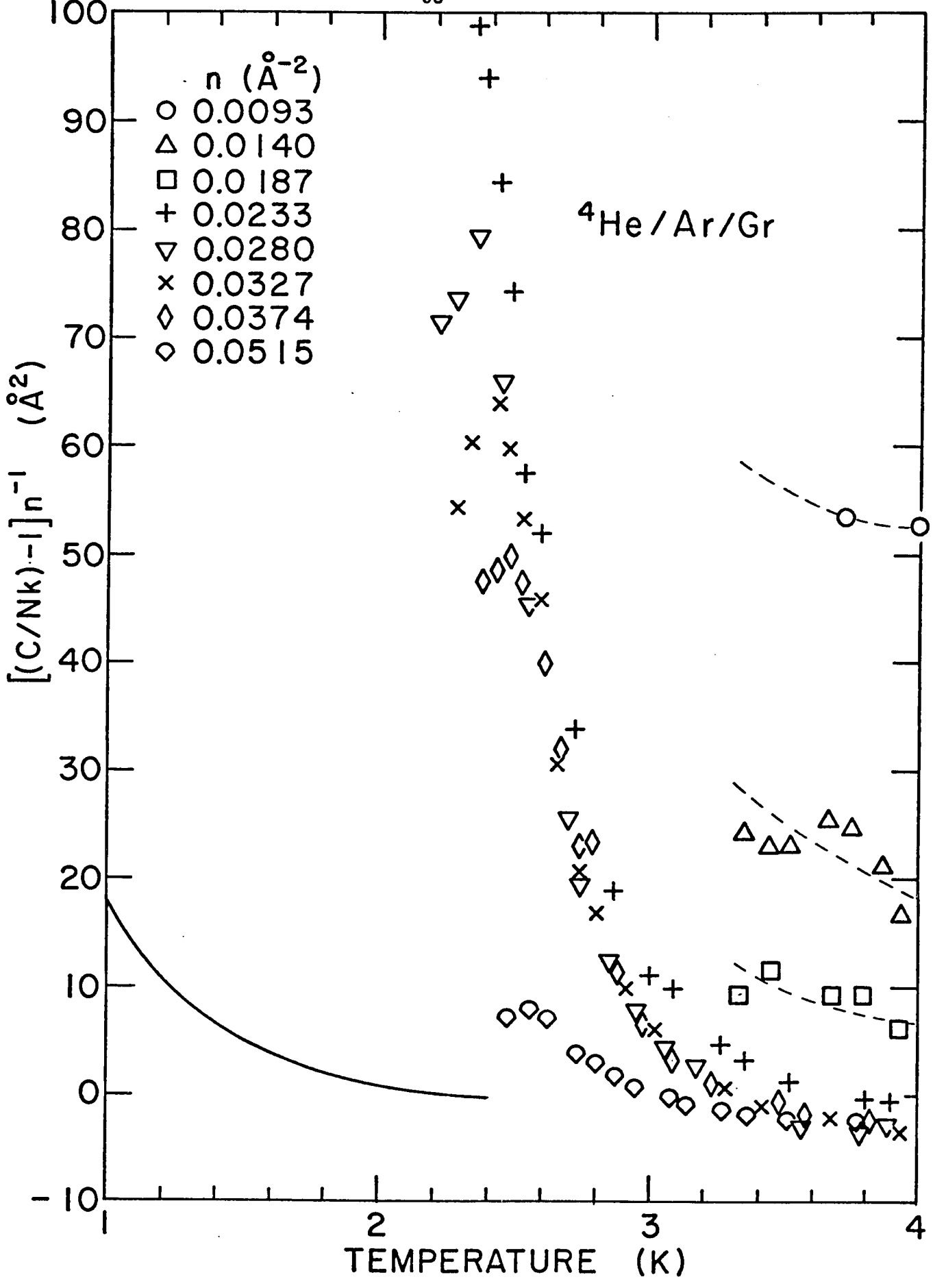
n (Å⁻²)
0.0093
0.0140
0.0187
0.0233
0.0280
0.0327
0.0374
0.0515
⁴He/Ar/Gr
[(C/Nk)-1]n⁻¹ (Å²)
TEMPERATURE (K)
100
90
80
70
60
50
40
30
20
10
0
-10
1
2
3
4

$C/Nk = \alpha(T)+\beta(T)n^{-1} + \gamma(T)n^{-2}$. Although one can attempt to fit the three low density tails of Fig. 6.2 by a suitable choice of the functions $\alpha(T)$, $\beta(T)$, and $\gamma(T)$, it is impossible for the dependence on n^{-1} or n^{-2} to abruptly halt in the density region where a single curve is followed. A more sophisticated model of the low density adsorption is needed.

The run at density $n=0.0515$ Å^{-2} deviates from the single curve at approximately 3.5 K, perhaps due to the importance of higher order virial terms. The two highest density runs have markedly different behavior and are not included in the figure.

The results of plotting the ^{4}He/Ne/Gr data in the same manner is shown in Fig. 6.3, again with the Siddon and Schick calculation for ^{4}He/Gr included for comparison. The figure demonstrates that the deviation of the specific heat from the classical value ($C/Nk = 1$) in the high temperature tail ($T>2$ K) and for densities $0.0233 \leq n \leq 0.0560$ Å^{-2} is nearly linear in areal density. This is in agreement with the virial expansion approximation. Deviations from the "single" curve occur for temperatures considerably above the peak temperatures, in contrast to the Ar-plated case.

Preplating the Grafoil substrate with a monolayer of Ar or Ne thus significantly alters the high temperature specific heat of the helium film. However, the data are qualitatively consistent with an interpretation in which the helium is nonetheless two dimensional, its high temperature specific heat being approximately unity and deviations being accounted for by a virial correction to the specific heat. The

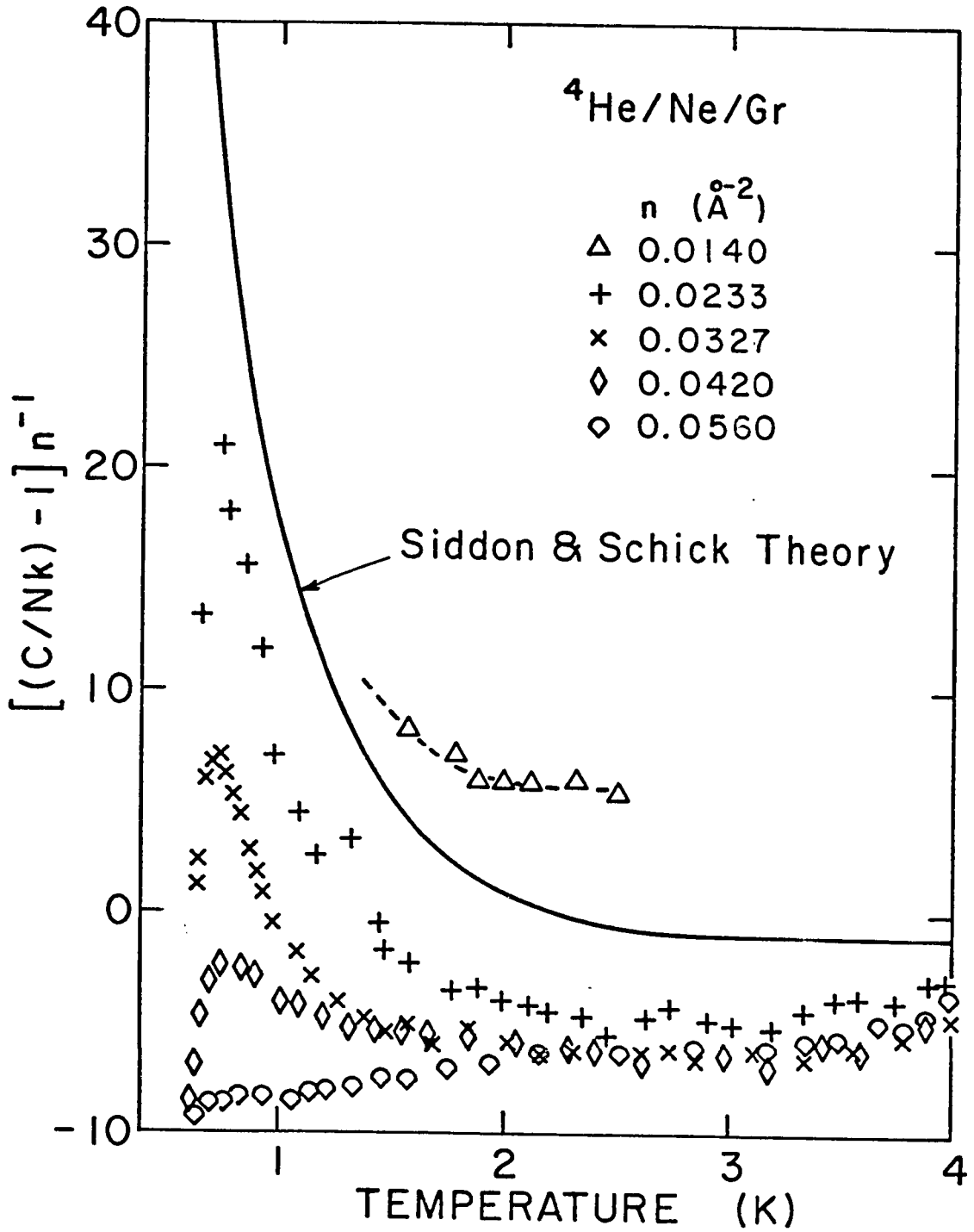

Figure 6.3 ^{4}He/Ne/Gr specific heat data and Siddon and Schick theory for two-dimensional helium.

effect of Ar-plating is to increase the temperature at which the specific heat shows a marked (>10%) increase over the classical high temperature value. Neon plating is seen to have the opposite effect.

6.3 Low Temperature Region

At temperatures below the peak in the ^{4}He/Gr data shown in Fig. the specific heat is monotonically increasing with temperature and decreasing with density. The same trend is followed by the Ar- and Ne-plated data for areal densities $n \leq 0.0515$ Å^{-2}.

Attempts to fit the data with exponential and localized oscillator functions were not successful. As a convenient way of demonstrating the differences in the low temperature behavior of ^{4}He on the three surfaces, log-log plots of C/Nk vs. T are shown in Figs. 6.4-6.6. Graphical fits to the plots at different temperatures show that the specific heat of individual runs cannot be described by a single power law except in the case of those ^{4}He/Ar/Gr runs for which the low temperature data extend over less than one-half of a decade in temperature. Excluding these runs, all curves show an increase with temperature of the value of the exponent r in the fitting curve $C/Nk=AT^r$. A few values of the exponent are shown in the figures. The ^{4}He/Gr run with $n=0.0279$ Å^{-2} can be fit over 0.8 decades with $r=2.2\pm0.2$. This is the largest temperature range with relatively constant r in all the data.

6.4 The Liquid Phase Argument, ^{4}He/Gr

Bulk ^{3}He and ^{4}He are the only known laboratory substances which do not solidify under their own vapor pressure as the temperature is

Figure 6.4 Log-log plot, ^{4}He/Gr specific heat data of Refs. 2 and 26 and three values of the exponent r in the fitting curve $C/Nk = AT^r$.

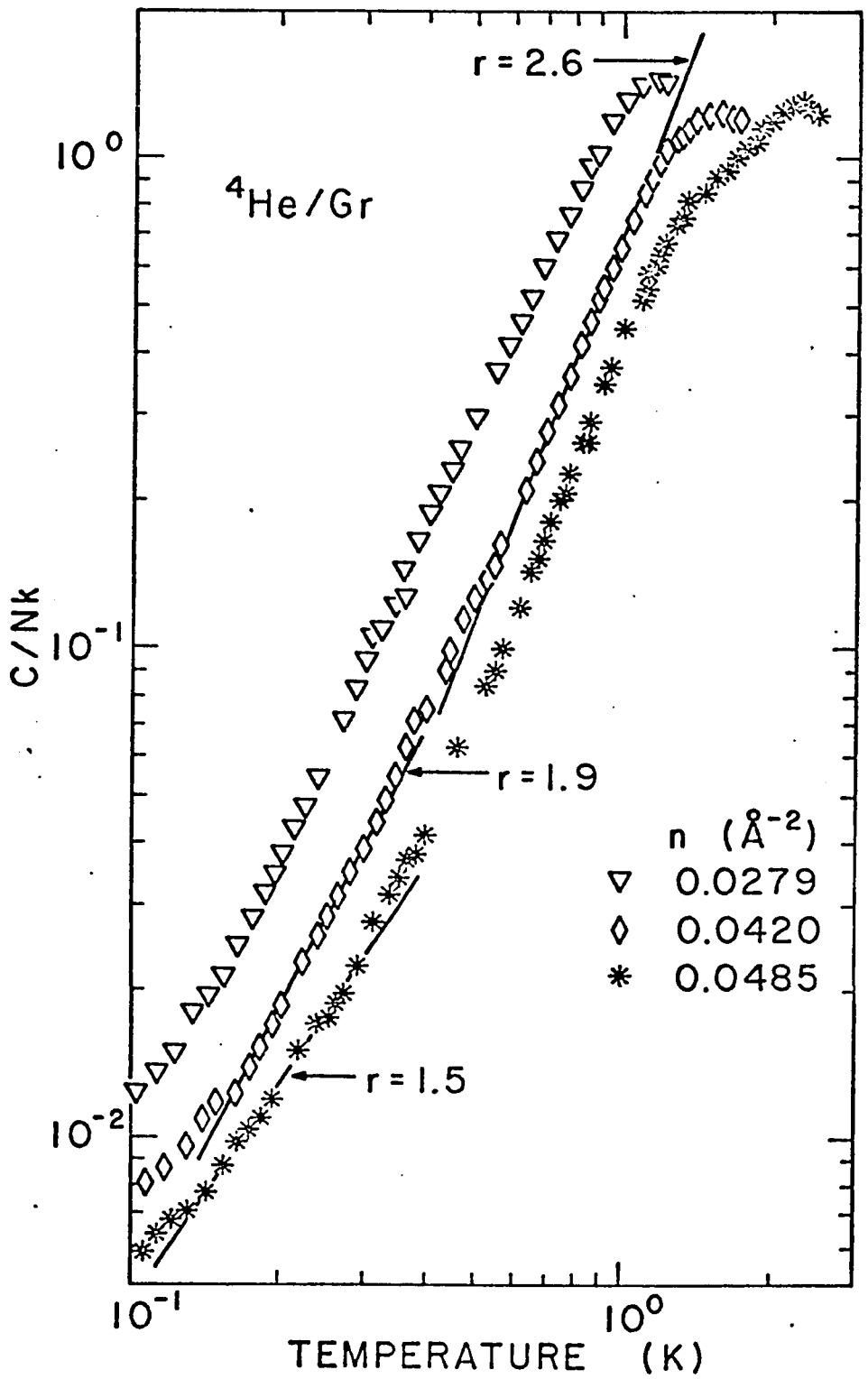
r = 2.6
10^0
^{4}He/Gr
C/Nk
10^{-1}
r = 1.9
n (Å^{-2})
0.0279
0.0420
0.0485
r = 1.5
10^{-2}
10^{-1}
10^0
TEMPERATURE (K)

Figure 6.5 Log-log plot, ^{4}He/Ar/Gr specific heat vs. temperature.

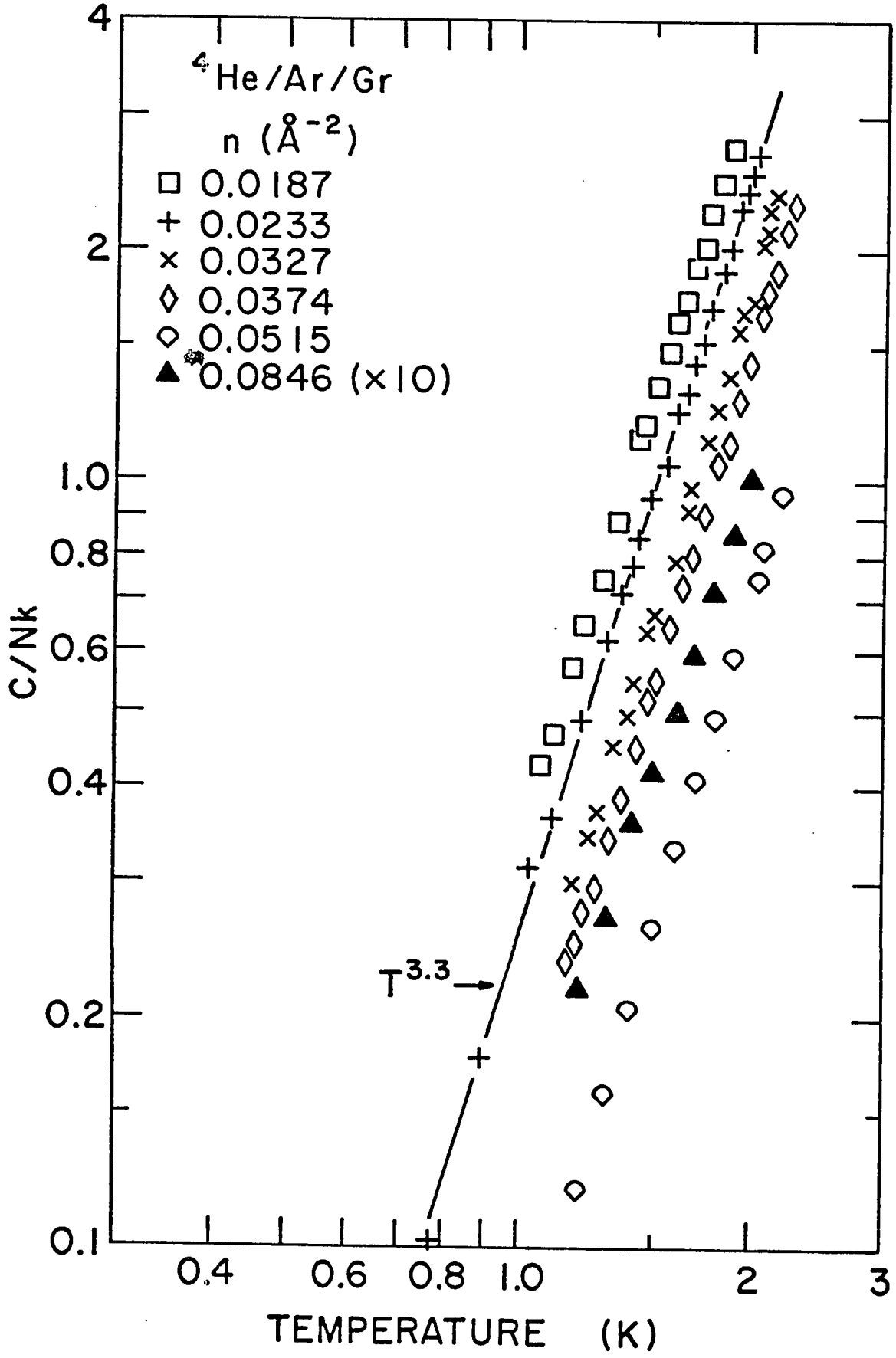
4
2
1.0
0.8
0.6
0.4
0.2
0.1
C/Nk
^{4}He/Ar/Gr
n (Å^{-2})
0.0187
0.0233
0.0327
0.0374
0.0515
0.0846 (×10)
$T^{3.3}$
0.4
0.6
0.8
1.0
2
3
TEMPERATURE (K)

Figure 6.6 Log-log plot, ^{4}He/Ne/Gr specific heat vs. temperature and four values of the exponent r in the fitting curve $C/Nk = AT^r$.

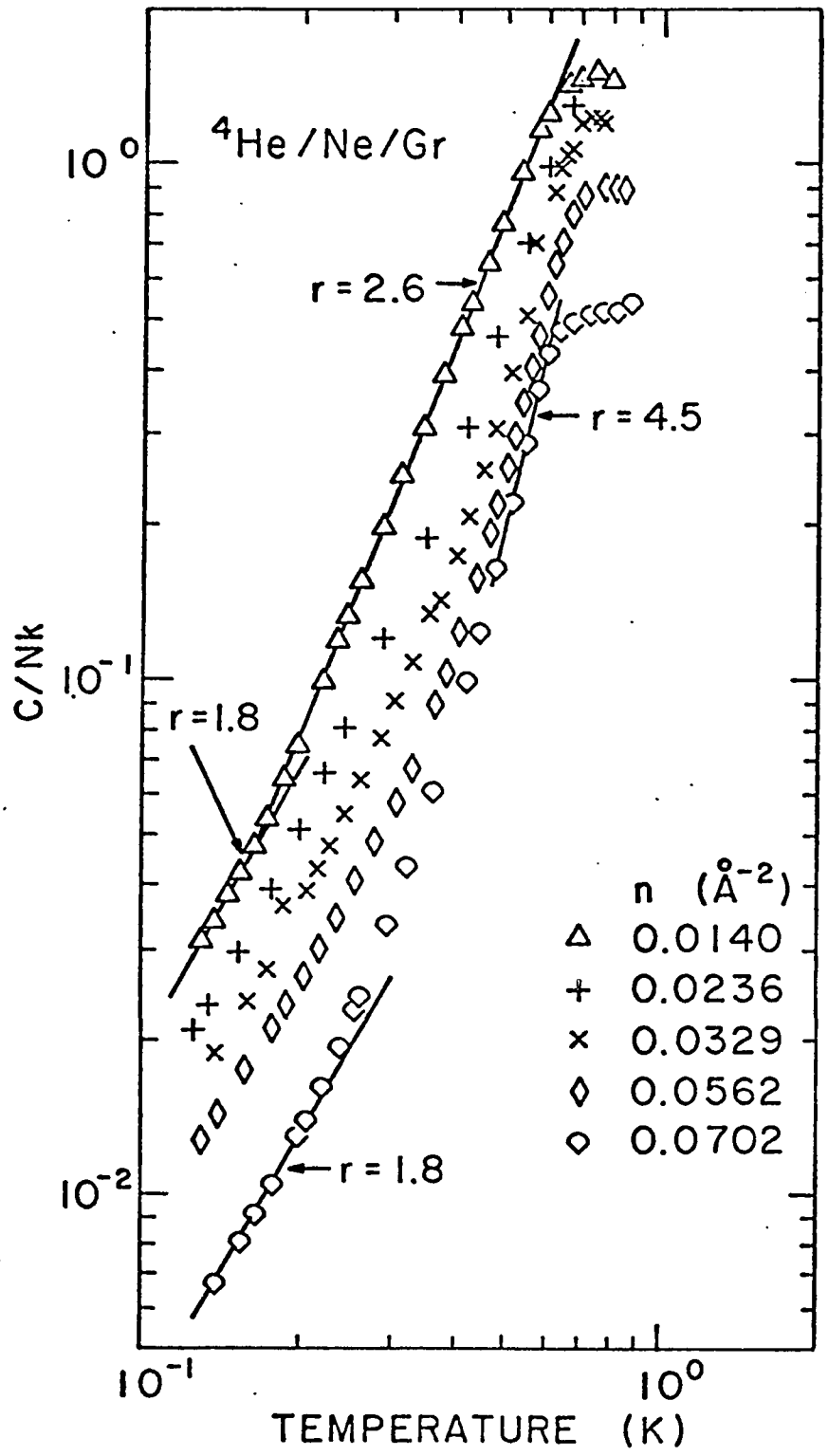
^{4}He/Ne/Gr
10^0
10^{-1}
10^{-2}
C/Nk
r = 2.6
r = 4.5
r = 1.8
r = 1.8
n (Å^{-2})
0.0140
0.0236
0.0329
0.0562
0.0702
10^{-1}
10^0
TEMPERATURE (K)

lowered toward absolute zero. The fact that their ground states are liquids is a result of their large zero-point kinetic energies and their relatively small interatomic attractive potential energy.[63]

Several authors have reported calculations which indicate that the situation is somewhat different in two dimensions.[31-34] The ground state of ^{4}He is predicted to be a liquid with an areal density of approximately n=0.036 $\text{A}^{\text{o}-2}$, whereas the ground state of ^{3}He is predicted to be a gas owing to its greater zero-point motion.[64] A realistic calculation must, however, take account of the periodic variation for the helium-substrate potential energy. If the periodic variation is strong enough, then it is expected that the low temperature phase will be one in which the helium is in registry with the substrate. Novaco[65] considered the competition between the liquid and superlattice phases for helium adsorbed on graphite and concluded that the ground state would be a liquid. However, he pointed out that the calculation was sensitive to any change in the He-He effective interaction such as that produced by He-substrate phonon interactions and that his conclusion that the ground state is liquid was only tentative.

Novaco and Campbell[34] calculated the equilibrium density and binding energy of the ^{4}He/Gr liquid and obtained the values 0.0365 $\text{A}^{\text{o}-2}$ and 0.62 K respectively. These values are in close agreement with calculations for the two dimensional ^{4}He liquid without periodic substrate variations.[31-34]

Assuming the ground state of ^{4}He/Gr is a liquid near density 0.04 $\text{A}^{\text{o}-2}$, a region of two phase coexistence terminating in a critical

point is expected, and the specific heat at constant areal density should abruptly drop as the coexistence region is crossed. The ^{4}He/Gr specific heat signals of Fig. 1.3 show a rounded peak in the specific heat in the range of density where liquefaction is expected. These peaks have been interpreted as the signature of liquefaction smeared somewhat by inhomogeneities.[2,30,66,67] Further support for the liquefaction interpretation and a discussion of unresolved difficulties follows.

Siddon and Schick[22] have demonstrated that the calculated second virial coefficient B(T) for ^{4}He in two dimensions can be fitted to the form of a van der Waals second virial coefficient

$$B(T) = b - a/kT \qquad (2)$$

to yield values of the critical temperature and density in the van der Waals theory. They obtained T_c=1.4 K and n_c=0.032 Å^{-2}*, approximately the temperature and density of the specific heat peaks shown in Fig. 1.3. Because the virial calculation deals with the effect of interactions and statistics as the system is cooled from high temperatures, the estimates of T_c and n_c are obtained in an essentially different manner from the ground state calculations and give additional support for the liquefaction interpretation.

Another piece of evidence supporting the liquefaction interpretation is provided by a calculation of the low temperature specific heat of

---

*In Ref. 22 the value of n_c was misprinted as 0.034 Å^{-2}.

two-dimensional ^{4}He carried out by Miller and Woo.[68] They found that the major contribution to the specific heat of two-dimensional ^{4}He is from longitudinal surface phonons, and reported preliminary numerical calculations which gave a linear dispersion relationship at low frequency. Treating the phonons as elementary excitations obeying Bose statistics the specific heat contribution is

$$\frac{C}{Nk} = \frac{1}{2\pi nkT^2} \int_0^\infty \varepsilon_\nu e^{\varepsilon_\nu/kT} (e^{\varepsilon_\nu/kT} - 1)^{-2} \nu d\nu \qquad (3)$$

where ε_ν is the energy of an excitation of wave vector ν. With linear dispersion this equation leads to a specific heat proportional to T^2/n.

The expected range of validity of this temperature and density dependence depends upon the range of validity of the linear dispersion approximation. This can be obtained from Miller and Woo[68] as being $0 \leq \varepsilon_\nu \tilde{<} 4$ K. Thus, within the assumptions of the approximation, one could expect T^2/n behavior for $T \tilde{<} 0.4$ K. Approximately quadratic temperature dependence is observed in this temperature range and in the vicinity of $n = 0.036$ Å^{-2} for ^{4}He/Gr (See Sec. 6.3). Furthurmore, the magnitude of the measured specific heat agrees reasonably well with the theoretical calculations.* However, it should be noted that the theoretically predicted proportionality to n^{-1} is not observed experimentally.

---

*Miller[69] mentions a factor of 4 error in the calculation of the specific heats and this has been taken into account.

There are three main difficulties with the interpretation that the peaks in the ^{4}He/Gr data signal liquefaction. The first is that the data do not show a discontinuity in the specific heat as would be expected when crossing a liquid-gas coexistence boundary. Dash[67] has argued that substrate inhomogeneities will produce variations in the local density of the two dimensional gas phase and that regions of different density will phase condense at different temperatures, thus producing a rounded specific heat peak. If n(T) describes the boundary of the coexistence region, then a small spread in density Δn will produce a spread in condensation temperature $\Delta T \approx (dn/dT)^{-1}\Delta n$. In addition, Novaco[30] has studied the effect of a distribution of adsorption energies on the shape of a model liquefaction peak and has reported similar rounding effects. While these mechanisms for rounding are plausible and more detailed models may lead to an understanding of the lack of a sharp drop in the specific heat, they do not explain the apparent absence of a critical point. This is the second main difficulty with the liquefaction interpretation.

The third difficulty has to do with a discrepancy between experimental results and theoretical predictions of the specific heat of adsorbed ^{3}He - ^{4}He mixtures. Miller[69] argues that if at low densities the ground state of ^{4}He/Gr is a liquid and the ground state of ^{3}He/Gr is a gas, then there should be a phase separation peak in the specific heat of ^{3}He - ^{4}He mixtures even for large ^{3}He concentrations. The heat capacity data of Hickernell, McLean, and Vilches[70] show no evidence of a peak for ^{3}He concentrations greater than 0.5.

These problems and the tentative nature of Novaco's determination that the ground state is a liquid thus preclude any unambiguous identification of the specific heat peaks as signaling evaporation from a liquid.

6.5 The Liquid Phase Argument, ^{4}He/Ar/Gr and ^{4}He/Ne/Gr

The similarity between the series of specific heat peaks of ^{4}He/Gr, ^{4}He/Ar/Gr, and ^{4}He/Ne/Gr for densities $n \lesssim 0.05$ Å^{-2} is strong evidence that they all signal the same effect modified in each case by the nature of the substrate. Further, because the peaks in the case of ^{4}He/Gr may signal liquefaction, it is important to consider whether the ^{4}He/Ar/Gr and ^{4}He/Ne/Gr results can also be understood as liquefaction peaks, and if so, to try to understand why the liquefaction temperature and the phase boundary are so strongly substrate dependent.

As was discussed in Chapter 1, plating Grafoil with a layer of Ar or Ne significantly increases the periodic component of the helium-substrate potential energy (Table 1.1). This has the effect of increasing the probability of finding a helium atom directly above a lattice site and of increasing the overall variation in probability at various locations on the unit cell. Perspective plots of the variations in the probability function for an isolated ^{4}He atom adsorbed on unplated graphite and on Ar-plated surface at T=0 have been published by Novaco and Milford and are shown in Fig. 6.7. The strong effect of Ar-plating is clearly evident.

The binding energy of a single helium atom on the Ar-plated surface is such that, if the system is treated classically, the atom is not

Figure 6.7 Comparison of perspective plots of the probability function $\psi^*(x,y)\psi(x,y)$ for a single ^{4}He atom adsorbed on unplated graphite and on argon-plated copper.

(a) Over a unit cell of the graphite lattice the probability function remains sizeable even directly above the substrate carbon atoms. From Hagen, Novaco, and Milford, Ref. 37.

(b) Calculation for ^{4}He adsorbed on argon plated copper which should be qualitatively the same as ^{4}He/Ar/Gr[39]. The probability function shows strong variations over the unit cell. There are two adsorption sites per unit cell. From Milford and Novaco, Ref. 71.

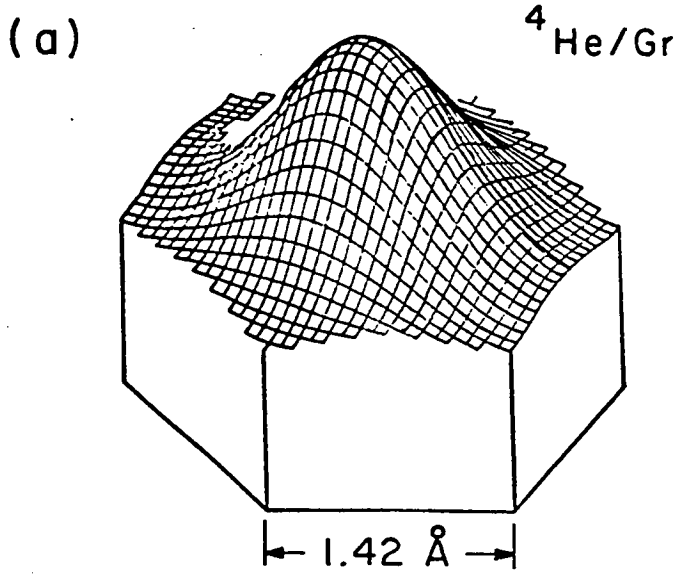
(a)
^{4}He/Gr
1.42 Å

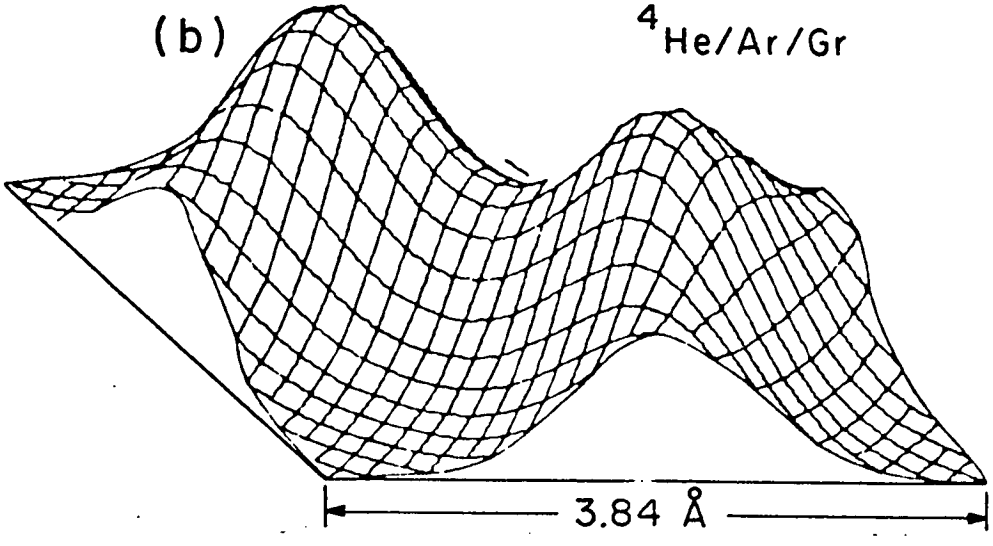
(b)
^{4}He/Ar/Gr
3.84 Å

restricted from free translation on energetic grounds (cf. Fig. 1.6). There would, of course, be classical scattering of the atom which would lead to a non-uniform probability function. In the temperature range of interest, ^{4}He has a thermal deBroglie wavelength $\lambda > 4$ Å and therefore quantum mechanical effects are important. In particular, the helium diffracts from the non-uniform potential and this diffraction leads to the probability functions of Fig. 6.7 and to single particle bands which differ from those of a free particle.[37,39,40,71]

The strong variation of the probability function along the surface can be viewed as a form of localization. But it is important to keep in mind that the theoretical calculations of binding energies imply that the helium is nonetheless highly mobile along the surface. The experimentally observed virial gas behavior is qualitatively consistent with this picture.

At non-vanishingly small areal densities, correlations between helium atoms will change the probability picture of Fig. 6.7. On unplated graphite the helium is predicted to condense into a liquid with density $n = 0.036$ Å^{-2}. (This density does not correspond to any simple superlattice structure.) It is expected that the increased localization of the helium on a plated surface will tend to decrease the zero-point repulsion of two neighboring atoms and allow them to take greater advantage of their mutual atraction.[5,72,73] Although the interatomic potential remains the same, the zero-point repulsion is reduced. A similar effect would be produced by increasing the mass of the helium.

It is interesting to consider whether the shift in the temperature of the specific heat peak observed for ^{4}He adsorbed on the plated

surfaces can be understood as an effective mass phenomenon. One approach to this question is offered by looking at the two dimensional critical point temperatures for different adsorbed atoms and using these to determine the importance of mass on critical point temperature. For bulk atoms with Lennard-Jones interactions the classical law of corresponding states predicts that the critical temperature is proportional to the value of the minimum of the Lennard-Jones potential.(74) Agreement with experiment is within 10% for the heavier gas species (Xe, Kr, Ar, O_2, and N_2)*, but less massive atomic species deviate from the classical value owing to the quantum mechanical effects of diffraction and statistics.(75) Processes involving diffraction become important when the thermal deBroglie wavelength $\lambda = h/(2\pi mkT)^{\frac{1}{2}}$ becomes comparable to the size of the atom, whereas statistics become important when λ is comparable to the interatomic spacing. The quantum mechanical law of corresponding states includes an additional dimensionless parameter $\Lambda^* = h/\sigma(m\epsilon)^{\frac{1}{2}}$ where σ and ϵ are the parameters of the Lennard-Jones potential. The theory predicts that kT_c/ϵ should be a function only of Λ^* for all atomic species with interaction potentials of the Lennard-Jones form and with the same statistics.(76) Fig. 6.8(a) shows such a plot for several noble gas species and demonstrates the dependence on the quantum parameter Λ^*. The diatomic molecules oxygen, nitrogen, and para-hydrogen are also included and follow roughly the

---

*For these atomic species and for Ne, H_2, ^4He, and ^3He in the discussion which follows, the Lennard-Jones parameters used are those given in Ref. 55. The critical temperatures of bulk Xe, Kr, and Ar are taken from Ref. 77; those of O_2 and N_2 are taken from Ref. 78.

Figure 6.8 (a) Law of corresponding states plot for several bulk atomic species showing dependence of the reduced critical temperature kT_c/ϵ on the quantum parameter Λ^*. Λ^*_{CF} is the maximum value of Λ^* for which a system of fermions will have a liquid ground state as determined in Ref. 73.

(b) Two dimensional law of corresponding states using the bulk Lennard-Jones parameters σ and ϵ. The boson branch is drawn through the ^{4}He point and through Λ^*_{CB}, the value of Λ^* which separates liquid and gas ground states. One possible fermion branch is also shown. The critical temperatures T_c are determined either from vapor pressure (VP) or heat capacity (HC) measurements, as follows:

Atom	T_c(K)	Method	Ref.
Xe	117	VP	77
Kr	97	VP	77
Ar	65	VP	77
N_2	48	HC	89
Ne	16.5	HC	54
p-H_2	11.5	HC	90
^{4}He	1.2	HC	2

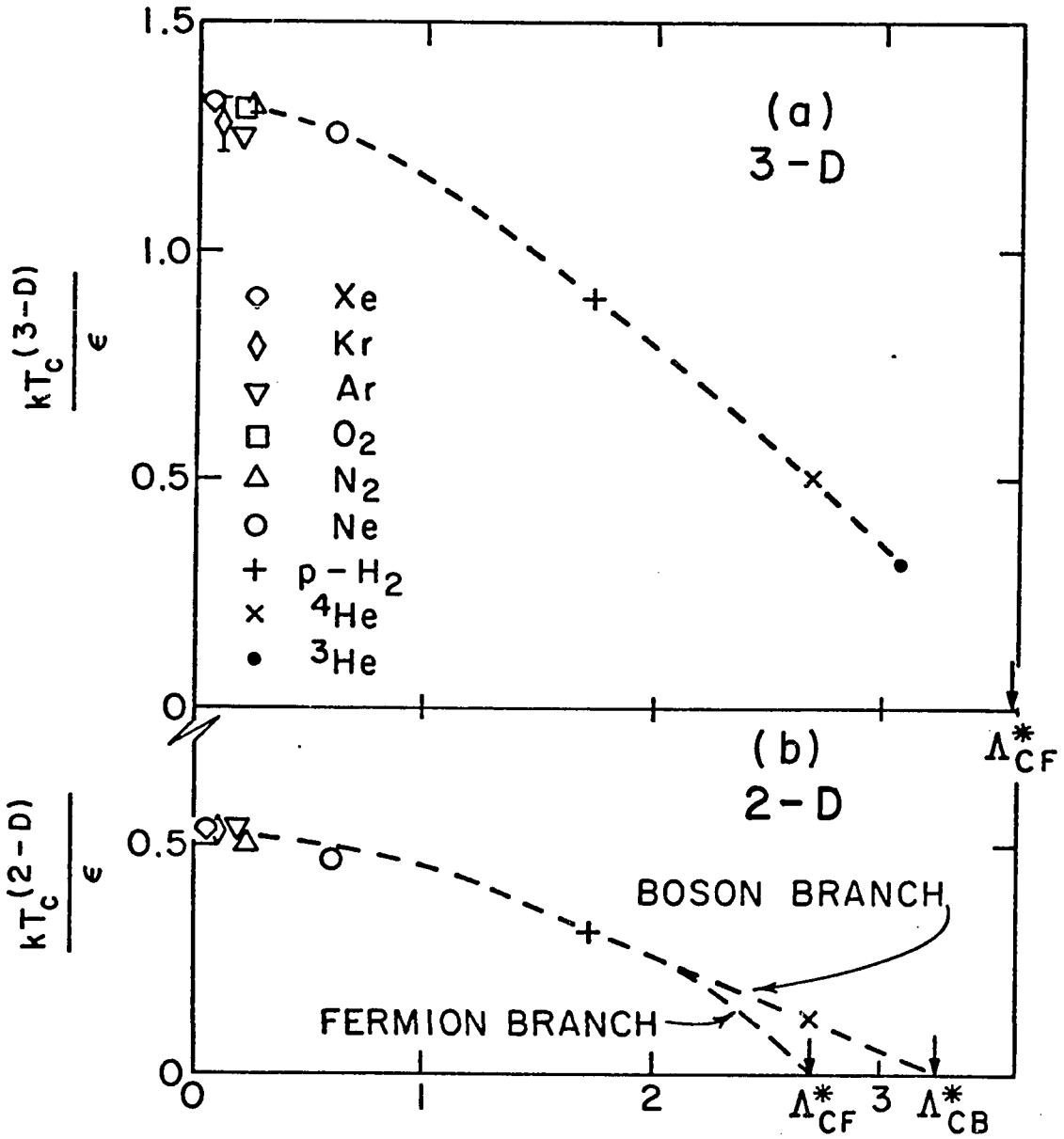
1.5
1.0
0.5
0
(a)
3-D
$kT_c^{(3-D)}/\epsilon$
Xe
Kr
Ar
O_2
N_2
Ne
$p-H_2$
^4He
^3He
Λ^*_{CF}
(b)
2-D
$kT_c^{(2-D)}/\epsilon$
0.5
BOSON BRANCH
FERMION BRANCH
0
0
1
2
Λ^*_{CF}
3
Λ^*_{CB}
QUANTUM PARAMETER $\Lambda^* = \frac{h}{\sigma\sqrt{m\epsilon}}$

same trend. The dotted line is just a guide for the eye. Miller, Nosanow, and Parish[79] have calculated the largest values of the quantum parameter for which bosons and fermions are expected to liquefy. These values are $\Lambda^*_{CB} = 4.24$ and $\Lambda^*_{CF} = 3.58$.

An analogous plot for two dimensions can be constructed from critical point temperatures inferred from vapor pressure and heat capacity studies. In the heat capacity studies, the temperature used is the temperature at which the specific heat is a maximum. The result is shown in Fig. 6.8(b). Several features are of interest. First, it can be seen that the critical temperature for an atomic species in two dimensions is significantly less than in three dimensions. The ratio is approximately 0.5 in the classical region, in agreement with simple calculations based upon the range dependence of the attractive part of the interatomic potential.[80] The theoretical upper limits of Λ^* for the occurrence of a critical point are shown.[73] The dotted line through the experimentally observed critical points continues smoothly to $\Lambda^*_{CB} = 3.26$ and is labeled "Boson Branch". The branch for particles with Fermi statistics is predicted to terminate at $\Lambda^*_{CF} = 2.74$ and a dotted line has been drawn to indicate a possible path of the branch.

The value of Λ^* for ^{3}He is 3.08 which is greater than Λ^*_{CF}. The figure then provides a way of visualizing the theoretical prediction that ^{3}He in two dimensions does not liquefy.

Fig. 6.9 shows an expanded version of the right half of the two dimensional law of corresponding states plot. A mass scale based on the helium Lennard-Jones values σ=2.556 Å and ε=10.22 K[55] is

Figure 6.9 Expanded law of corresponding states plot for two dimensions showing region of boson and fermion branches. The temperatures of measured maxima in the specific heat of ^{4}He/Gr, ^{4}He/Ar,Gr, ^{3}He/Ar/Gr, and ^{4}He/Ne/Gr are used for T_c. A separate non-reduced temperature scale and a mass scale based on the helium Lennard-Jones parameters are shown.

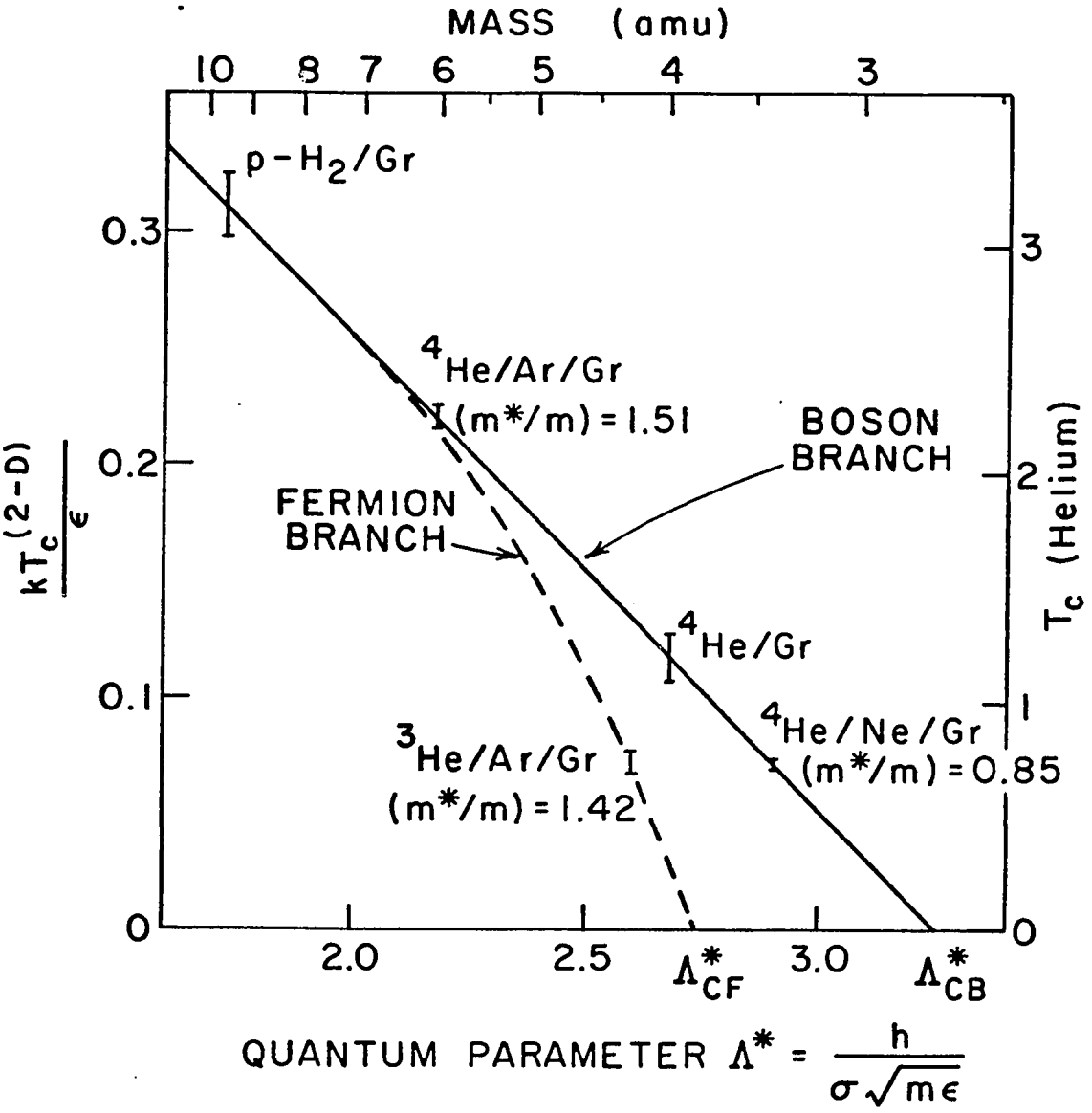
MASS (amu)
10
8
7
6
5
4
3
p-H2/Gr
4He/Ar/Gr
(m*/m) = 1.51
BOSON
BRANCH
FERMION
BRANCH
4He/Gr
4He/Ne/Gr
(m*/m) = 0.85
3He/Ar/Gr
(m*/m) = 1.42
0.3
0.2
0.1
0
3
2
1
0
2.0
2.5
3.0
Λ*CF
Λ*CB
kTc(2-D)/ε
Tc (Helium)
QUANTUM PARAMETER Λ* = h/σ√mε

included, along with a scale of non-reduced temperature for helium. The plotted points corresponding to the values of Λ^* and the temperatures of the tallest specific heat peak for para-H_2/Gr and ^{4}He/Gr happen to be colinear with the point Λ^*_{CB} on the abscissa and a straight line is shown drawn through these points.

If the ^{4}He/Ar/Gr results are viewed as due to the same effect as the ^{4}He/Gr results, then a comparison can be made between features which the two sets of data have in common. The temperature of the tallest specific heat peak is the most obvious choice. If this feature occurs at approximately the critical point, then the law of corresponding states plot can provide effective mass values for ^{4}He on the plated substrate. On the other hand, if the tallest specific heat peak is the signal of some other effect, then the applicability of the law of corresponding states picture is questionable, and at best can provide a qualitative way of understanding the shifts in temperature of the observed feature.

The temperature at which the specific heat of ^{4}He/Ar/Gr is greatest is 2.3 K. Fig. 6.9 shows this result plotted along the boson branch and indicates that such a shift in temperature would be expected for a helium atom of mass approximately 6 amu on a structureless substrate. Thus the effect of Ar-plating may be understood, within the framework of this picture, as enhancing the mass of the helium by a factor $m^*/m=1.5$.

A shift of effective mass by a factor 1.5 is enough to reduce the quantum parameter of ^{3}He below Λ^*_{CF}. It is possible therefore that ^{3}He/Ar/Gr may show evidence of liquefaction, or at least that the data

may display a feature similar to the peaks seen for ^{4}He. This is indeed the case. Whereas the ^{3}He/Gr data show no evidence for liquefaction, the ^{3}He/Ar/Gr results of Fig. 5.3 show a specific heat peak at 0.74 K. Plotted on the fermion branch of Fig. 6.9 a mass shift of $m^*/m=1.4$ is inferred. If the fermion branch is drawn differently, this value will change somewhat. However, it must be at least $m^*/m=[\Lambda^*(^3\text{He})/\Lambda^*_{CF}]^2 = 1.26$ for the peak to be placed on the fermion branch. Furthermore, m^*/m cannot be greater than 1.9 without violating the reasonable requirement that the difference between the boson and fermion branches increases monotonically with Λ^*.

This picture, although only semi-quantitative, nonetheless argues strongly that if the specific heat peaks seen at low areal density in the ^{4}He/Gr data are signals of liquefaction, then the ^{3}He/Ar/Gr system may also liquefy. If this interpretation is confirmed, then ^{3}He/Ar/Gr represents a new two dimensional liquid. The possibility exists, however, that the specific heat feature which has been focused on here is the signal of some other effect, such as the film atoms becoming ordered with the substrate. In that case it still remains an interesting observation that a law of corresponding states picture does quite well in explaining the temperature shifts of the maximum in the specific heat.

A similar analysis of the ^{4}He/Ne/Gr results gives an effective mass $m^*=0.85$ m, where m is the mass of ^{4}He. This shift in mass is in the opposite sense from that expected on the qualitative grounds of increased localization and indicates that within the law of corresponding states picture the effect of Ne-plating is to increase the effective

value of the quantum parameter Λ^* for helium.

A possible explanation for the apparent increase in Λ^* is offered by considering the spread of the helium wavefunctions in the direction normal to the surface. Using a model which allows for the z-wise spread, Sander, Bretz, and Cole,[81] and later Novaco[82] demonstrated that the effect of the spread is to modify the effective He-He interaction. The two dimensional interaction can be calculated as a function of the lateral separation of two atoms and an assignment made of effective Lennard-Jones parameters σ_{eff} and ε_{eff}. For a given lateral separation two helium atoms are on average further apart because of the motion normal to the surface. In addition, there is no lateral distance at which the averaged Lennard-Jones interaction energy can be equal to the value ε, the minimum of the unaveraged interaction. The result is that σ_{eff} and ε_{eff} have values less than their respective standard values σ and ε. The effective values can then be used to calculate an effective quentum parameter

$$\Lambda^*_{eff} = \frac{h}{\sigma_{eff}(m\varepsilon_{eff})^{\frac{1}{2}}} \quad . \tag{4}$$

For ^{4}He/Gr at low temperatures the root mean square deviation of the normal distance of a helium atom from its average position has been estimated to be 0.27 Å.[82] Using the analysis of Ref. 81, this leads to an approximately 1% increase in Λ^*. For ^{4}He/Ar/Gr, the r.m.s. deviation can be estimated from Fig. 3 of Ref. 39 to be 0.35 Å, and this produces a shift in Λ^* of less than 2%. The effect is expected to be more sizeable, however, in the case of the second layer of helium

adsorbed on graphite (^{4}He/^{4}He/Gr) partly because the top layer of ^{4}He atoms are less strongly bound to the ^{4}He-plated surface ($E_{binding} \simeq 30$ K)[83] and partly because of an added contribution from the oscillations of the first layer solid helium atoms in the direction normal to the surface. The combined effect is estimated to produce an r.m.s. deviation of 0.73 Å,[82] approximately half being due to the oscillation of the solid underlayer. The result is that Λ^*_{eff} is increased 8% over Λ^*. The same increase in the quantum parameter would be expected if σ and ε remained constant and the helium were viewed as having an effective mass m*=0.85 m. Using the law of corresponding states plot (Fig. 6.9) a shift of Λ^* by this amount would shift the expected critical temperature of ^{4}He/^{4}He/Gr to 0.75 K, approximately the temperature of the tallest specific heat peak in the data of Polanco and Bretz[84] for this system. It should be kept in mind, however, that the calculation above does not take into consideration any change in the effective quantum parameter due to lateral localization of the helium wavefunctions or due to other possible effects such as exchange of phonons between the surface atoms and the substrate.[85]

An estimate of the shift in Λ^* for ^{4}He/Ne/Gr can be made by comparing the ^{4}He-^{4}He bare interaction with the effective interaction on Ne-plated graphite. Using the parameters for the Beck potential calculated by Novaco,[40] the minimum in the potential is calculated to shift from $(r_{min}, E(r_{min})/k)$ = (2.969 Å, 10.35 K) to (2.934 Å, 10.15 K). This is a 1.2% decrease in lateral spacing at the minimum and a 1.9% decrease in the minimum value of E(r). A rough estimate of the effect of these shifts on the value of Λ^* can be made by assuming that the

effective Lennard-Jones parameters are shifted proportionally. This gives $\Lambda^*_{eff} = 1.02\ \Lambda^*$, which is equivalent to an effective mass shift $m^*/m=0.96$. This shift is considerably smaller than that estimated for the second layer of ^{4}He and is not enough to account for the approximately 40% shift in temperature of the specific heat peak of ^{4}He on Ne-plated as opposed to unplated Grafoil.

Although ^{3}He/Ne/Gr does not display a peak in the specific heat, the analysis can be extended to this case by focusing on a different feature of the data. Any feature which depends on the quantum parameter Λ^* would then be expected to occur at lower temperatures in the plated case. Fig. 6.10 shows a ^{3}He/Gr specific heat run taken by Hickernell, McLean, and Vilches[61] with areal density $n=0.0279\ \text{Å}^{-2}$ and one of slightly less density taken with Ne-preplating as part of this study. In both runs the high temperature specific heat has an approximately constant value, whereas at lower temperatures the specific heat falls to lower values. It can be seen qualitatively that the temperature at which significant deviations from the high temperature value occur in the plated case is about one-half that observed in the unplated case. Although it is not clear how this shift in temperature can be related quantitatively to a change in effective mass, the shift is consistent with the earlier observation that Ne-preplating reduces the effective mass and lowers the temperature of the occurrence of the maximum in the specific heat.

6.6 Other Interpretations, ^{4}He/Ar/Gr

The preceding section presented a discussion of the possibility that

Figure 6.10 Comparison of specific heats, ^{3}He/Gr (from Ref. 61) and ^{3}He/Ne/Gr.

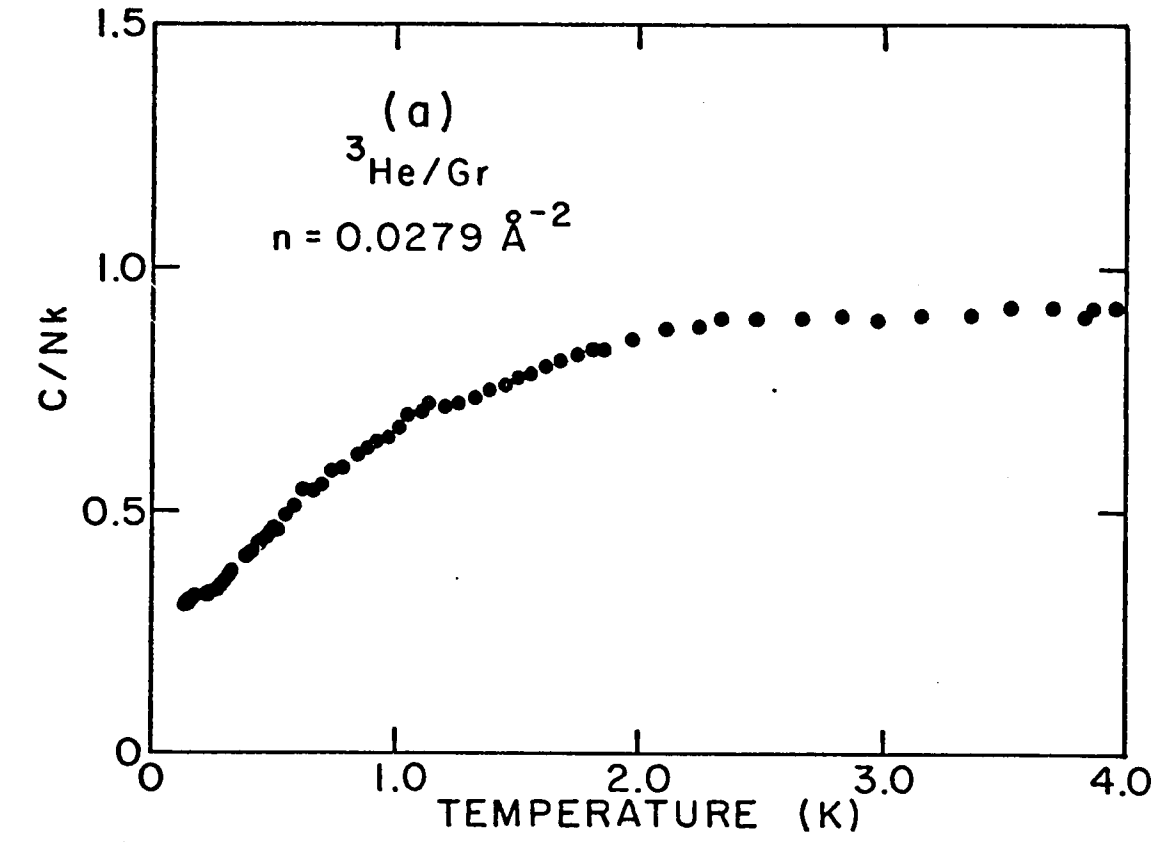
(a)
^{3}He/Gr
n = 0.0279 Å^{-2}
C/Nk
TEMPERATURE (K)
0
0.5
1.0
1.5
1.0
2.0
3.0
4.0

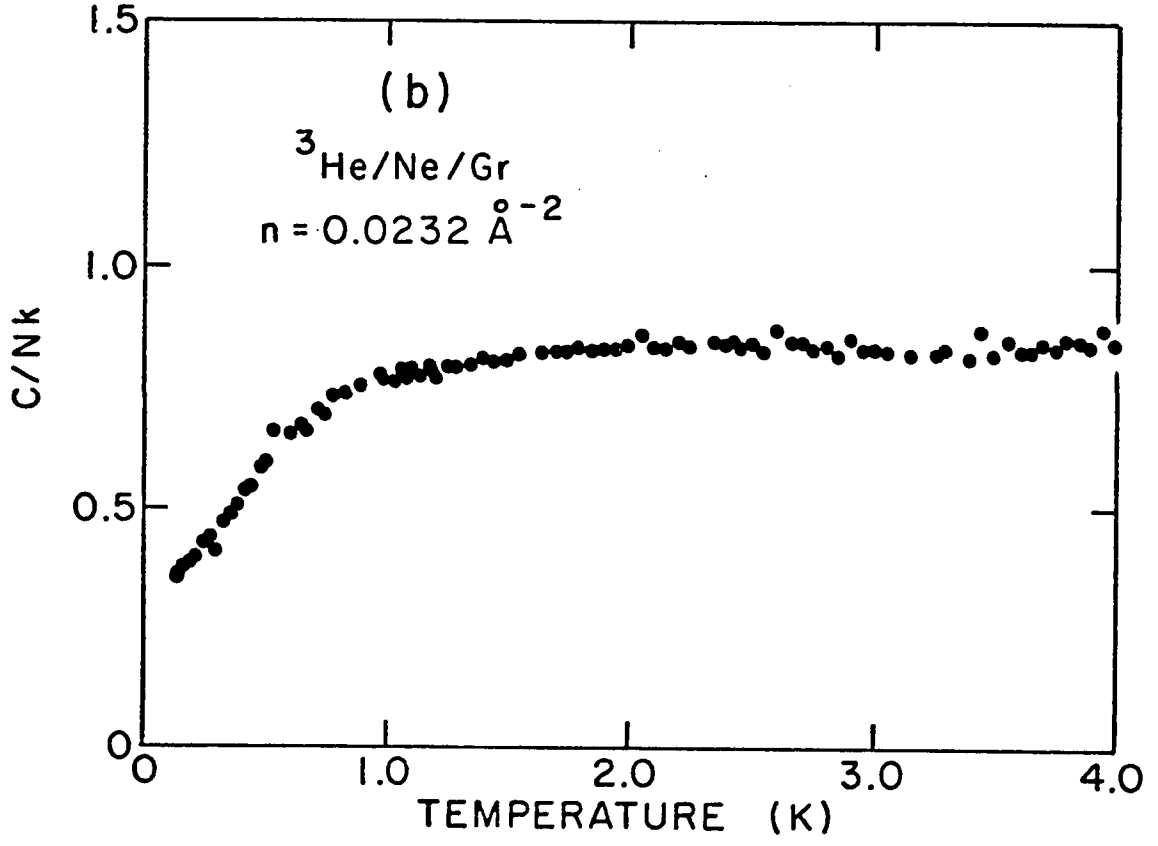
(b)
^{3}He/Ne/Gr
n = 0.0232 Å^{-2}
C/Nk
TEMPERATURE (K)
0
0.5
1.0
1.5
1.0
2.0
3.0
4.0

the dominant peaks in the specific heat of the ^{4}He/Ar/Gr system are the signal of liquefaction. This possibility was prompted primarily by the similarity of the heat capacity signal with that of ^{4}He/Gr, a system for which liquefaction had been predicted on theoretical grounds. However, because of the strong variation in the He-substrate potential in the case of ^{4}He/Ar/Gr, consideration must be given to the possibility that the series of specific heat peaks signal the presence of registered or solid phases. These two possibilities are discussed in this section.

Recently, Rehr and Tejwani[86] have calculated the second virial coefficient correction to the heat capacity of helium adsorbed on rare gas substrates. Their theory uses helium wavefunctions localized on a triangular array of adsorption sites and assumes the interaction energy to be equal to the value of the He-He Lennard-Jones 6-12 potential at the site separation distance. The theory thus neglects the spread of the wavefunctions in both the lateral and normal directions and can be expected to predict only qualitative trends of the specific heat. Fig. 6.11 shows the calculated deviation of the specific heat from the single particle value C^o plotted versus a reduced temperature scale. Curves are shown for five values of the ratio u/t, where u and t are the two particle He-He interaction energy and the one-particle energy, respectively. The single particle energy includes both kinetic and helium-substrate energies. The solid lines are the results when only the lowest band in the theory is considered and the dotted lines include corrections for higher bands. A few of the ^{4}He/Ar/Gr experimental points from Fig. 6.2 are shown plotted as (C-1)/nNk versus T.

Figure 6.11 Heat capacity calculated from the theory of Rehr and Tejwani for five values of u/t. Solid lines are the results when only the lowest band is included. The dotted lines include contributions from higher bands. The circles and squares show specific heat results for the systems ^{4}He/Ar/Gr (this study) and ^{4}He/Gr (Ref. 2) plotted as $[(C/Nk)-1]n^{-1}$ vs. T. A non-reduced temperature scale is shown.

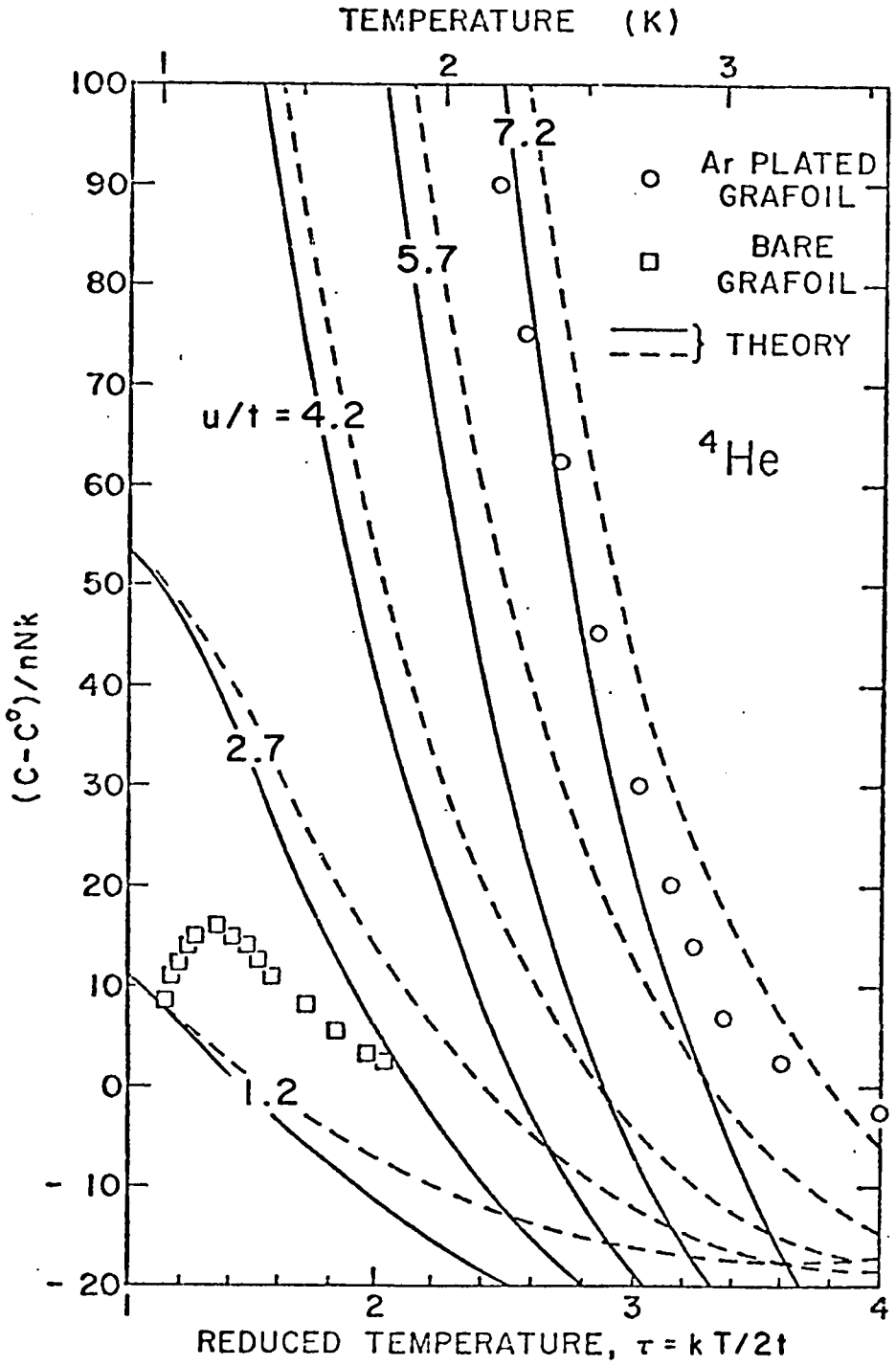
TEMPERATURE (K)
1
2
3
100
90
80
70
60
50
40
30
20
10
0
- 10
- 20
(C-C°)/nNk
7.2
5.7
u/t = 4.2
2.7
1.2
Ar PLATED GRAFOIL
BARE GRAFOIL
THEORY
⁴He
1
2
3
4
REDUCED TEMPERATURE, τ = kT/2t

Assuming that only every other adsorption site is available for occupation, the theory gives u/t=5.8. The theory does very well at qualitatively demonstrating the shift in the high temperature specific heat of ^{4}He/Ar/Gr, and suggests that the specific heat peaks may be related to a registered phase in which there is one helium atom for every two adsorption sites on the argon lattice. This would be expected at a density of approximately 0.086 Å^{-2}.

The two runs taken in the vicinity of this density (n=0.0846 and 0.0887 Å^{-2}) display small shoulders in the heat capacity between 2 and 3 degrees Kelvin. The shoulder for the lower density run appears to be the last of the series of specific heat peaks which occur for all lower density runs. The phase diagram (Fig. 5.1(b)) shows that the shoulder for the run with density n=0.0887 Å^{-2} does not follow the same trend, but rather has moved to higher temperatures and appears to lie on the helium melting line defined by the unplated Grafoil data. A plot of C/Nk versus T^2 for these two runs gives two dimensional Debye temperatures of 41 K and 31 K respectively (Fig. 6.12). This decrease in experimental Debye temperatures with increasing density is counter to the expectation for solids and indicates that it is unlikely that films for both densities are solids at temperatures below their respective peaks. The value of 31 K for the Debye temperature of the run with density 0.0887 Å^{-2} is somewhat higher than the value of 24 K obtained by interpolation to this density from the ^{4}He/Gr data of Hering.[46] This difference may be attributed to uncertainties in the actual areal density of the film or to modifications of the solid produced as a result of Ar-preplating.

Thus it seems that the ^{4}He/Ar/Gr solidifies rather than forming a registered phase at areal density n=0.086 Å^{-2}. However, it should be recognized that when the density is close to that of the possible superlattice structure, the solid may be able to lower its energy significantly by taking advantage of the variation in helium-substrate potential energy and that this may in fact be a rather complex region.

Assuming that the specific heat shoulder for the highest density run is the signal of melting, then the possibility exists that the line of peaks in the ^{4}He/Ar/Gr phase diagram (Fig. 5.1(b)) define a two phase coexistence region between the solid and a lower density gas phase. The line of peaks would then be a sublimation line, and the intersection of the sublimation and solid lines would be either a tricritical point or a critical end point depending on whether the intersection is the highest temperature point on the sublimation line or not.[87] A major problem with the two phase identification, however, is that isotherms of the heat capacity when plotted versus density are not linear (Fig. 5.11) as would be expected for a coexistence region on thermodynamic grounds.[88] A model of the possible two phase region which includes inhomogeneities and a distribution of areal densities over individual Grafoil crystallites may be able to resolve this difficulty.

Although the nature of the specific heat peaks is not clear at the moment, the study points to many potentially interesting areas for future research. Among these are a study of the interplay between the

Figure 6.12 C/Nk vs. T^2 for the two highest density ^{4}He/Ar/Gr runs shown with Debye temperatures obtained from eyeball fits to the data. A single ^{4}He/Gr run from Ref. 46 is shown for comparison.

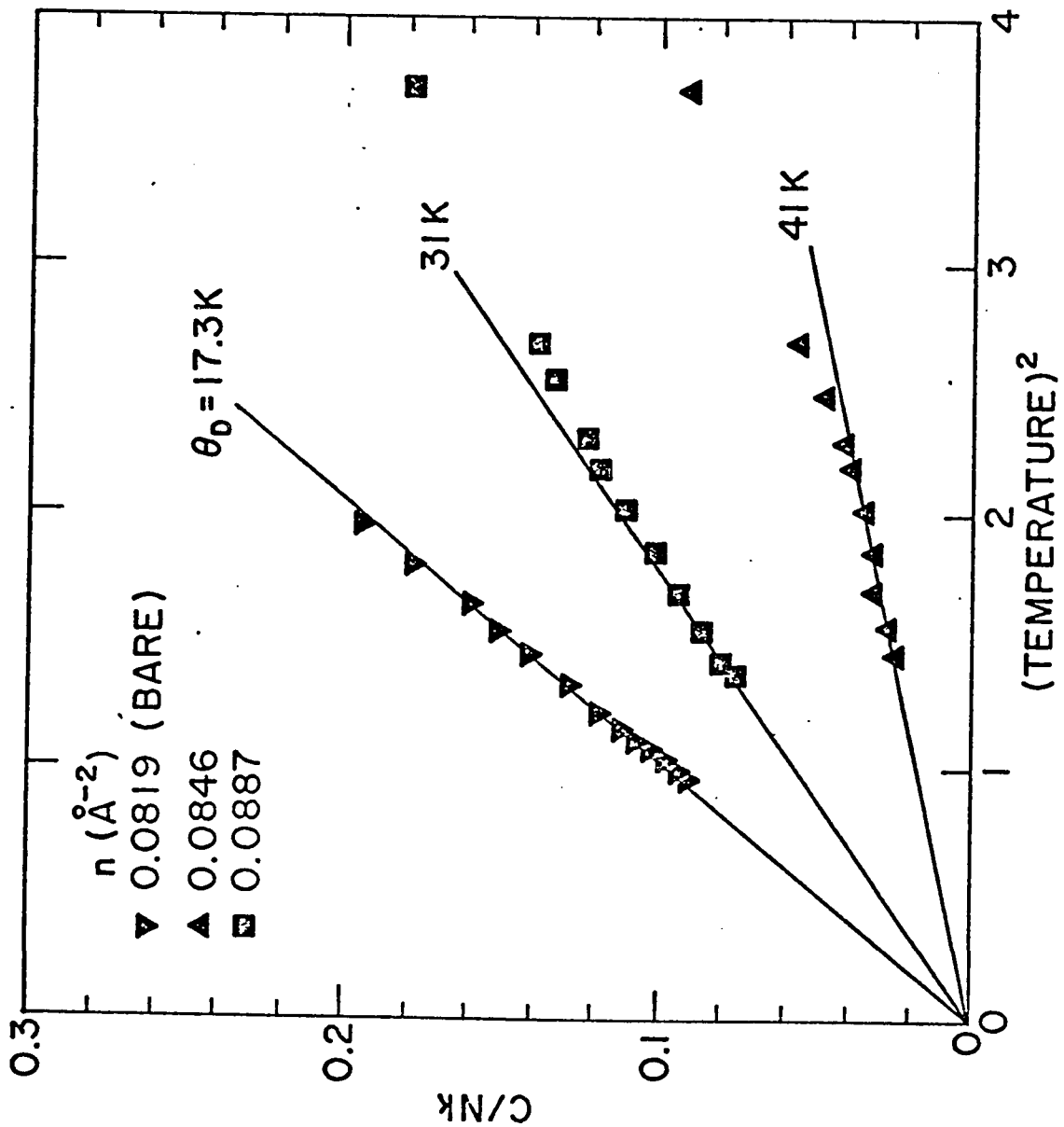
0.3
0.2
0.1
0
C/Nk
0
1
2
3
4
(TEMPERATURE)²
θD = 17.3K
31K
41K
n (Å⁻²)
▼ 0.0819 (BARE)
▲ 0.0846
■ 0.0887

presumed solid and the substrate near the density n=0.086 Å^{-2} and an exploration of the possibility of a tricritical point or critical endpoint.

6.7 Other Interpretations, ^{4}He/Ne/Gr

The high density phase diagram for ^{4}He/Ne/Gr (Fig. 5.9) is similar to the phase diagrams[21] for ^{3}He/Gr and ^{4}He/Gr in that there is a series of peaks observed over a narrow temperature range for densities just below what appears to be a melting line. The tall peak observed at areal density n=0.0841 Å^{-2} for both isotopes on the Ne-plated substrate and the other peaks in the density range $0.0841 \leq n \leq 0.0889$ Å^{-2} are thus probably signals of a transition similar to the one reported by Hering, Van Sciver and Vilches[21] on unplated Grafoil, the nature of which is not completely understood. The shape of the line of peaks on the phase diagram for both surfaces is similar to that of the registry-deregistry transitions observed for ^{3}He/Gr and ^{4}He/Gr at approximately 0.064 Å^{-2} and an important question is whether the ^{4}He/Ne/Gr peaks at approximately 0.084 Å^{-2} could be the result of a transition from a registered phase.

The only simple superlattice structure in this density range is one with one helium atom for every three lattice sites (cf. Fig. 1.8(d)). Assuming that the nearest neighbor distance of the plated neon is 3.08 Å and that the area available for helium adsorption is the same as in the case of unplated Grafoil, this registered phase would occur at areal density n=0.083 Å^{-2}. Each helium atom would then have three nearest neighbors at a distance of 3.08 Å. This distance is less than

the spacing between atoms for even the highest areal density helium solid adsorbed on unplated Grafoil. A close-packed solid with nearest neighbor distance 3.08 $\mathring{A}$ has an areal density 0.122 $\mathring{A}^{-2}$. This fact seems to indicate that the possibility of the open structure at density $n=0.083\ \mathring{A}^{-2}$ can be eliminated on the grounds that the spacing between helium atoms is too small. However, this spacing is still within the attractive part of the He-He potential which has a minimum at 2.87 $\mathring{A}$, and it is possible that the energetic advantage of sitting in the adsorption sites provided by the underlying neon layer is enough to overcome the energy price of localizing the helium wavefunctions in the open structure.

It should be pointed out that the energy required for localization may be less than that required for the close packed solid with the same interatomic spacing for three reasons. First, in the open structure the helium may be able to take advantage of the larger "rattle space" per atom and the wavefunctions may be less localized than in the close packed case. Also, the periodic nature of the helium-substrate potential has already localized the helium wavefunctions to some extent, thus reducing the energy expense of localizing the atoms on sites. Thirdly, because of the greater spread of the helium wavefunction normal to the surface, the effective Lennard-Jones hard core diameter is less for helium on Ne-plated graphite than for helium on unplated graphite.

If the registered phase exists, then it is possible that the part of the phase diagram at temperatures below the series of peaks observed for $n\leq 0.0702\ \mathring{A}^{-2}$ is a region of coexisting registered and gas phases.

the heat capacity versus density isotherms (Fig. 5.12) are

not linear over this region as would be expected, and a definite identification of the low temperature phase(s) awaits further work either in the form of a more detailed heat capacity study including a model of heat capacity rounding effects or a neutron scattering study which could give structural information.

Chapter 7

CONCLUSION

The heat capacity measurements of this study demonstrate that rare gas plating of a graphite substrate is an effective means of producing new crystalline substrates for the study of helium films. In both the Ar-plated and Ne-plated cases, monolayer ^{4}He films with areal densities $n<0.05$ Å^{-2} are seen to display a series of heat capacity peaks similar in many respects to the series of peaks observed in earlier studies of ^{4}He adsorbed on unplated graphite and interpreted as the signal of liquefaction.

The effect of rare gas plating of the substrate is to modify the effective interactions of the helium film in such a way as to produce rather dramatic shifts in the condensation temperature of the film, increasing the temperature by a factor of almost two in the Ar-plated case and decreasing the temperature by a factor of about one-half in the Ne-plated case. Within the law of corresponding states framework these shifts are equivalent to changes in the effective mass of the helium, the shift being $m^*/m = 1.5$ for the case ^{4}He/Ar/Gr and $m^*/m = 0.85$ for ^{4}He/Ne/Gr. The shifts are understood as resulting in part from the increased lateral localization of the helium wavefunctions which enhances m^*, and in part from the competing effect of decreased localization normal to the surface plane. Heat capacity data using ^{3}He are qualitatively consistent with the effective mass interpretation.

At temperatures above the peak temperatures, the heat capacity of the helium films on Ar- and Ne-plated graphite have the temperature and

density dependence characteristic of a two-dimensional gas describable by virial corrections to the equation of state of an ideal two-dimensional gas. The measurements have stimulated theoretical investigation of the role of the substrate in determining the properties of the film in this phase, and in the case of Ar-plating a comparison is possible between the experiment and theory.

The few runs taken with ^{4}He adsorbed on Ar-plated graphite at coverages above n=0.05 Å^{-2} indicate that the film seems to form a solid at roughly the same temperature and density as is found in the case of ^{4}He adsorbed on unplated graphite. The most likely registered phase, that of one helium atom for every two argon adsorption sites, is not seen, although further work is required to identify the high areal density features with certainty. The possibility exists that the entire ^{4}He/Ar/Gr system is dominated by the presence of the solid and that the heat capacity peaks at lower n are due to sublimation.

The higher areal density runs with Ne plating indicate a complex region of features similar to those observed on unplated graphite, including a series of peaks at densities slightly below the occurrence of the solid line.

The results presented here suggest that the study of adsorption on plated surfaces may be an interesting and fruitful avenue for future research. There are many unanswered questions concerning the ^{4}He/Gr, ^{4}He/Ar/Gr, and ^{4}He/Ne/Gr systems, as well as more general questions concerning the role the substrate plays in determining the properties of atoms at solid surfaces.

As far as the ^{4}He/Gr, ^{4}He/Ar/Gr, and ^{4}He/Ne/Gr systems are concerned, an unambiguous identification of the low temperature phase of the helium films at low to moderate areal densities is, of course, the key to an understanding of these systems. A spectroscopic investigation of the structure of the helium film for one or more of these systems would be most useful. Another approach would be to perform a more detailed heat capacity study using one of the new forms of high areal density graphites with the hope of substantially reducing the problems introduced by the small fraction of inhomogeneous adsorption sites present in Grafoil.

If the low temperature moderate areal density phase of ^{4}He/Ar/Gr is a liquid, then considerable attention should be given the ^{3}He/Ar/Gr system, which will most likely have a liquid region as well. The nature of both Bose and Fermi two-dimensional liquids could, in fact, be studied on a succession of different rare gas plated substrates. If, on the other hand, the ^{4}He/Ar/Gr film is a registered or solid phase, the physics of the strong isotopic dependence of the specific heat would be of considerable interest.

The high areal density regions deserve more attention than was possible in this study. Of particular interest in the He/Ar/Gr case would be the nature of the solid helium film, especially near the density of the possible $X_g=\frac{1}{2}$ superlattice phase. In the Ne-plated case, the nature of the peaks at areal densities just below the solid line are a possible area for investigation. For example, do they signal a region of two phase solid-registered equilibrium as is expected in the He/Gr case?

In addition to the possible monolayer platings with rare gas atoms, investigations of plating with two or more solid layers of a rare gas or of plating with partial rare gas layers are potentially fruitful areas of research. Studies of the effects of reduced adsorption domain area or of progressively weaker adsorbate-substrate potential are possibilities.

In the broader view, questions of the influence of the substrate on two-dimensional melting, transport properties, and atomic scattering may be approachable using rare gas plated substrates. It is not unlikely that plated substrates will play an increasingly important role in future investigations of the interaction of atoms at solid surfaces.

REFERENCES

1. The review articles and books listed in references 2-6 provide perhaps the best guide to the expanding volume of literature on physically adsorbed monolayers.

2. M. Bretz, J. G. Dash, D. C. Hickernell, E. O. McLean, and O. E. Vilches, Phys. Rev. A8, 1589 (1973), and Phys. Rev. A9, 2814 (1974).

3. J. G. Dash, Films on Solid Surfaces (Academic, New York, 1975).

4. J. G. Dash, in Quantum Liquids, edited by J. Ruvalds and T. Regge (North Holland-Elsevier, New York, 1978), p. 63.

5. C.-W. Woo, in The Physics of Liquid and Solid Helium, edited by K. H. Bennemann and J. B. Ketterson (Wiley, New York, 1976), Part I, sec. 5.7.

6. J. G. Dash and M. Schick, in The Physics of Liquid and Solid Helium, edited by K. H. Bennemann and J. B. Ketterson (Wiley, New York, to be published, 1978), Part II.

7. D. L. Goodstein, W. D. McCormick, and J. G. Dash, in Proceedings of the Ninth International Conference on Low Temperature Physics, Columbus, Ohio, 1964 (Plenum, New York, 1965), Part B, p. 368.

8. D. L. Goodstein, J. G. Dash, and W. D. McCormick, Phys. Rev. Lett. 15, 447 (1965), and Phys. Rev. Lett. 15, 740 (1965).

9. W. D. McCormick, D. L. Goodstein, and J. G. Dash, Phys. Rev. 168, 249 (1968).

10. G. A. Stewart and J. G. Dash, J. Low Temp. Phys. 5, 1 (1971).

11. G. A. Stewart and J. G. Dash, Phys. Rev. A2, 918 (1970).

12. P. Mahadev, M. F. Panczyk, R. A. Scribner, and J. G. Daunt, Phys. Lett. 41A, 221 (1972).

13. D. F. Brewer, A. J. Symonds, and A. L. Thompson, Phys. Rev. Lett. 15, 182 (1965).

14. D. F. Brewer, J. Low Temp. Phys. 3, 205 (1970).

15. H. M. Guo, D. O. Edwards, R. E. Sarwinski, and J. T. Tough, Phys. Rev. Lett. 27, 1259 (1971).

16. A. A. Antoniou, J. Chem. Phys. 62, 779 (1975).

17. Because of the large number of studies of helium monolayers which have used exfoliated graphite, reference is made to the reviews listed in Refs. 2-6.

18. J. G. Dash, Ref. 3, sec. 3.4.

19. W. A. Steele, The Interaction of Gases with Solid Surfaces, Topic 14, Vol. 3 of The International Encyclopedia of Physical Chemistry and Chemical Physics (Pergamon, New York, 1974), sec. 2.8.

20. R. L. Elgin and D. L. Goodstein, Phys. Rev. A9, 2657 (1974).

21. S. V. Hering, S. W. Van Sciver, and O. E. Vilches, J. Low Temp. Phys. 25, 793 (1976).

22. R. L. Siddon and M. Schick, Phys. Rev. A9, 907, (1974).

23. R. L. Siddon and M. Schick, Phys. Rev. A9, 1753 (1974).

24. G. A. Stewart, Phys. Rev. A10, 671 (1974).

25. M. Schick and R. L. Siddon, Phys. Rev. A8, 339 (1973).

26. M. Bretz, Phys. Rev. Lett. 38, 501 (1977).

27. M. Nielsen, J. P. McTague, and W. Ellenson, J. Physique 38, C4-10 (1977).

28. J. G. Dash, Ref. 4, p. 78 and private communication.

29. D. C. Hickernell, Ph.D. dissertation (University of Washington, 1972)(unpublished).

30. A. D. Novaco, J. Low Temp. Phys. 9, 457 (1972).

31. D. S. Hyman, Ph.D. dissertation (Cornell University, 1970) (unpublished).

32. C. E. Campbell and M. Schick, Phys. Rev. A3, 691 (1971).

33. M. D. Miller, C.-W. Woo, and C. E. Campbell, Phys. Rev. A6, 1942 (1972).

34. A. D. Novaco and C. E. Campbell, Phys. Rev. B11, 2525 (1975).

35. J. G. Dash, R. Ecke, J. Stoltenberg, O. E. Vilches, and O. J. Whittemore, Jr., "Uniform MgO Adsorbents", (to be published, J. Phys. Chem., 1978).

36. W. A. Steele, Ref. 19, p. 13.

37. D. E. Hagen, A. D. Novaco, and F. J. Milford, in Proceedings of the Second International Conference on Adsorption-Desorption Phenomena, Florence, Italy, 1971 (Academic, New York, 1972).

38. H. Taub, K. Carneiro, J. K. Kjems, L. Passell, and J. P. McTague, Phys. Rev. B16, 4551 (1977).

39. A. D. Novaco and F. J. Milford, Phys. Rev. A5, 783 (1972).

40. A. D. Novaco (preprint).

41. G. A. Somorjai, Surf. Sci. 34, 156 (1973).

42. M. Bretz and J. G. Dash, Phys. Rev. Lett. 26, 963 (1971).

43. A. D. Novaco, Phys. Rev. A5, 1653 (1973); also Ref. 4, p. 87.

44. E. Domany, M. Schick, and J. S. Walker, Phys. Rev. Lett. 38, 1148 (1977).

45. S. Van Sciver, Ph.D. dissertation (University of Washington, 1976) (unpublished).

46. S. V. Hering, Ph.D. dissertation (University of Washington, 1974) (unpublished).

47. O. V. Lounasmaa, Experimental Principles and Methods Below 1K (Academic, New York, 1974), p. 225.

48. Ibid, pp. 220-221.

49. E. O. McLean, Ph.D. dissertation (University of Washington, 1972) (unpublished).

50. Leybold-Heraeus, Inc., Seco Road, Monroeville, Pennsylvania.

51. Handbook of Chemistry and Physics, 49th Edition (Chemical Rubber Company, Cleveland, Ohio, 1968), p. D-139.

52. C.-H. Fagerstroem and A. C. Hollis Hallett, in Proceedings of the Ninth International Conference on Low Temperature Physics (Plenum, New York, 1965), Part B, pp. 1092-1094.

53. T. T. Chung (preprint).

54. G. B. Huff, Ph.D. dissertation (University of Washington, 1972) (unpublished).

55. J. O. Hirschfelder, C. F. Curtiss, R. B. Bird, Molecular Theory of Gases and Liquids (Wiley, New York, 1954), p. 1110.

56. E. R. Grilly, Cryogenics 2, 226 (1962).

57. E. Lerner and J. G. Daunt, J. Low Temp. Phys. 10, 299 (1973).

58. J. G. Dash, Ref. 2, pp. 94-96.

59. J. G. Dash, R. E. Peierls, and G. A. Stewart, Phys. Rev. A2, 932 (1970).

60. G. T. McConville, Cryogenics 9, 122 (1969).

61. D. C. Hickernell, E. O. McLean, and O. E. Vilches, Phys. Rev. Lett. 28, 789 (1972).

62. J. G. Dash, Ref. 2, p. 97.

63. F. London, Superfluids (Dover, New York, 1954), Vol. II, Sec. B.

64. However, a recent calculation by R. D. Puff and M. Schick predicts that ^{3}He in two dimensions will condense into a liquid ground state (private communication).

65. A. D. Novaco, Phys. Rev. 7, 1653 (1973).

66. J. G. Dash, Ref. 3, pp. 141-142.

67. J. G. Dash, Ref. 3, pp. 232-234.

68. M. D. Miller and C.-W. Woo, Phys. Rev. A7, 1322 (1973).

69. M. D. Miller, Phys. Rev. B17, 1139 (1978).

70. D. C. Hickernell, E. O. McLean, and O. E. Vilches, J. Low Temp. Phys. 23, 143 (1976).

71. F. J. Milford and A. D. Novaco, Phys. Rev. A4, 1136 (1971).

72. M. Bretz and J. G. Dash, Phys. Rev. Lett. 26, 963 (1971).

73. M. D. Miller and L. H. Nosanow, "Liquid-to-Gas Phase Transitions in Two-Dimensional Quantum Systems at Zero Temperature", (to be published, J. Low Temp. Phys., 1978).

74. J. O. Hirschfelder, Ref. 55, sec. 4.1.

75. J. O. Hirschfelder, Ref. 55, sec. 6.6.

76. L. H. Nosanow, L. J. Parish, F. J. Pinski, Phys. Rev. B11, 191 (1975).

77. A. Thomy and X. Duval, J. Chim. Phys. 67, 1101 (1970).

78. Handbook of Chemistry and Physics, Ref. 51, p. F-64.

79. M. D. Miller, L. H. Nosanow, and L. J. Parish, Phys. Rev. B15, 214 (1976).

80. J. G. Dash, Ref. 3, p.123.

81. L. M. Sander, M. Bretz, and M. W. Cole, Phys. Rev. B14, 61 (1976).

82. A. D. Novaco, Phys. Rev. B13, 3194 (1976).

83. C. E. Campbell, F. J. Milford, A. D. Novaco, and M. Schick, Phys. Rev. A6, 1648 (1972).

84. S. E. Polanco and M. Bretz, Phys. Rev. B17, 151 (1978).

85. M. Schick and C. E. Campbell, Phys. Rev. A2, 1591 (1970).

86. J. J. Rehr and M. Tejwani, Bull. Amer. Phys. Soc. 23, 261 (1978), and preprint.

87. R. B. Griffiths, Phys. Rev. B12, 345 (1975).

88. J. G. Dash, Ref. 3, p. 83.

89. T. T. Chung and J. G. Dash, Surf. Sci. 66, 559 (1977).

90. M. Bretz and T. T. Chung, J. Low Temp. Phys. 17, 479 (1974).

APPENDIX A

^{4}He/Ar/Gr specific heat for runs with areal densities $n \leq 0.0515$ $\mathring{A}^{-2}$. The values are interpolated from smoothed specific heat vs. temperature curves.

T	0.0093	0.0140	0.0187	0.0233	0.0280	0.0327	0.0374	0.0515
0.500	0.080			0.028				0.012
.540	.098			.034				.014
.580	.112			.040				.016
.620	.130			.046				.018
.660	.150			.054				.020
.700	.176			.070				.023
.740	.215			.088				.026
.780	.258			.102				.030
.820	.304			.122				.035
.860	.360	0.258		.146				.042
.900	.415	.312		.173				.048
.940	.482	.370	0.274	.204				.055
.980	.560	.430	.316	.242				.062
1.020	.655	.495	.364	.284				.071
1.060	.770	.565	.406	.324				.079
1.100	.890	.640	.460	.365				.090
1.140	.995	.722	.512	.410				.100
1.180	1.095	.810	.564	.462		0.302		.115
1.220	1.210	.900	.620	.510	0.414	.340	0.266	.130
1.260	1.340	1.000	.686	.564	.452	.375	.298	.145
1.300	1.465	1.102	.760	.620	.502	.416	.326	.160
1.340	1.610	1.220	.862	.680	.564	.455	.366	.180

T	0.0093	0.0140	0.0187	0.0233	0.0280	0.0327	0.0374	0.0515
1.380	1.735	1.315	0.956	0.750	0.620	0.500	0.400	0.198
1.420	1.870	1.450	1.050	.822	.680	.555	.446	.215
1.460	2.000	1.575	1.174	.902	.744	.605	.490	.238
1.500	2.130	1.710	1.284	.985	.812	.655	.532	.260
1.540	2.250	1.860	1.400	1.075	.888	.725	.586	.290
1.580	2.370	2.010	1.506	1.170	.970	.795	.648	.315
1.620	2.475	2.175	1.640	1.275	1.050	.860	.704	.345
1.660	2.592	2.355	1.768	1.370	1.140	.935	.766	.380
1.700	2.655	2.520	1.900	1.475	1.234	1.000	.820	.408
1.740	2.705	2.665	2.022	1.570	1.334	1.085	.890	.422
1.780	2.746	2.810	2.170	1.685	1.434	1.175	.960	.480
1.820	2.770	2.935	2.314	1.835	1.560	1.260	1.028	.510
1.860	2.778	3.030	2.492	1.970	1.660	1.360	1.108	.558
1.900	2.774	3.140	2.660	2.130	1.794	1.470	1.200	.595
1.940	2.747	3.208	2.840	2.310	1.956	1.585	1.300	.640
1.980	2.698	3.250	2.990	2.460	2.104	1.710	1.418	.685
2.020	2.620	3.255	3.120	2.620	2.320	1.850	1.540	.730
2.060	2.555	3.220	3.252	2.770	2.460	1.985	1.656	.780
2.100	2.490	3.135	3.358	2.925	2.592	2.130	1.770	.840
2.140	2.425	3.015	3.432	3.110	2.768	2.290	1.870	.900
2.180	2.380	2.910	3.426	3.250	2.944	2.470	2.000	.960
2.220	2.325	2.820	3.358	3.375	3.086	2.620	2.144	1.020
2.260	2.280	2.705	3.254	3.490	3.220	2.730	2.288	1.095

T	0.0093	0.0140	0.0187	0.0233	0.0280	0.0327	0.0374	0.0515
2.300	2.228	2.595	3.108	3.485	3.284	2.900	2.402	1.155
2.340	2.180	2.475	2.926	3.360	3.270	3.010	2.560	1.220
2.380	2.125	2.355	2.712	3.150	3.214	3.100	2.686	1.280
2.420	2.080	2.260	2.478	3.000	3.084	3.100	2.800	1.330
2.460	2.035	2.150	2.304	2.785	2.740	3.010	2.852	1.375
2.500	1.990	2.065	2.156	2.570	2.450	2.870	2.840	1.420
2.540	1.940	1.994	2.040	2.340	2.210	2.620	2.760	1.428
2.580	1.896	1.915	1.940	2.160	2.042	2.400	2.602	1.405
2.620	1.855	1.845	1.850	2.030	1.882	2.190	2.404	1.372
2.660	1.825	1.795	1.770	1.905	1.740	2.000	2.212	1.335
2.700	1.792	1.740	1.704	1.800	1.640	1.820	1.992	1.285
2.740	1.760	1.694	1.652	1.695	1.540	1.670	1.810	1.235
2.780	1.735	1.652	1.600	1.590	1.464	1.575	1.688	1.195
2.820	1.705	1.615	1.554	1.500	1.392	1.490	1.588	1.150
2.860	1.685	1.580	1.512	1.435	1.328	1.410	1.460	1.120
2.900	1.664	1.545	1.466	1.375	1.280	1.345	1.362	1.080
2.940	1.645	1.520	1.430	1.330	1.238	1.290	1.300	1.065
2.980	1.625	1.495	1.396	1.292	1.200	1.235	1.246	1.045
3.020	1.602	1.472	1.362	1.255	1.158	1.190	1.198	1.020
3.060	1.592	1.458	1.332	1.220	1.120	1.150	1.158	1.000
3.100	1.580	1.442	1.306	1.195	1.094	1.120	1.120	.990
3.140	1.572	1.430	1.286	1.170	1.072	1.092	1.090	.970

T	0.0093	0.0140	0.0187	0.0233	0.0280	0.0327	0.0374	0.0515
3.180	1.560	1.416	1.270	1.148	1.052	1.070	1.060	0.960
3.220	1.548	1.405	1.254	1.126	1.032	1.052	1.038	.950
3.260	1.540	1.392	1.240	1.108	1.014	1.032	1.018	.942
3.300	1.535	1.382	1.226	1.092	.996	1.015	1.002	.932
3.340	1.528	1.372	1.216	1.074	.980	1.000	.990	.925
3.380	1.522	1.362	1.206	1.060	.966	.985	.978	.915
3.420	1.518	1.354	1.198	1.050	.954	.972	.966	.906
3.460	1.514	1.346	1.190	1.038	.942	.962	.956	.902
3.500	1.510	1.340	1.182	1.026	.930	.952	.946	.900
3.540	1.505	1.332	1.178	1.018	.918	.940	.938	.890
3.580	1.500	1.325	1.174	1.008	.906	.932	.932	.885
3.620	1.498	1.320	1.170	1.000	.900	.920	.930	.882
3.660	1.496	1.315	1.166	.998	.894	.915	.926	.880
3.700	1.494	1.308	1.164	.992	.890	.908	.922	.878
3.740	1.492	1.305	1.162	.990	.892	.902	.920	.875
3.780	1.490	1.300	1.160	.985	.894	.898	.916	.874
3.820	1.485	1.296	1.158	.978	.896	.892	.912	.874
3.860	1.482	1.292	1.154	.976	.900	.885	.908	.874
3.900	1.480	1.288	1.152	.972	.906	.884	.906	.874
3.940	1.480	1.284	1.154	.965	.912	.884	.904	.874
3.980	1.478	1.282	1.156	.962	.922	.884	.902	.874

APPENDIX B

^{4}He/Ne/Gr specific heat for several runs with areal densities $0.0140 \leq n \leq 0.0888$ Å^{-2}. The values are interpolated from smoothed specific heat vs. temperature curves.

For the three highest density runs, the temperature at which the desorption contribution is significant is indicated by a horizontal line and the correction made for the specific heat values at higher temperatures.

T	0.0140	0.0236	0.0329	0.0422	0.0562	0.0702	0.0841	0.0888
0.140	0.0346	0.0252	0.0190	0.0140	0.0066	0.0122		
.160	.0446	.0320	.0240	.0178	.0084	..0152		
.180	.0582	.0400	.0300	.0216	.0104	.0188		
.200	.0764	.0514	.0366	.0256	.0128	.0228		
.220	.0990	.0642	.0440	.0302	.0178	.0272		
.240	.124	.0788	.0522	.0354	.0194	.0320		
.260	.153	.0946	.0620	.0416	.0240	.0374		
.280	.187	.113	.0736	.0500	.0290	.0434		
.300	.222	.133	.0872	.0556	.0352	.0502		
.320	.260	.156	.103	.0638	.0430	.0570		
.340	.304	.181	.123	.0740	.0716	.0640		
.360		.211	.138	.0870	.0620	.0714		
.380	.412	.246	.159	.103	.0738	.0788		
.400		.282	.182	.120	.0868	.0866		
.420	.525	.322	.209	.140	.103	.0944		
.440			.241	.163	.122	.102		
.460	.663	.427	.278	.190	.146	.111		
.480			.320	.221	.187	.119		
.500	.815	.553	.360	.261	.204	.128	.0113	.0086
.520				.308	.239	.144	.0123	.0092
.540	.970	.707	.500	.355	.278	.159	.0133	.0098
.560						.165	.0144	.0102
.580	1.168	.920	.722	.510	.383	.167	.0155	.0106
.600						.170	.0167	.0110
.620	1.335	1.110	.937	.690	.460	.175	.0179	.0116
.640						.182	.0191	.0122
.660	1.434	1.370	1.118	.797	.487	.189	.0203	.0128
.680						.195	.0216	.0136

T	0.0140	0.0236	0.0329	0.0422	0.0562	0.0702	0.0841	0.0888
0.700	1.484	1.467	1.216	0.884	0.504	0.201	0.0230	0.0142
.720						.204	.0243	.0148
.740	1.504	1.488	1.234	.905	.514	.207	.0257	.0154
.760						.218	.0272	.0160
.780	1.480	1.462	1.217	.903	.523	.223	.0287	.0166
.800						.228	.0303	.0174
.820	1.420	1.410	1.167	.897	.530	.232	.0323	.0182
.840						.237	.0343	.0190
.860	1.370	1.355	1.106	.891	.532	.240	.0363	.0200
.880						.243	.0384	.0208
.900	1.325	1.304	1.056	.878	.534	.245	.0405	.0218
.920						.246	.0429	.0226
.940	1.293	1.243	1.019	.853	.533	.247	.0453	.0236
.960						.248	.0478	.0244
.980	1.270	1.200	.990	.830	.528	.249	.0504	.0254
1.000						.251	.0530	.0266
1.020	1.247	1.164	.966	.827	.521	.253	.0558	.0278
1.060	1.231	1.132	.946	.829	.522	.261	.0617	.0302
1.100	1.217	1.102	.930	.826	.525	.269	.0677	.0332
1.140	1.203	1.076	.912	.812	.530	.275	.0742	.0366
1.180	1.192	1.053	.898	.803	.535	.280	.0810	.0400
1.220	1.180	1.036	.886	.798	.539	.284	.0878	.0436
1.260	1.170	1.023	.877	.793	.544	.290	.0953	.0472
1.300	1.161	1.010	.868	.789	.550	.296	.104	.0514
1.340	1.153	.995	.859	.783	.558	.301	.119	.0560

T	0.0140	0.0236	0.0329	0.0422	0.0562	0.0702	0.0841	0.0888
1.380	1.145	0.985	0.851	0.781	0.564	0.309	0.133	0.0614
1.420	1.138	.975	.846	.780	.570	.316	.152	.0670
1.460	1.132	.968	.841	.779	.576	.324	.172	.0730
1.500	1.125	.960	.835	.778	.581	.331	.194	.0800
1.540	1.118	.952	.830	.777	.585	.337	.217	.0884
1.580	1.114	.947	.826	.775	.589	.340	.246	.0974
1.620	1.110	.942	.823	.773	.593	.347	.292	.107
1.660	1.106	.937	.820	.771	.596	.355	.352	.120
1.700	1.102	.933	.818	.769	.599	.363	.444	.136
1.740	1.098	.930	.816	.767	.603	.371	.497	.153
1.780	1.094	.927	.814	.764	.606	.378	.398	.172
1.820	1.091	.913	.812	.761	.609	.385	.254	.193
1.860	1.088	.917	.811	.758	.611	.391	.210	.216
1.900	1.086	.912	.810	.755	.613	.397	.209	.240
1.940	1.084	.907	.810	.753	.615	.403	.210	.265
1.980	1.082	.904	.809	.752	.617	.409	.212	.287
2.020	1.081	.901	.807	.750	.619	.414	.215	.298
2.060	1.081	.899	.804	.749	.620	.420	.220	.297
2.100	1.081	.897	.801	.748	.621	.426	.226	.288
2.140	1.081	.894	.800	.747	.623	.432	.232	.282
2.180	1.081	.892	.800	.746	.625	.437	.237	.273
2.220	1.081	.891	.799	.745	.627	.442	.243	.275

T	0.0140	0.0236	0.0329	0.0422	0.0562	0.0702	0.0841	0.0888
2.260	1.081	0.890	0.798	0.743	0.629	0.447	.250	.281
2.300	1.081	.889	.797	.741	.631	.453	.257	.284
2.340	1.081	.888	.797	.739	.633	.459	.265	.292
2.380	1.081	.887	.797	.737	.634	.465	.273	.302
2.420	1.081	.886	.797	.735	.636	.471	.282	.314
2.460	1.081	.884	.797	.733	.638	.478	.291	.327
2.500	1.080	.883	.796	.730	.640	.484	.301	.343
2.540	1.080	.882	.795	.728	.641	.490	.312	.360
2.580	1.080	.881	.794	.726	.641	.497	.323.	.377
2.620	1.080	.880	.793	.724	.641	.503	.334	.396
2.660	1.080	.880	.792	.723	.640	.509	.346	.415
2.700	1.080	.879	.791	.722	.640	.514	.358	.433
2.740	1.080	.879	.791	.721	.641	.520	.372	.452
2.780	1.080	.878	.791	.720	.641	.526	.387	.473
2.820	1.080	.878	.792	.720	.642	.532	.403	.496
2.860	1.080	.878	.793	.720	.642	.537	.419	.518
2.900	1.080	.879	.794	.720	.642.	.542	.436	.540
2.940	1.080	.880	.794	.720	.643	.547	.453	.564
2.980	1.080	.880	.795	.720	.644	.553	.472	.590
3.020	1.081	.881	.795	.721	.644	.557	.491	.618
3.060	1.082	.881	.795	.722	.644	.562	.513	.647
3.100	1.083	.882	.795	.722	.643	.567	.535	.677

T	0.0140	0.0236	0.0329	0.0422	0.0562	0.0702	0.0841	0.0888
3.140	1.084	0.883	0.794	0.723	0.643	0.573	0.357	0.707
3.180	1.086	.885	.794	.723	.643	.579	.382	.738
3.220	1.088	.887	.794	.724	.647	.585		
3.260	1.089	.889	.794	.725	.651	.591		
3.300	1.090	.891	.794	.726	.655	.598		
3.340	1.092	.893	.794	.728	.658	.605		
3.380	1.094	.895	.793	.729	.662	.612		
3.420	1.096	.897	.793	.731	.666	.619		
3.460	1.098	.899	.794	.732	.669	.627		
3.500	1.100	.900	.794	.735	.671	.635		
3.540	1.103	.902	.795	.737	.674	.643		
3.580	1.108	.904	.794	.740	.677	.653		
3.620	1.114	.906	.795	.743	.679	.663		
3.660	1.122	.909	.796	.747	.682	.675		
3.700	1.132	.912	.796	.750	.683	.688		
3.740	1.141	.915	.796	.754	.687	.701		
3.780	1.150	.919	.796	.756	.690	.714		
3.820	1.160	.924	.797	.760	.694	.729		
3.860	1.171	.930	.798	.763	.697	.744		
3.900	1.183	.937	.799	.766	.700	.759		
3.940	1.195	.943	.800	.769	.704	.776		
3.980	1.207	.950	.802	.772	.707	.796		

BIOGRAPHICAL NOTE

Selden B. Crary was born May 10, 1949, in Schenectady, New York, the son of Selden B. and Marjorie S. Crary. He graduated from Niskayuna High School in 1967 and received the Sc.B. degree with honors in Physics from Brown University in 1971. While a graduate student he has been teaching assistant, research assistant, and staff assistant at the University of Washington, where he received the M.S. degree in Physics in 1973. He married Susan F. Engert in 1975, and they enjoy hiking and bicycling in their free time.